



MRE11-RAD50-NBS1 complex disassembly from DNA double-strand breaks after ionising radiation.

Msc by Research Thesis

Stelios Alexander Raymond Koukouravas

University number – 1492928

Supervised by

Prof Kristijan Ramadan

Department of Oncology,

Medical sciences division,

University of Oxford

Trinity term 2022

Acknowledgements

I would like to thank my supervisor, Professor Kristijan Ramadan, for offering me the opportunity to conduct exciting research in his group. I am grateful for many of his insightful discussions and guidance, which have shaped me strongly as a young scientist.

I will always be thankful to multiple lab members Ignacio Torrecilla, Annamaria Ruggiano and Pauline Lascaux who were my mentors during the year. All three are excellent scientists, who offered me great support, assistance, and feedback both technically and mentally. They have all helped me to become a better independent thinker and scientist. I thank all the rest of the members Ramadan group: Juntong, Gwennie, Ftoon, Christiano, Susan, Wei, Abhay. It was wonderful sharing the laboratory with all of them. They provided me with the friendship that I needed and many fond memories to look back upon. I look forward to spending more time with them in the coming years.

Lastly but not least, I would like to thank my family for their incredible support on multiple levels and for making it possible for me to study for this degree.

Achievements

Awarded Medical Research Council (MRC) funding by Medical Science Division (MSD) for my DPhil, starting 2022.

Blue performance scheme for elite athletes 2021/22 https://www.sport.ox.ac.uk/steliosalex-koukouravas

Awarded the Adrian Mee Vincent's Scholarship for Team Sports a fund for scholar-athletes who also display leadership qualities and a willingness to participate in outreach activities for 2022/23 (not yet announced).

Published a co-authored paper in Biosystems during my placement in Singapore (2018) titled - Probability of change in life: Amino acid changes in single nucleotide substitutions (Published 2020) (1)

Declaration of originality

This dissertation is submitted for the degree of Msc by Research in Oncology. I hereby declare that the work in this thesis is my own original work, except where explicitly otherwise stated. I declare that this work has not been submitted for any other degree at this or any other university.

Table of Content

Acknowledgements 2

Achievements 2

Declaration of originality 3

Table of Content 4

Abbreviations 9

Abstract 10

List of Figures 11

1. Introduction 13

1.1. Hallmarks of Cancer 13

Figure 1. Hallmarks of cancer 13

1.2. Genomic Instability and DNA Damage Repair in Cancer 13

Figure 2. DNA damage agents and repair responses. 14

1.3. Ionising Radiation 15

Figure 3. Types of ionising radiation (IR) and the damage caused by these agents. 16

1.4. Double-Strand Break Response 17

Figure 4. Overview of main double-strand break (DSB) repair pathways. 19

1.5. MRN complex 19

1.5.1. Introduction of Structure and Function of the MRN complex 19

Figure 5. The MRN complex structure and conformational states. 21

1.5.2. Recognising DSB 22

Figure 6. Three step bidirectional model of end resection, initiating homologous recombination (HR). 23

1.5.3. Resecting DNA 23

1.5.4. Disassembly 24

Figure 7. Model of excess resection without presence of long-range resection factors 26

Figure 8. Key interaction partners of the MRN-CtIP complex. 27

1.5.5. Other roles of the MRN complex 27

1.6. DNA Damage Response Pathways 28

1.6.1. Homologous Recombination 28

Figure 9. DSB pathways with a focus on regulation of double ended HR sub-pathways and resolution. 31

Figure 10. Schematic of break-induced replication of single ended double-strand breaks. 33

1.6.2. Non-Homologous End Joining 34

1.6.3. Pathway Choice with a focus on the MRN Complex 35
Figure 11. Factors effecting pathway choice after IR. 36
1.7. HR and the MRN complex Role in Tumourigenesis and Treatment Outcomes 37
Tabular Figure 12. Investigation of MRN complex alterations involvement in tumourigenesis and progression. 40
1.8. DSB PTMs with a Focus on the MRN Complex 40
1.8.1. Phosphorylation 40
1.8.2. Methylation 41
1.8.3. Ubiquitination 41
Figure 13. Schematic of known E3 ligase's role in HR. 45
1.8.4. SUMOylation 46
1.8.5. Other PTMs 47
1.8.6. CtIP 48
1.8.7. PTM Crosstalk and Overview 48
1.9. p97 in Genome Stability 49
1.9.1. Structure and Function 51
Figure 14. p97 Structure and function 51
1.9.2. Cofactors 52
1.9.3. p97's Role in DSB and HR 53
Figure 15. p97 functions in the DNA damage response. 54
1.9.4. p97 Interaction with the MRN Complex 54
1.9.5. Other Roles of p97 in the Nucleus 55
1.9.6. Clinical Application 55
Figure 16. Small molecule inhibitors targeting different components of the ubiquitin proteasome system 56
Tabular Figure 17. p97 alteration's role in tumourigenesis, progression or treatment resistance. 59
2. Aims 59
2.1. Specific Objectives 59
Figure 18. Schematic overview of project 60
3. Methods 60
3.1. Tissue Culture 60
3.2. Plasmid Transfections 61
3.3. Molecular Cloning 61
3.3.1. PCR Amplification 62
3.3.2. Band Extraction 63

3.3.3. DNA Assembly and Ligation 63
3.3.4. Transformation 64
3.3.5. Colony PCR 64
3.3.6. DNA Sequencing 65
3.4. DNA Purification 66
3.5. Stable Cell Line Generation 67
3.6. Protein Analysis 68
3.6.1. Western Blotting 68
3.6.2. Co-Immunoprecipitation 71
3.6.3. Denaturing IP 72
3.7. Ionising Radiation Treatment 72
3.8. Solutions and Reagents 73
3.8.1. Antibodies 73
3.8.2. Buffers 73
4. Results 75
4.1. Introduction 75
Figure 19. Research project plan and progression to answer research questions. 75
4.2. Molecular Cloning 75
Figure 20. Molecular cloning overview. 76
4.3. Primer Design 76
Figure 21. Plasmid map example of the construct synthesised 77
Figure 22. Primer design table. 77
4.4. DNA Amplification and Extraction 78
4.4.1. Overcoming Limitations 78
Figure 23. PCR amplicon run on a 1% agarose electrophoresis gel. 79
Figure 24. PCR amplicons run on 1% agarose electrophoresis gels from various rad50 amplification strategies 80
4.5. Ligation and Transfection 81
4.5.1. Overcoming Limitations 81
Figure 25. Transformed bacteria post ligation 82
4.6. Cloning Validation – Colony PCR and Sanger Sequencing 82
Figure 26. Candidate colony PCR result of 1% agarose electrophoresis gel. 83
4.6.1. Overcoming Limitations 84
Figure 27. Candidate multiple sequence alignment result. 85
Figure 28. Alignment similarity table. 85

4.7. Validation of Plasmids in a Mammalian System 86
4.8. Western Blotting 87
Figure 29. Western blot validation of SSH and FLAG/APEX2 tagged synthetic plasmids in mammalian cells. 88
4.9. Co-Immunoprecipitation Validation 88
Figure 30. Co-Immunoprecipitation (Co-IP) testing of functionality of APEX2 synthetic plasmids. 90
4.10. Post-translational Modification Investigation 90
4.10.1. Denaturing Immunoprecipitation 90
4.10.2. Co-Immunoprecipitation 92
Figure 31. Co-immunoprecipitation of MRE11 to identify ubiquitination status of the MRN complex 93
4.11. Stable Cell Line Generation 94
Figure 32. Schematic of the Flp-In system used to create stable cell lines. 94
5. Discussion 95
6. Conclusion 100
7. References 101
8. Appendix 110
Figure 33. Mass spectrometry results from a MRE11 pulldown. 110
Figure 34. Mass spectrometry results of p97 pulldown. 111
Figure 35. Graphical representation of table in Figure 17. 111
Figure 36. Mass spectrometry results of p97 pulldown. 111
Figure 37. Example of tables used for HiFi cloning to ensure correct PCR amplification prior to ligation. 112
Figure 38. Candidate 1% agarose electrophoresis gel of PCR amplicons. 113
Figure 39. Band excision prior to gel extraction. 113
Figure 40. DNA quantification after gel extraction using nanodrop. 114
Figure 41 Agar plates containing ampicillin (50µg/ml) showing colonies transfected with synthetic DNA constructs after DNA assembly and ligation. 114
Figure 42. Candidate colony PCR result of 1% agarose electrophoresis gel from unspecific PCR amplification. 115
Figure 43. Patch plates of colonies screened by colony PCR. 115
Figure 44. Failed DNA alignment result showing the beginning and end regions of the RAD50 insert into the pCDNA5 vector backbone as well as a region of interest where the alignment resumed. 118
Figure 45. Schematic of the proposed ligation reaction causing the failed alignment. 118
Figure 46. Protein alignment result of the variant found in the NBN gene (ACC39752.1) aligned to multiple different species. 118

Figure 47. An example of a failed Sanger sequencing result. 119

Figure 48. DNA concentrations in ng/µl of plasmids after maxiprep DNA purification once colony PCR and sequencing reactions. 119

Figure 49. Candidate 'failed' denaturing IP results where MRE11 is not observed as SUMOylated or Ubiquitinated despite evidence from the literature. 120

Figure 50. Candidate 'failed' denaturing IP results where MRE11 is not observed as Ubiquitinated despite evidence from the literature. 121

Figure 51. Positive control denaturing IP results where RNF8 is potentially observed as ubiquitinated although NBS1 is not. 123

Figure 52. UBE4A and UBXD8 regulate accumulation of MRE11 on DNA damage similarly to p97. 123

Figure 53. Gantt chart displaying masters work completed along with planned work for first couple months of DPhil. 124

Abbreviations

MRE11	Meiotic recombination 11
RAD50	RAD50 Double Strand Break Repair Protein
NBS1	Nijmegen Breakage Syndrome 1 or Nibrin
CtIP	CtBP (carboxy-terminal binding protein) interacting protein
53BP1	P53 Binding Protein 1
AT	Ataxia Telangiectasia
ATM	Ataxia Telangiectasia mutated
ATR	Ataxia Telangiectasia and Rad3 related
BRCA1	Breast Cancer gene 1
BS	Bloom syndrome
DDR	DNA Damage Response
DNA-PK	DNA-dependent protein kinase
DSB	Double-Strand Break
HR	Homologous Recombination
IR	Ionising Radiation
NBS	Nijmegen Breakage Syndrome
NHEJ	Non-Homologous End Joining
PARP	Poly (ADP-ribose) polymerase
PIAS4	Protein inhibitor of activated STAT 4
PROTACs	Proteolysis targeting chimeric
PTM	Post-translational modification
RNF4	Ring Finger Protein 4
SSA	Single Strand Annealing
SSB	Single Strand Break
STUbL	SUMO-targeted ubiquitin ligases
UPS	Ubiquitin Proteasome System
UV	Ultraviolet
γHA2X	Phosphorylation of the Ser-139 residue of the histone variant H2AX
PCR	Polymerase Chain Reaction
APEX2	Apurinic/Apyrimidinic Endodeoxyribonuclease 2

Abstract

The complex formed by MRE11 –RAD50 and –NBS1, designated the MRN complex is essential for the DNA damage response (DDR). The MRN complex has a well-studied role in DNA end resection as part of the homologous recombination (HR) pathway. HR repairs double-strand breaks (DSB), the most toxic lesions that can arise in cells. The ATPase, p97, also called VCP, is a major component in the ubiquitin-proteasome system (UPS) and has an intrinsic unfoldase activity. It has been shown that loss of p97 strongly radiosensitises cells to ionising radiation (IR). Previous work shows that p97 provides timely removal of MRE11 from DSB sites thus preventing excessive end resection. Although the crucial role of the MRN complex in repairing DSBs has been well studied, the mechanism by which p97 controls the activity of the complex remains unknown. A better characterisation of the crosstalk between the MRN complex and p97 could lead to improving cancer prevention, diagnosis, and treatment. Indeed, drugs targeting the MRN complex and p97 are currently under clinical trial as sole or as combination (radiosensitiser) therapy (NCT03921021 and NCT04402541). This thesis aims to generate tools to answer the vital biological question of, **how is p97 directed to disassemble the MRN complex from DNA after DSBs**. To achieve this aim, it is intended to elucidate both the binding partners and post-translational modification (PTMs) of the MRN complex, using APEX2 proximity ligation assays in combination with mass spectrometry analysis. To this end, molecular cloning techniques were used to synthesise plasmids expressing fusion proteins of MRE11, RAD50 and NBS1 tagged with either APEX2 or SSH. The expression and functionality of these fusion proteins were validated using western blotting and co-immunoprecipitation, respectively. Subsequent stable cell lines were generated using these plasmids via the Flp-In system.

Additional studies identified post-translational modifications of the MRN complex using co-immunoprecipitation where ubiquitination of MRN complex was observed.

List of Figures

Figure 1. Hallmarks of cancer. 13
Figure 2. DNA damage agents and repair responses. 14
Figure 3. Types of ionising radiation (IR) and the damage caused by these agents. 16
Figure 4. Overview of main double-strand break (DSB) repair pathways. 19
Figure 5. The MRN complex structure and conformational states. 21
Figure 6. Three step bidirectional model of end resection, initiating homologous recombination (HR). 23
Figure 7. Model of excess resection without presence of long-range resection factors. 26
Figure 8. Key interaction partners of the MRN-CtIP complex. 27
Figure 9. DSB pathways with a focus on regulation of double ended HR sub-pathways and resolution. 31
Figure 10. Schematic of break-induced replication of single ended double-strand breaks. 33
Figure 11. Factors effecting pathway choice after IR. 36
Tabular Figure 12. Investigation of MRN complex alterations involvement in tumourigenesis and progression. 40
Figure 13. Schematic of known E3 ligase's role in HR. 45
Figure 14. p97 Structure and function. 51
Figure 15. p97 functions in the DNA damage response. 54
Figure 16. Small molecule inhibitors targeting different components of the ubiquitin proteasome system. 56
Tabular Figure 17. p97 alteration's role in tumourigenesis, progression or treatment resistance. 59
Figure 18. Schematic overview of project. 60
Figure 19. Research project plan and progression to answer research questions. 75
Figure 20. Molecular cloning overview. 76
Figure 21. Plasmid map example of the construct synthesised. 77
Figure 22. Primer design table. 77
Figure 23. PCR amplicon run on a 1% agarose electrophoresis gel. 79
Figure 24. PCR amplicons run on 1% agarose electrophoresis gels from various rad50 amplification strategies. 80
Figure 25. Transformed bacteria post ligation. 82
Figure 26. Candidate colony PCR result of 1% agarose electrophoresis gel. 83
Figure 27. Candidate multiple sequence alignment result. 85
Figure 28. Alignment similarity table. 85
Figure 29. Western blot validation of SSH and FLAG/APEX2 tagged synthetic plasmids in mammalian cells. 88
Figure 30. Co-Immunoprecipitation (Co-IP) testing of functionality of APEX2 synthetic plasmids. 90
Figure 31. Co-immunoprecipitation of MRE11 to identify ubiquitination status of the MRN complex 93
Figure 32. Schematic of the Flp-In system used to create stable cell lines. 94
Figure 33. Mass spectrometry results from a MRE11 pulldown. 110
Figure 34. Mass spectrometry results of p97 pulldown. 111
Figure 35. Graphical representation of table in Figure 17. 111

Figure 36. Mass spectrometry results of p97 pulldown. 111
Figure 37. Example of tables used for HiFi cloning to ensure correct PCR amplification prior to ligation. 112
Figure 38. Candidate 1% agarose electrophoresis gel of PCR amplicons. 113
Figure 39. Band excision prior to gel extraction. 113
Figure 40. DNA quantification after gel extraction using nanodrop. 114
Figure 41 Agar plates containing ampicillin (50µg/ml) showing colonies transfected with synthetic DNA constructs after DNA assembly and ligation 114
Figure 42. Candidate colony PCR result of 1% agarose electrophoresis gel from unspecific PCR amplification. 115
Figure 43. Patch plates of colonies screened by colony PCR. 115
Figure 44. Failed DNA alignment result showing the beginning and end regions of the RAD50 insert into the pCDNA5 vector backbone as well as a region of interest where the alignment resumed. 118
Figure 45. Schematic of the proposed ligation reaction causing the failed alignment. 118
Figure 46. Protein alignment result of the variant found in the NBN gene (ACC39752.1) aligned to multiple different species. 118
Figure 47. An example of a failed Sanger sequencing result. 119
Figure 48. DNA concentrations in ng/µl of plasmids after maxiprep DNA purification once colony PCR and sequencing reactions. 119
Figure 49. Candidate 'failed' denaturing IP results where MRE11 is not observed as SUMOylated or Ubiquitinated despite evidence from the literature 120
Figure 50. Candidate 'failed' denaturing IP results where MRE11 is not observed as Ubiquitinated despite evidence from the literature. 121
Figure 51. Positive control denaturing IP results where RNF8 is potentially observed as ubiquitinated although NBS1 is not. 123
Figure 52. UBE4A and UBXD8 regulate accumulation of MRE11 on DNA damage similarly to p97 123
Figure 53. Gantt chart displaying masters work completed along with planned work for first couple months of DPhil 124

1. Introduction

1.1. Hallmarks of Cancer

In the ever-growing field of cancer research, the landmark 'Hallmarks of Cancer' reviews have provided a foundation to characterise neoplastic cells (2-4). The original 6 hallmarks (2) with additional emerging and enabling characteristics which were added in 2011 (3) and 2022 (4). Genomic alterations facilitate cancer formation by providing certain subclones with a selective advantage - enabling hallmark(s) e.g., uncontrolled proliferation to propagate and outcompete non-cancerous cells. The current list of hallmarks is shown in figure 1. One of the hallmarks of interest is genome instability and mutation. Initially highlighted as an enabling characteristic since it underpins cancer formation as a whole (3) subsequent evidence has confirmed it as a hallmark (4).

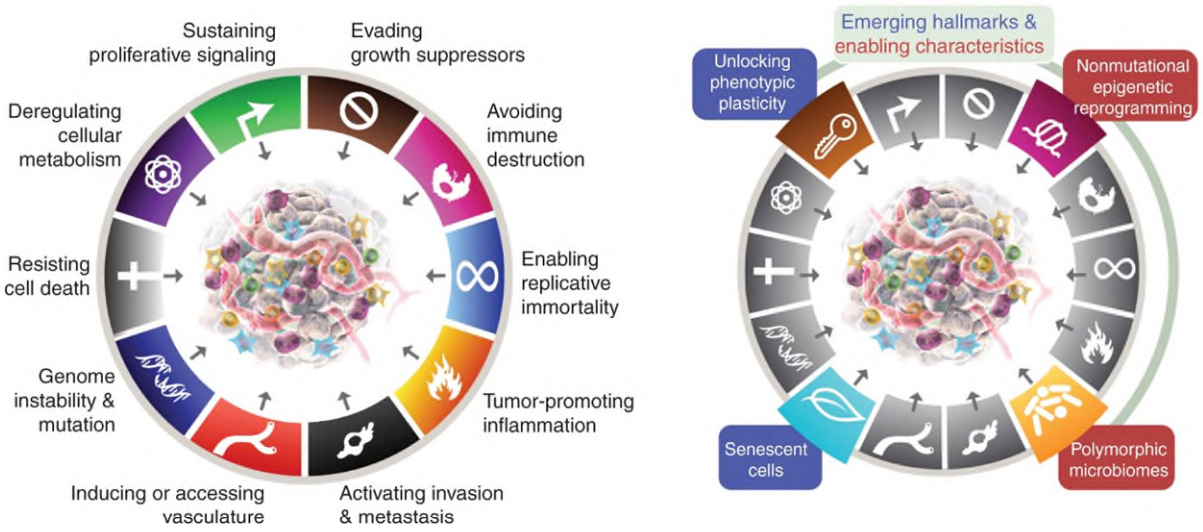


Figure 1. Hallmarks of cancer.

Figure showing the confirmed, (left) and emerging, (right) hallmarks as well as enabling characteristics (right) that facilitate tumourigenesis and progression. Figure adapted from (4).

1.2. Genomic Instability and DNA Damage Repair in Cancer

Cancer cells often exhibit an increased mutation rate and genome instability compared to normal cells (5). Faulty DNA repair machinery is one of the reasons for this as it compromises the protection of the genome, causing errors. For example, the *brca1* gene heterozygosity is a key risk factor for breast cancer, as the loss of this key regulator of an 'error-free' DNA damage repair pathway (homologous

recombination - HR) increases the risk for cancerous mutations to arise (6). Endogenous and exogenous agents can also damage DNA and other macromolecules within the cell. Some common endogenous agents include oxidising producing reactive oxygen species (ROS) and alkylating agents e.g., methyl groups added by S-adenosylmethionine (SAM). Common environmental agents include UV radiation and ionising radiation (IR). These agents can result in different types of DNA damage (Figure 2), these include single and double strand breaks.

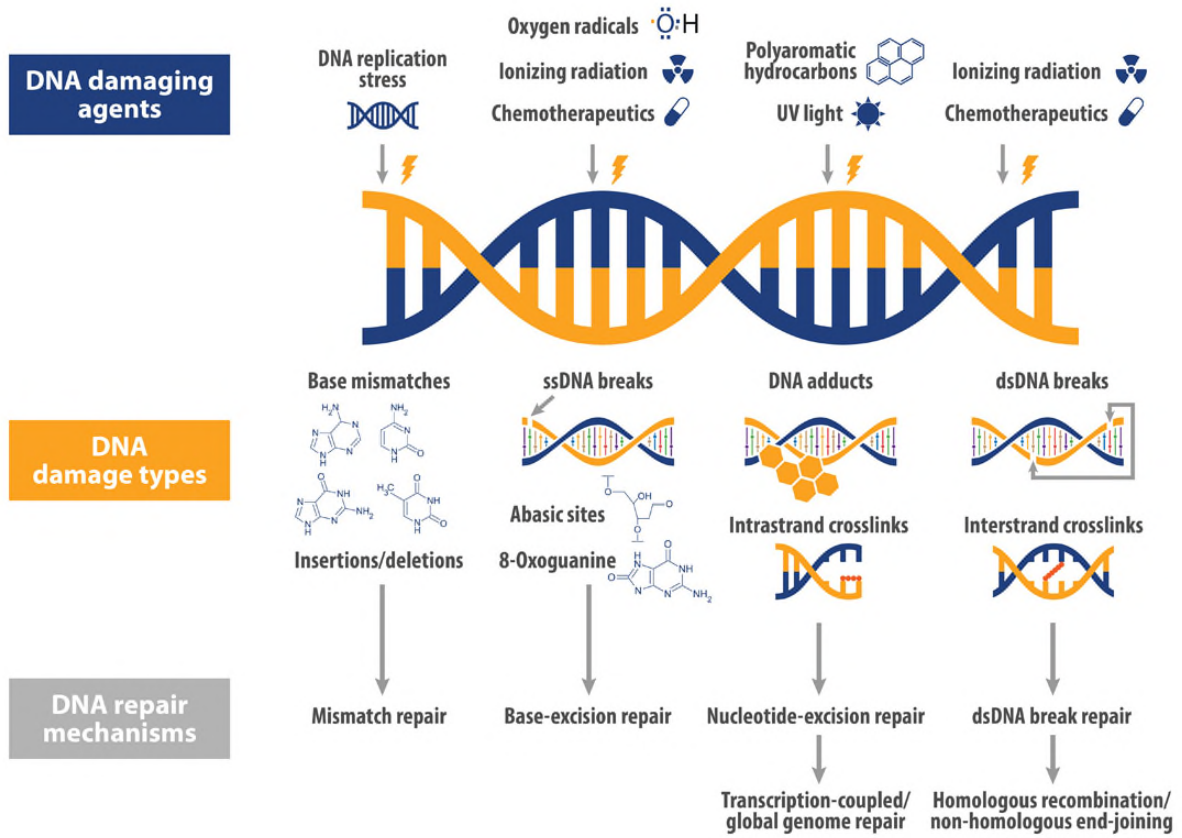


Figure 2. DNA damage agents and repair responses.

The figure shows different types of DNA damaging agents, the damage they cause and the mechanisms that mediate their repair. Of interest, ionising radiation and chemotherapeutics caused double-strand breaks which are repaired generally by homologous recombination and non-homologous end-joining. Figure adapted from CrownBioscience.

Single strand breaks (SSB) are the most common lesion type, where only one strand is damaged, although these do not often compromise genome stability (7). However, if SSBs are left unrepaired they can form double-strand breaks (DSBs). This can occur during the DNA replication process where the replication fork can collapse upon encountering an SSB. This blocks the replisome from

progressing, causing DSBs. As DSBs are the most toxic genomic lesion to cells and compromise genome stability, the repair of these lesions is imperative (7). If incorrectly repaired, DSBs can lead to mutations and chromosomal rearrangements resulting in cell death or may lead to cancer formation (7, 8). Furthermore, in cancer, cell cycle checkpoint control is dysregulated therefore the progression of the cell cycle continues despite these lesions occurring, resulting in greater accumulation of mutations and genome instability.

However, DSBs toxicity is also used to treat cancer, e.g., using IR. The inability of cancer cells to repair these lesions as efficiently as normal cells, results in cancer specific toxicity.

1.3. Ionising Radiation

Ionising radiation (IR) encompasses particles or electromagnetic waves with enough energy to ionise or detach electrons from a molecule. These include gamma and x-rays (waves) and alpha, beta and neutron particles (Figure 3). One gray of IR generally produces thousands of SSBs and tens of DSBs along with other types of damage within the cell (9, 10). The type of damage is radiation dependent. IR can cause direct damage e.g., to macromolecules such as DNA or indirect damage e.g., free radicals' production by water ionisation (Figure 3). IR can cause immediate DNA damage or secondary damage such as replication fork collapse (11). IR causes a variety of lesions in close proximity, and these are termed complex, clustered or dirty lesions (12). The clustering of these lesions at a precise nanometre scale is a signature of IR (10). One of the most important mechanisms of cellular toxicity induced by IR is based on these DNA damage lesions inducing SSB, DSB and DNA adducts (Figure 3).

IR is commonly used as an anticancer therapy as it preferentially affects rapidly dividing cancer cells. More than 50% of cancer patients receive radiotherapy at some point in their treatment. IR is generally given in fractions, where dosages are given over a designed time period (13). The 5 Rs of radiation are used when treating patients to assess the biological effect of fractionated radiotherapy and to optimise safety. These factors are Repair, Repopulation, Redistribution, Reoxygenation and Radiosensitivity (14). These factors consider 1) how likely cells within the tumour repair the damage,

2) the rate of tumour regeneration, 3) the tumour cell cycle phase, as those in the G2 and M phase are most sensitive, 4) how oxygenated the tumour tissue is; hypoxic tissues are more resistant to radiation (as ROS formation is limited) and 5) how inherently sensitive the specific tissue/tumour type is to radiation. Fractionated radiotherapy is often compared to peeling the skin off an onion with each fraction of radiation exposing another layer of the tumour to more oxygen and more damage. One negative impact of each fractionated treatment is that a rebound effect is experienced where there is a period of increased growth due to the lack of intra-tumour competition.

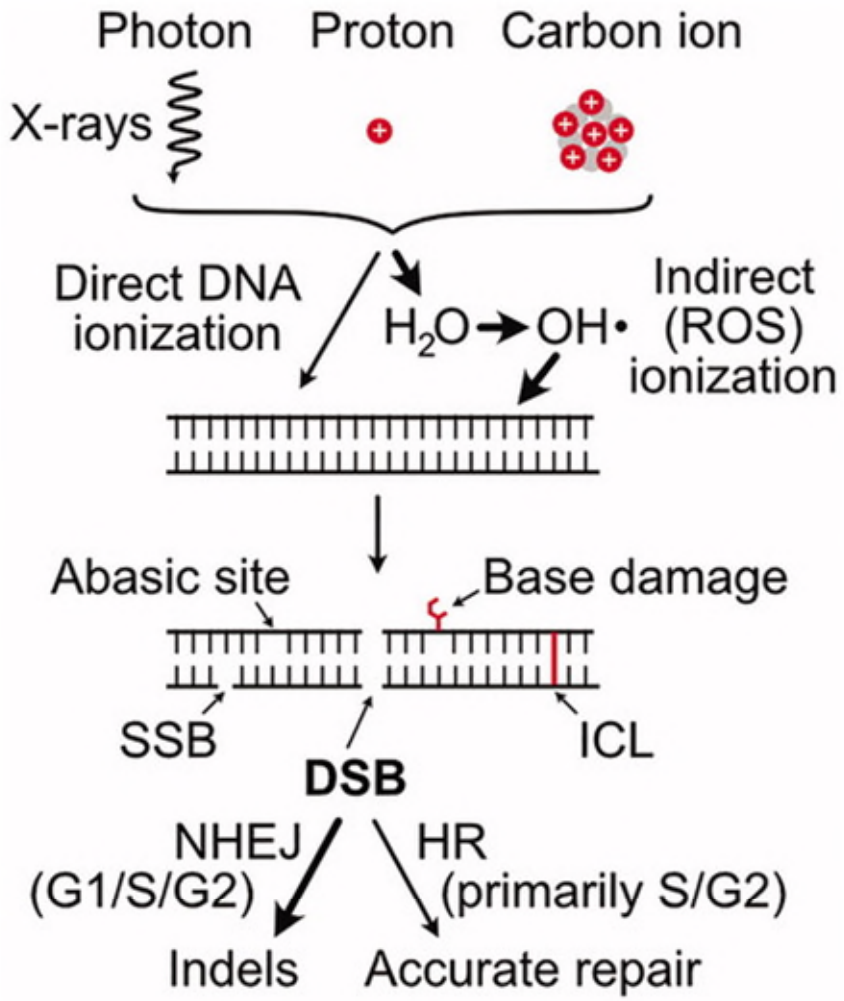


Figure 3. Types of ionising radiation (IR) and the damage caused by these agents.

IR shown at the top can cause direct or indirect damage (through ROS formation) to DNA. This can cause several lesions to DNA such as abasic sites, single strand breaks (SSB), double strand breaks and more including those not shown in the figure such as intra-strand crosslinks or protein DNA crosslinks. This shows the complex breaks that IR can induce. DSB are repaired

by non-homologous end joining (NHEJ) or homologous recombination (HR) depending on the cell cycle stage. These repair mechanisms have different outcomes. Figure adapted from (11)

Methods to increase the efficiency and minimise side effects of IR treatment not only include fractionation therapy but also combination therapy, which is a promising area of treatment. Radiosensitisers are described as agents which increase the efficacy of IR treatment while limiting side effects. Using insight gained from the 5 Rs of fractionated radiotherapy, cell cycle and DNA damage regulators as well as oxygenating agents are being explored as radiosensitisers. These methods are particularly effective in reducing side effects because therapies may be sub-lethal for normal cells i.e., normal cells can repair the damage, but the damage level is lethal for cancer cells. Potential radiosensitisers such as the inhibition of proteins and complexes in the DSB response have been suggested (ref). The loss of integrity of one of these, the MRN (MRE11 (meiotic recombination 11)-RAD50 (DNA double strand protein RAD50)-NSB1 (Nijmegen breakage syndrome 1) complex) complex, which consists of a group of 3 proteins involved in the homologous recombination (HR) pathway has been shown to radiosensitise cancer (15-17). Furthermore, it has been shown that multiple cancers develop radioresistance by increasing HR and MRN efficiency (11, 18-20) (Figure 12) therefore studying the role of the MRN complex could provide a therapeutic target as a radiosensitiser.

1.4. Double-Strand Break Response

Double-strand breaks are caused by ultraviolet (UV) light, Ionising radiation (IR), other agents or where replication forks collapse at the site of SSB which disrupts the replisome machinery. These are the most cytotoxic breaks as they can lead rapidly to the loss of genetic information, cell death or tumourigenesis (21). These breaks can be described as clean or dirty (Figure 3 and 11). For example, dirty DSBs may contain DNA adducts and covalent bound proteins, while clean breaks do not. IR generally is thought to generate dirty breaks whereas a cleavage by a restriction enzyme would generate a clean break. Dirty breaks are more difficult, and require a longer time, to repair with some breaks deemed unrepairable (11, 12). Type of breakage can also be defined by the status of their ends - single-ended breaks normally occurs after replication and double-ended breaks from DNA damaging

agents as seen in figures 10 and 9 respectively. The type of break, cell cycle stage and nuclear localisation dictate the repair pathway choice (22) (Figure 11).

Different pathways can repair DSBs. The main two pathways are non-homologous end joining (NHEJ) and homologous recombination (HR) (Figure 4). Although in reality, these are not simple hard-defined pathways as other sub and alternative pathways such as, but not exclusive to, alternative-NHEJ and single-strand annealing (SSA) exist (Figure 9). NHEJ is an error prone repair pathway which is the most frequently involved in DSB repair. NHEJ occurs throughout the cell cycle and its factors are rapidly recruited at DSB sites (23). HR on the other hand is deemed 'error-free' but it generally only occurs during S and G2 phases, when a sister chromatid present acts as a template for the repair of the lesion and displays slower kinetics (23). More detail regarding these pathways can be found below particularly regarding HR due to its role in this project. DSB repair is not only essential to repair damage but is also important during telomere lengthening, VDJ recombination, class switch recombination and meiosis. Multiple hereditary conditions that are linked with cancer formation involve faulty DSB machinery e.g., ataxia telangiectasia (AT), Nijmegen breakage syndrome (NBS) and Bloom syndrome (BS). Targeting the DSBs is an anti-cancer therapy as tumours have greater dependencies on specific DSBs pathways to repair lesions. Among the drugs developed to target the DDR, several have reached clinical trial stage, such as kinase inhibitors (ATM, ATR and DNA-PK) (24), other small molecule inhibitors and PROTACs (Proteolysis targeting chimera, containing a protein head specific for the protein of interest and a E3 ubiquitin ligase therefore can selectively degrade a target protein) (25).

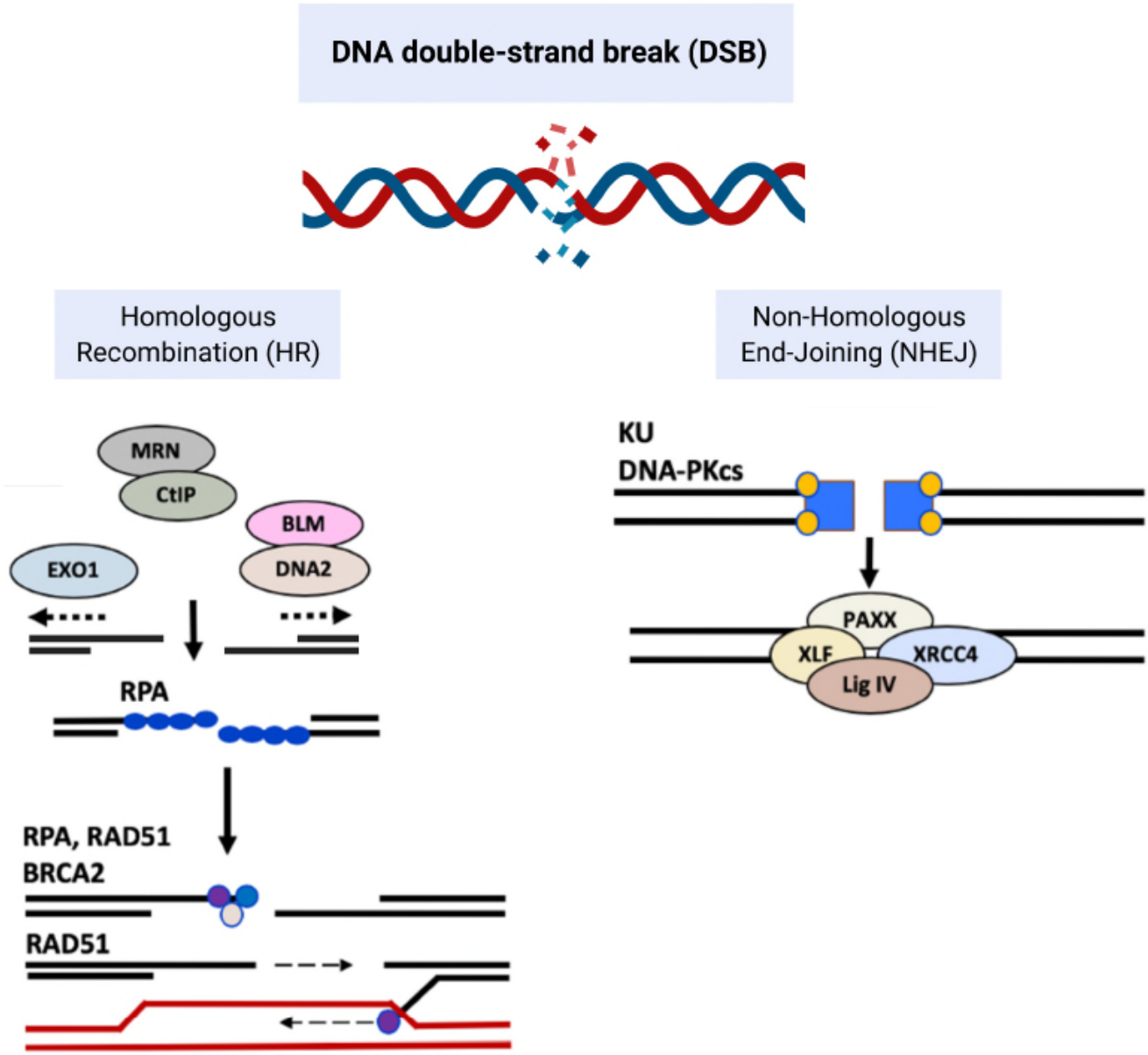


Figure 4. Overview of main double-strand break (DSB) repair pathways.

Homologous recombination shows resection factors MRN-CtIP, EXO1 and DNA2-BLM revealing ssDNA which subsequently get bound by RPA. BRCA2 mediates the formation of a nucleofilament with Rad51 replacing RPA. Homology search is then completed where strand invasion with a homologous sequence (shown in red) occurs, and repair is completed. Non-homologous end-joining shows Bound DSB ends by Ku which recruit DNA-PKc's which further recruit other machinery (PAXX, XLF, LigIV and XRCC4) to process the DSB ends and facilitate end joining. Figure adapted from (26)

1.5. MRN complex

1.5.1. Introduction of Structure and Function of the MRN complex

The MRN is a hetero-hexametric complex comprising of two MRE11-RAD50-NBS1 proteins which act as an initial sensor of DSBs in the HR pathway. The MRN complex initiates HR by performing DNA end resection of the DSB site. The MRE11-RAD50 complex is conserved across species, while the role of

NBS1 in the complex can differ in different systems (27). The MRN complex has four functions; DSB recognition, DNA bidirectional end processing via intrinsic exo and endonucleic nuclease abilities, DNA bridging, and signalling in the DDR pathways.

The MRN complex structure can be divided in three sections, the head, the coil, and the hook. The head contains a MRE11 homodimer each of which interacts with RAD50 and NBS1 proteins using different domains as can be seen in Figure 5a. RAD50 contains a coiled-coil domain which proceeds from the RAD50 ABC ATPase domains forming the coil and ending in the zinc hook (27) (Figure 5b).

MRE11 is the core nuclease of the complex, its activity depends on the interaction with its partners. MRE11 consists of a catalytic nuclease core made of a Mn^{2+} dependent phosphodiesterase domain. The RAD50 protein is a member of the SMC (structural maintenance of chromosomes) family characterised by two long intramolecular coiled-coil domains that run anti-parallel. The bridging of the N- and C-termini, form a globular ABC ATPase head nucleotide binding domain which spatially lies next to MRE11 (Figure 5B). RAD50 coiled-coils end in a zinc hook which dimerise with the other RAD50 zinc hook (intramolecularly). These can in turn interact with a further two RAD50 zinc hooks (intermolecularly) via zinc ion chelation allowing the MRN complex to interact with itself and another MRN molecule (Figure 5B-D). This action allows the bridging of DNA ends and tethering of sister chromatids (inter- or intra-molecular tethering) (28) (Figure 5A-D). RAD50 mediated tethering of sister chromatids increases the efficiency of homologous search in the HR pathway and maintains the DSB site in a close proximity for efficient DDR signalling. RAD50's ATPase activity causes a confirmational change that supports MRE11's nuclease activity via 'opening' of the complex and the removal the steric obstruction of RAD50 which allows MRE11 to bind (Figure 5B). NBS1 uses a nuclear localisation signal to support the role of the MRN complex. Its functions include contributing to the DNA binding function of the MRN complex and mediating the interactions with multiple cofactors such as CtIP, BRCA1, ATR, and ATM via its FHA and BRCT domains (Figure 5A) (28). NBS1 binds to MRE11 via its two

MRE11-interacting regions on the C-terminus of the protein. There is some evidence that NBS1 has MRN-independent roles in cells (23, 29).

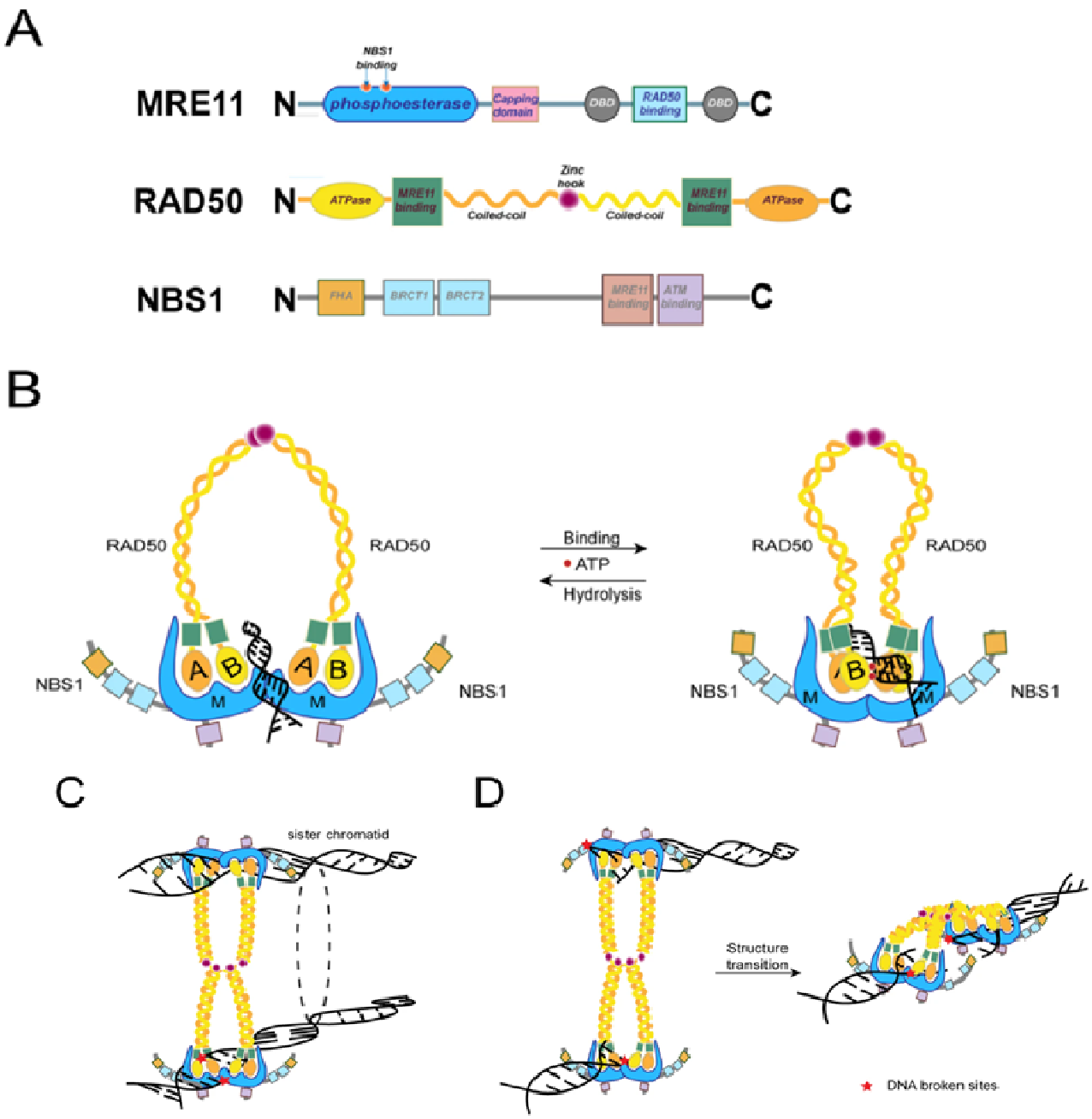


Figure 5. The MRN complex structure and conformational states.

A) Protein domains of MRE11, RAD50 and NBS1 highlighting key domains and interaction domains. B) cartoon of the structure of the MRN complex and its conformational change during ATP binding and hydrolysis. MRE11 dimer interacts with DNA and each MRE11 bind a single NBS1 and RAD50 molecule. In the ADP bound state an open clamp is shown where it can freely diffuse along DNA. ATP bound state a closed clamp structure is induced allowing to engage DNA for end processing. RAD50 tails change conformational state allowing for tethering activities. ATP hydrolysis mediates the conversion between these two states. C and D) tethering function of the MRN complex between sister chromatids (C) and double ended DSB (D). Figure adapted from (30).

The MRN complex diffuses along the DNA strand and senses DBS sites. Conformational changes allow the MRN complex to recognise and start the repair at the DBS site. ATP hydrolysis disengages the RAD50 dimer from blocking the MRE11 nuclease domain allowing the opening of the conformation and initiation of resection (31). Moreover, NBS1 recruits CtIP (CtBP (carboxy-terminal binding protein) interacting protein and MRN end resection initiation factor) which aids in end resection initiation (32). *In vitro* it has been shown that the MRN complex is able to partially unwind DNA for efficient end resection (33). Taken together this highlights the importance of the structure of the MRN complex and how that structure impacts the main function of the MRN complex as an end resection, signalling and DNA bridging factor. More detail regarding these functions can be seen in subchapters 1.5.2-5.

1.5.2. Recognising DSB

The MRN complex is recruited to the site of DSB within seconds and facilitates the signalling of the lesion by propagating ATM signalling via NBS1 interaction. There is a feedback loop between the MRN complex and ATM where the MRN complex activates ATM, ATM in turn phosphorylates all three subunits of the MRN complex (34). MRN accesses DSBs via facilitated diffusion along the DNA strand (35). Engagement of DNA is thought to be mediated by cofactor CtIP binding and ATP hydrolysis, mediating the conformational change allowing MRE11 to access the DNA break site (28) (Figure 5). Signalling molecule activation and post translational modification (PTM) manipulation regulates availability and the rate of assembly of the MRN complex, therefore regulating DSB recognition rate (32, 36). For example, PIH1D1, a subunit of heat shock protein 90, stabilises MRE11, NBS1 and ATM (37). C1QBP1 also stabilises MRE11 and RAD50, while amplified METTL16 levels have also been shown to sequester MRE11. Both of these processes are controlled via phosphorylation (38, 39). In addition, DYNLL1 has been shown to interact with MRE11 in BRCA1 deficient cells which limits end resection initiation (40). Furthermore, PTMs such as ubiquitination of NBS1 by RNF8, and UPS4 auto-deubiquitylation and others highlighted in section 1.8.3 aid in MRN complex formation and recruitment to DSB sites (41-43). MRN interacting protein, MRNIP also promotes MRN loading to DNA. This is thought to be via lipid droplet formation (44). Whilst it has been shown that in yeast the 9-1-1

complex seems to prevent MRN binding to DNA (45). An understanding of how these mechanisms interplay to regulate the MRN complex activity is needed, especially in the context of radiation-induced breaks.

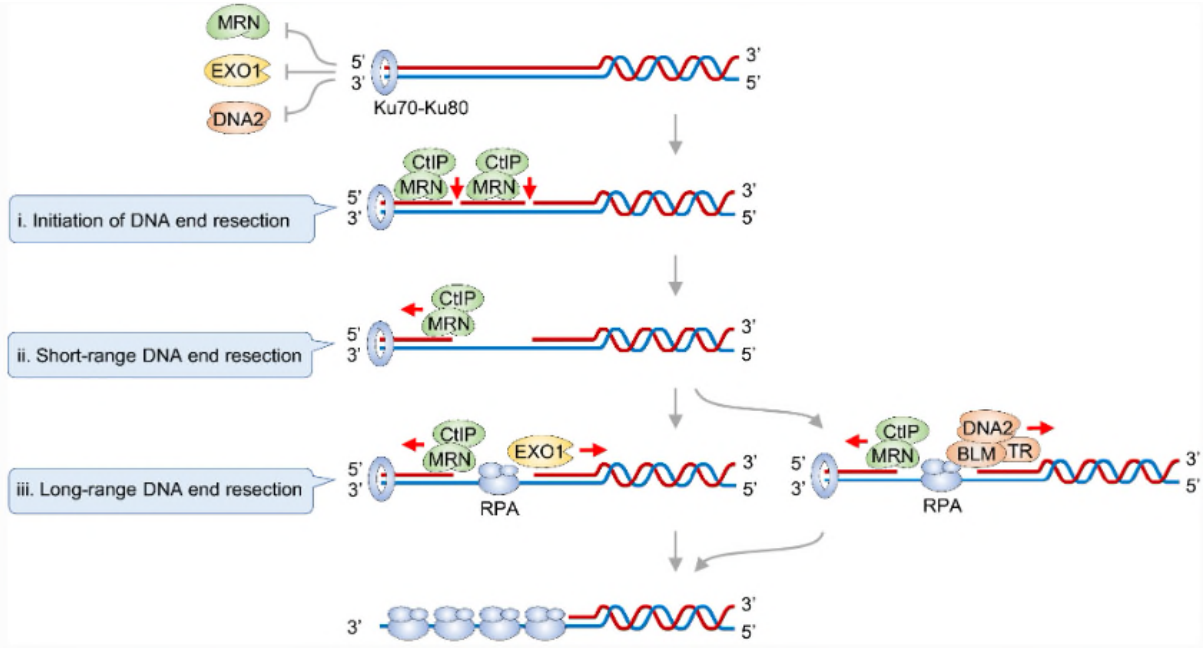


Figure 6. Three step bidirectional model of end resection, initiating homologous recombination (HR).

Ku bound ends compete with the MRN complex impacting pathways choice. Under Hr submissive conditions the MRN complex can bind DNA upstream of the double-strand break (DSB) site. I) MRN with the help from CtIP initiate end resection by making an initial endonucleic cut. ii) short-range resection by the MRN-CtIP complex occurs 3' to 5' revealing ssDNA. iii) long-range resection machinery can now access the resection site and processive resection occurs revealing large sections of ssDNA. Long-range machinery is either the EXO1 nuclease or the DNA2-BLM-TR complex. RPA binds and protects ssDNA ready for the next steps of HR. Figure adapted from (32)

1.5.3. Resecting DNA

End resection describes the digestion of single strand DNA (ssDNA) at the DSB site to expose long sections of ssDNA allowing for homology searching. End resection is a three-step, bidirectional process of initiation, short-range and long-range resection (Figure 6). The MRN complex completes two of these steps, initiation, and short-range resection via its endo and exonucleic activity respectively. These functions also dictate the bidirectionality of end resection. The endonucleic activity creates a nick on one strand of the DNA roughly 35-45 nucleotides (nt) upstream of the DSB site by bending the DNA homoduplex (46). Initiation of end resection by MRN requires the presence of NBS1 and its endonuclease activity is mediated by the hydrolysis of ATP on RAD50 and CtIP binding (32, 47) (Figures

5 and 6). It is thought that phosphorylated CtIP interacts with NBS1 which in turn triggers the ATP hydrolysis and resection (48, 49). Additional endonucleic nicks are made in roughly 20nt increments upstream of the break (Figure 7). This allows the exonucleic function of the MRN complex to digest the ends back to the break sight and remove potential protein blocks such as the Ku complex, exposing ssDNA of about 100-200 nucleotides (36). The MRN complex partially unwinds the DNA strand aiding its processivity (50). Furthermore, MRNIP condensates are proposed to accelerate end resection (44). Specific inhibitors for MRNs endo and exonucleic function showed differential effects which support the above outline (51). This process of short-range resection allows access of long-range resection machinery to the DSB site due to the nick created via the MRN complex endonuclease activity. MRN also promotes long-range resection by direct signalling recruitment of long-range resection factors, increasing the processivity of both Exo1 and the DNA2 complex (15, 26, 35, 52). This process initiates HR, the subsequent steps will be highlighted in chapter 1.6.1.

1.5.4. Disassembly

Excessive ssDNA formation promotes genome instability therefore it is hypothesised that once a certain threshold of resection is met, resection machinery is dissembled from chromatin (15, 53). Loss of multiple proteins regulating the MRN complex has caused a phenotype of excess resection and genome instability. Therefore, these proteins are assumed to regulate the disassembly of the MRN complex.

Inhibition of p97, a segregase that will be discussed in chapter 1.7, results in MRE11 and RAD50 foci accumulation, excess MRE11 dependent resection (Exo1 independent) resulting in more ssDNA and an increase in SSA (15, 26). The removal of MRE11 was shown to be proteasome independent, implying that p97 processing of the complex does not lead to its degradation by the proteasome. This has it has been shown for several other p97 substrates (54). The implication is that p97 redirects MRE11 by removing it from chromatin for reuse into the nucleosol.

Inhibition of proteasomal ubiquitin shuttle factor UBQLN4 also causes MRE11 accumulation. Although here, UBQLN4 directs MRE11 to the proteasome, excessive end resection is not observed while increased initiation of end resection is (55, 56). ATM phosphorylates UBQLN4 activating it to regulate the MRN complex resulting in a negative feedback loop (57). Furthermore, ATM dependent phosphorylation has been shown to regulate MRN retention again in a negative feedback loop (52). When ATM cannot phosphorylate MRE11 at multiple residues, excessive end resection (Exo1 independent), defective HR and an increased reliance on SSA occurs (52).

A recent study showed that global SUMOylation increased after DSBs and found specifically an upregulation of MRE11 and RAD50 SUMOylation. MRE11 SUMOylation after DSBs protects it from ubiquitin-mediated degradation, in an opposing manner as a STUbL (SUMO-targeted ubiquitin ligases) would act (58). Overexpression of a deSUMOylating enzyme SENP3 or presence of an MRE11 mutant without SUMOylation sites caused MRE11 accumulation and excessive end resection. This may provide a mechanism for regulating the disassembly of the MRN complex, although further studies are required, especially regarding the spatiotemporal dynamics of these reactions (58). It was also found that there was differential regulation of the MRN complex subunits (58). RAD50 may be SUMOylated in a STUbL dependant manner, where SUMOylation is recognised by RNF4 resulting in subsequent ubiquitin-mediated degradation (59). Interestingly RNF4 associated ubiquitination is often coupled to p97 (60). NBS1 SUMOylation is downregulated after DSBs unlike MRE11 and RAD50 where SUMOylation increases (58).

PLk1 and subsequent CK2 dependent phosphorylation of residues in MRE11's DNA binding domain have been shown to prevent MRN complex assembly and binding to DNA and this has been suggested to be a mechanism of MRN complex disassembly (61). A mechanism has been proposed to explain the decrease in the affinity for DNA. The decreased affinity is caused by alterations in the electrostatic interactions between the MRN complex and DNA. As negatively charged phosphate groups are added

to MRE11, the electrostatic repulsion hinders its interaction with negatively charged DNA (61, 62). Electrostatic alterations were found to affect the binding affinity of the MRN complex elsewhere (35).

Disassociation of the MRN complex in budding yeast was found to be associated with Sae2 interaction (CtIP budding yeast homolog) presence suggesting CtIP could have a role in disassembly (50). Furthermore, the disassembly of the MRN complex is dependent on MRE11 nuclease and CtIP homolog (Ctp1) activity in fission yeast (63). Evidence suggests PIAS4 a E3 SUMO ligase recognises ATM dependent phosphorylation of CtIP and SUMOylates CtIP causing RNF4 based STUbL ubiquitination which may regulate end resection termination and MRN complex disassembly. Without this SUMOylation, a similar phenotype of HR deficiency and SSA compensation is observed (64). Whether CtIP SUMOylation affects MRN complex disassembly from DNA is unknown.

The exact mechanism in which the MRN complex causes excess end resection is not known. It is counter-intuitive as the current model for the 5'-3' exonucleic digestion by MRN would not explain the excess ssDNA, it could be that MRN continues to bind to upstream sequences although this would not warrant excess retention, rather excess loading (Figure 7). A speculation is that since the MRE11 nuclease may be needed to facilitate the MRN complex removal from DNA ends (63), more MRN complex is loaded further upstream to aid this removal, although without downstream removal factors aiding this process – disassembly cannot happen. This results in a positive feedback loop of MRN complex loading, furthermore it may promote end resection by other nucleases.

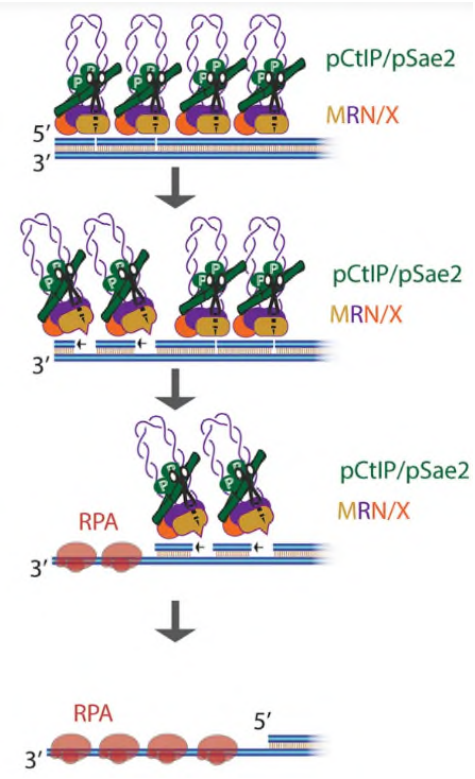


Figure 7. Model of excess resection without presence of long-range resection factors.

3' to 5' resection of DNA is completed by the MRN-CtIP complex after the initial endonucleic cut. RPA then binds ssDNA to protect these ends. Multiple MRN-CtIP mediated endonucleic cuts and resection upstream of the beginning of the ssDNA is a proposed method of excess resection driven solely by the MRN complex. Figure adapted from (48)

Although the role of Exo1 has been investigated, showing that MRN regulated excess resection is independent of Exo1 (26). This still leaves the other long- range machinery, the DNA2 nuclease complex to be investigated as MRN has also been found to increase processivity of this complex (65). Furthermore, long-range resection factors were found in a recent study using DNA repair reporter assays to promote SSA over HR compared to short-range resection factors (66). This makes sense as hyper-resection causes SSA preference.

Taken together this information shows the phenotype of MRN dependent excess/hyper-resection is not completely understood and further study is needed to clarify how all these factors could be involved. A list of MRN interacting proteins can be found in Figure 8.

Protein	Interaction Partner	Biological function
MRE11	UBQLN4	Remove ubiquitylated MRE11 from DSBs and prevent excessive DNA end resection.
	PARP1	Promote replication fork restart by recruiting MRE11.
	SAMHD1	Promote restart of stalled replication forks by stimulating MRE11 exonuclease activity toward nascent DNA.
MRN	DYNLL1	Limit DNA end resection by inhibiting MRE11 exonuclease activity.
	MRNIP	Enhance DDR by recruiting MRN complex
MRN, CtIP	ATM	Augment DDR cascade of phosphorylation; facilitate MRN turnover from DSB sites.
	USP4	Promote CtIP recruitment and DNA repair.
MRE11, RAD50	p97	Help MRN turnover from damaged chromatin.
	C1QBP	Stabilize MRE11 and RAD50 proteins; inhibit MRE11 exonuclease activity by preventing its DNA binding.
NBS1, CtIP	BRCA1	Enhance DNA end resection and antagonize 53BP1, RIF1 and the Shieldin complex.
CtIP	EXD2	Functionally interact with MRN to strengthen resection via its 3'-5' exonuclease activity.
	FANCJ	Promote DNA end resection via facilitating the recruitment of CtIP
	AUNIP	Facilitate CtIP accumulation at DSB sites and DNA end resection.

Figure 8. Key interaction partners of the MRN-CtIP complex.

Figure adapted from (32)

1.5.5. Other roles of the MRN complex

Beyond the scope of this thesis, the MRN complex is also involved in the resolution of stressed or broken replication forks, maintenance of the cohesion chromosome complex, telomere elongation,

meiosis, R-loop formation, (28, 67, 68), viral immune response (27, 69) and VDJ and class switch recombination (32, 47, 50).

1.6. DNA Damage Response Pathways

1.6.1. Homologous Recombination.

Tight regulation of HR is required as it can only generally take place during S and G2 phases of the cell cycle when a sister chromatid is present. Initiation without a homologous template can result in the loss of genetic information after unregulated end resection. The MRN complex is thought to be the initial sensor of DSBs as it is one of the first proteins to be recruited to DSB sites (23). It is debatable whether PARP recognises the sites of DSB prior to MRN binding (70). The MRE11-RAD50 head of the MRN complex binds homoduplex DNA and scans the genome via facilitated diffusion along the DNA strand independent of NBS1 (35). This complex recognises the site of DSBs in a time scale of seconds to minutes, along with other proteins such as the Ku complex and PARP (28, 70). One of the main functions of MRN is to activate ATM, a kinase acting as a master regulator of the DSB response and the DDR in general. ATM acts on numerous substrates to promote the DSB response, notably histone 2A which it phosphorylates converting it to 'γH2AX'. This in turn initiates a signal transduction cascade upon chromatin, propagating the signal for efficient recruitment and repair of DSBs. γH2AX leads to the recruitment of MDC1 which gets sequentially ubiquitinated by RNF8 and RNF168 causing 53BP1 to bind to said ubiquitin moieties. This marks the start of the chromatin-based DDR signalling (24). BRCA1 can remove 53BP1 from chromatin and this interaction of 53BP1 and BRCA1 is a control mechanism of pathway choice, regulating the onset of resection (71). 53BP1 has also been shown to regulate the choice between HR and SSA, potentially by limiting hyper-resection (72). Dysregulation of players in this process can affect pathway choice and the DDR as a whole. For example, depletion of RNF8 affects both HR and NHEJ while RNF168 depletion solely affects NHEJ (73). DDR dysregulation is exploited during PARP inhibitor treatment of HR deficient cancers inducing synthetic lethality. In these circumstances DSBs induced by the treatment cannot be repaired using the error free

mechanism of HR, resulting in excess genome instability and death. Interestingly a method of resistance to PARP inhibitors is to downregulate 53BP1, thereby restoring HR (71, 74).

During S and G2 phase of the cell cycle, cyclin-dependent kinases (CDKs), phosphorylate CtIP, DNA2 (a long-range resection factor) and NBS1. These phosphorylation events are thought to be a key regulation step, initiating end resection, and committing the cell to HR. Furthermore, BRCA1 interacts with CtIP and MRN to aid initiation and progression of end resection (75). End resection describes the digestion of one strand of DNA around the DSB site to expose long sections of ssDNA allowing for downstream processes such as homology searching. End resection is a three-strep bidirectional process comprising of initiation, short-range and long-range end resection (Figure 6). MRN completes two of these steps (initiation and short-range resection) via its endo and exonucleic activity respectively and these functions also dictate the bidirectionality of end resection (chapter 1.5.3). The action of MRN facilitates long-range nucleases EXO1 or the DNA2 complex (with the help of WRN/BLM helicases) to complete long-range resection 3' to 5' revealing 3' ssDNA overhangs of around 1 Kilobase. This three-step bidirectional end resection allows HR to repair all types of DSBs (single or double ended, clean, or dirty breaks) and can remove protein blocks from break sites. This is due to the multifunctional nature of the MRN complex which can process complex breaks at slower processivity, leaving the DSB site for long-range factors which can process DNA with faster processivity (76) (Figures 6 and 9).

To prevent unwanted digestion, binding, and formation of ssDNA secondary structures, replication protein A (RPA) binds the naked ssDNA formed after end resection. RPA also acts to recruit and activate the ATR pathway which phosphorylates substrates involved in DDR pathways (77). Subsequently, BRCA2 mediates the exchange of RPA to Rad51 that forms a nucleofilament which marks a key step in HR, where homologous searching results in downstream DNA pairing and strand invasion (29). Homologous search occurs after the nucleofilament probes multiple sequences and finds a homologous sequence with 7nt or more (47). Once a homologous sequence has been found a

displacement loop (D-loop) forms with the lesion strand invading the template strand. This is termed strand invasion (Figure 9). Rad51 activity is dictated by a number of factors. Much of this regulation is thought to be mediated via regulating Rad51 ATP binding and hydrolysis which effects Rad51 affinity for ssDNA (47). Annealing then occurs in the formed D-loop, Rad51 is removed by Rad54 and the remaining ssDNA from the sister template strand is used to fill in the resected and potentially missing bases using DNA polymerase δ or ε. DNA synthesis in HR is more error-prone than in DNA replication thought to be due to limited DNA mis-match repair capabilities of the DNA polymerases used during

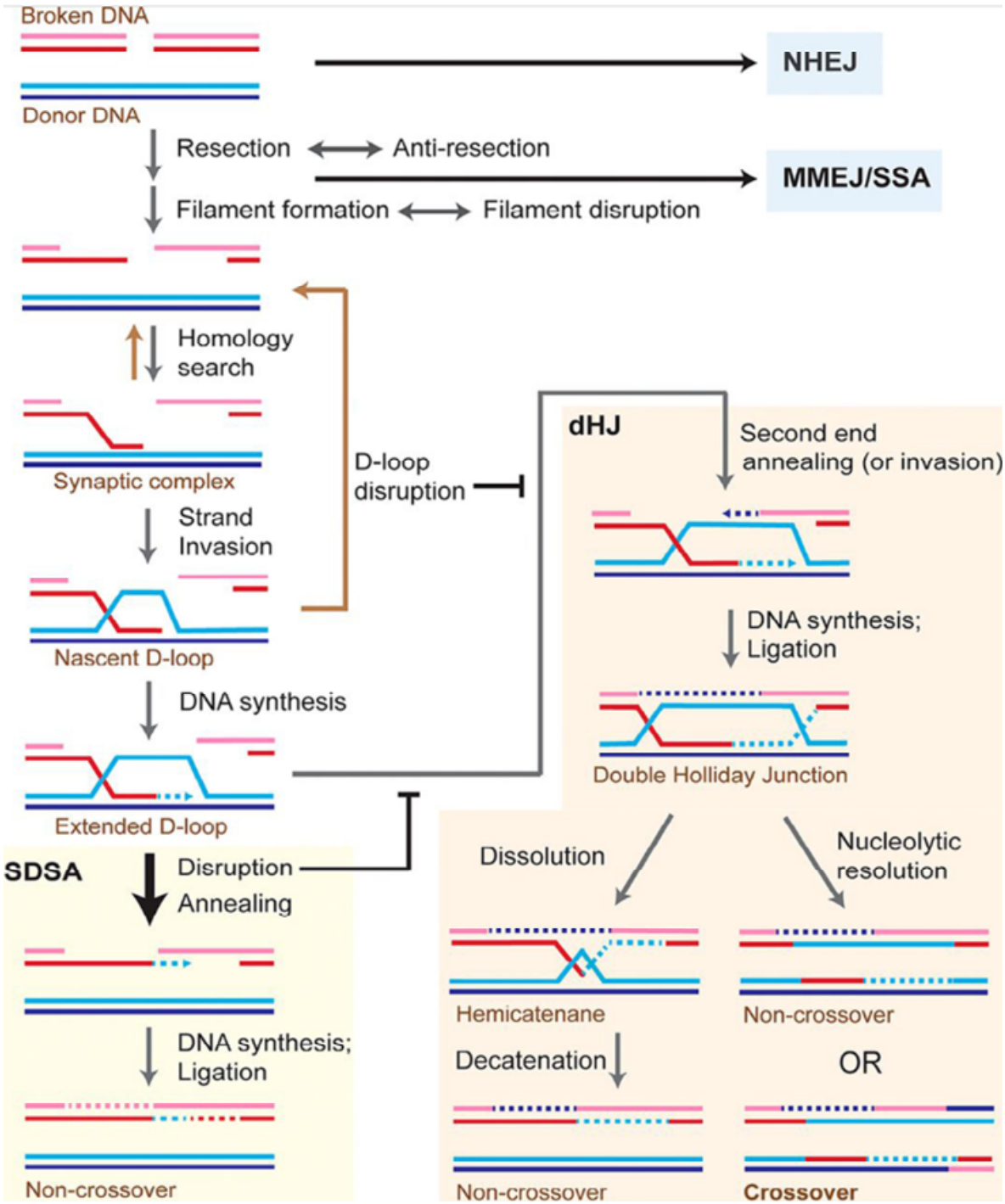


Figure 9. DSB pathways with a focus on regulation of double ended HR sub-pathways and resolution.

DSB can be repaired by non-homologous end joining without resection occurring, microhomology mediated end joining or alternative NHEJ require varied amounts of resection and preceded Rad51 nucleofilament formation. Nucleofilament/filament formation results in homology search and if successful formation of a synaptic complex and invades the template strand in strand invasion. This results in D-loop formation and subsequent extension. Most extended D-loops are disrupted resulting in annealing of the original break and repair via DNA synthesis and ligation, resulting in a non-crossover, this is called synthesis-dependent strand annealing (SDSA). If the D-loop is not disrupted the second end of the DSB anneals forming a stable D-loop which formed a double holiday junction after DNA synthesis and ligation. The holiday junction can be dissolved resulting in non-crossover events or resolved by nucleolytic digestion resulting in either crossover or non-

crossover events. To note break induced replication (BIR) where single ended breaks are repaired, shown in Figure 7. Figure adapted from (78)

HR synthesis (47). Once DNA synthesis starts, different HR resolutions can be formed these are; synthesis-dependent strand annealing (SDSA), holiday junction (HJ) pathway, and break-induced replication (BIR) (Figure 9 and 10) (79). As highlighted in figure 9 the formation, stability, length, and type of D-loop effects the outcome of repair, with different sub-pathways possible.

SDSA is the most common type of resolution of the D-loop (78) and occurs via disassembly of the extended D-loop before HJ formation. The 3' overhang is extended in the D-loop, the D-loop then gets disrupted after complete elongation occurs. The extended strand then forms a complementary complex with the other side of the double ended break and acts as a template for the other strand on the broken DNA. DNA synthesis and ligation completes this process. This results in a non-crossover event as the genetic material is maintained.

The other resolution of doubled ended HR occurs via HJ formation. The D-loop migrates along the template DNA as DNA synthesis elongation of the 3' overhang occurs. This continues until the overhang is extended to meet the other side of the DSB which is used as a template for the other strand for repair. Therefore, both strands of the template DNA are used to fill in the resected sequence and repair the break. The holiday junction can be resolved by nucleases causing a crossover or non-crossover event or may simply be dissolved causing a non-crossover event (figure 9). A crossover events describes the exchange of genetic material between complementary DNA strands. Holiday junction dissolving occurs when the strands migrate towards the centre point of the HJ and 'untangle' causing a non-crossover event (47, 79). Dissolution using 'dissolvasome' is preferred by cells after HJ formation due to the limit of crossover events (47).

BIR is used during one sided DSBs which often arise from replication fork collapse after the replisome encounters a lesion e.g., an SSB. BIR is similar to SDSA as one strand gets extended after D loop formation which is then used to extend the other, although there is no complementary meeting with the other side of the DSB as it is a one-sided DSB (Figure 10). This pathway is also used in telomer

lengthening where one strand gets elongated until the end of the template and the other pair is extended with it. This only occurs during single ended DSB due to the increased mutational burden of this pathway compared to those pathways reliant on double ended breaks (79).

These processes are often mutagenically silent. However, ectopic crossover exchanges of non-identical template sequences e.g., repetitive sequences, can result in genomic rearrangements and potential instability. Furthermore, if the template has slight allelic variation, incorrect genetic information can be transferred potentially resulting in a loss of heterozygosity. Therefore, HR is not completely 'error-free' due to the fidelity of the DNA polymerase and crossover events of non-identical information (80).

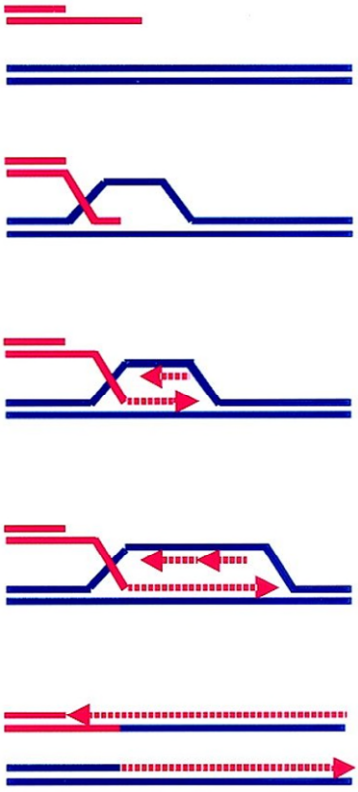


Figure 10. Schematic of break-induced replication of single ended double-strand breaks.

A sub-pathway of Homologous recombination. A single ended break is respected by end resection machinery and subsequent nucleofilament, homology search and strand invasion. A D-loop is formed during strand invasion where subsequent elongation occurs of the invading strand. The invading strand is then used as a template for the resected strand where DNA synthesis and ligation occurs. Figure adapted from (81)

In situations where a D-loop is not formed SSA can occur (Figure 9) where the 3' overhang forms a complementary pair with a homologous sequence and ligation occurs. This process, however, is highly error prone as it may result in large deletions.

Of academic and medical interest, HR is also used in genomic editing where precise DSBs are induced via CRISPR or other methods, and a homologous sequence can be introduced resulting in the insertion/alteration of a sequence of interest (70). Increasing the propensity towards certain pathways may aid in knock in/out technologies. This is often completed by using pathway inhibitors or cell-cycle regulators (82).

1.6.2. Non-Homologous End Joining

Canonical NHEJ describes a pathway in which DSB ends are ligated together after minimal processing. NHEJ can only be used during double ended breaks i.e., not after replication induced DSBs. Dirty breaks may also inhibit the direct ligation as processing may be required and therefore clean breaks are the more likely to be repaired by NHEJ (Figure 11). Another type of NHEJ termed alternative or microhomology mediated end joining (MMEJ). MMEJ as the name suggests uses a small homologous region to directly ligate DSB. It is similar to SSA, but smaller homologous sequences are required and is thought to be resection independent. Recent evidence suggests that there are two defined kinetic types of canonical NHEJ, one is a "fast-kinetic" NHEJ where no/minimal processing is needed and repair is almost immediate and the other, more widely studied is "slow-kinetic" NHEJ where processing is required which is discussed below and is illustrated in figure 4 (70). The Ku complex (Ku70 and 80 heterodimer) is synonymous with NHEJ, where it binds and maintains DNA ends and regulates downstream recruitment of the pathway. The Ku complex forms a ring like structure around the DSB DNA ends to protect them from degradation and recruits other proteins to the site of damage (63). DNA-PKcs are one of the first proteins to be recruited by the Ku complex forming an active complex that can bridge broken ends (Figure 4). Further factors such as Artemis, DNA polymerases (μ and λ), X-ray cross-complementing protein 4 (XRCC4), DNA ligase 4 and others are then recruited to the complex (70). Artemis is a nuclease that processes 3' overhangs then DNA polymerases (μ and λ) perform strand filling if overhangs are present. The MRN complex is also thought to play a role in NHEJ although its role is not completely understood. Current evidence suggests that it performs more of a facilitating role via its signalling and DNA bridging capabilities (83). The break type and DNA processing gives rise to the possibility of introducing errors, hence NHEJ is labelled as an error prone repair mechanism. NHEJ is used in genomic editing where it induces frameshifts after end processing resulting in the target gene dysfunctionality, 'knocking out' the gene.

1.6.3. Pathway Choice with a focus on the MRN Complex

Pathway choice describes the regulation of DDR machinery to 'decide' which pathway to use to repair lesions. The type and cellular context of the break dictates pathway choice (Figure 11). The key process mediating the crossroad between the main two DSB pathways, HR and NHEJ, is end resection, either minimal, in NHEJ or extensive, in HR. The context of the break i.e., single or double ended, as well as the type of break i.e., clean or dirty, simple or complex also dictates which pathway may be chosen. Resection is also regulated by the cell cycle via CDKs phosphorylating multiple substrates such as CtIP and DNA2 which promotes HR (84). CDK phosphorylation activates the MRN complex resection capabilities which reveals ssDNA and removes the Ku complex from DNA ends (85). The axis between Ku and MRN complex retention is thought to be a key identifier between the two pathways. MRN complex activity seems to not only control the balance between HR and NHEJ, but also HR and SSA. Shown by excessive retention of MRN causing increased usage of SSA (15). Therefore, the MRN complex activity has to be tightly regulated as dysregulation could result in an increase in error prone DSB pathways.

This shows regulation of end resection is vital to pathway choice, and with the MRN complex role as a key resection factor understanding how it is regulated is vital to understand this biology. We aim to increase this understanding by elucidating how MRN complex disassembly is regulated. Therefore, gaining insight into the balance between HR and NHEJ, SSA and other pathways.

As alluded to in a previous section (1.6.1) other key proteins are involved in pathway choice. Such as 53BP1 and BRCA1 who function in DSB response signalling, their respective actions counteract each other as negative regulators. Simplistically the Shieldin complex and other proteins act to maintain 53BP1 to promote NHEJ, whilst BRCA1 removes 53BP1 promoting HR (71). CDK dependent CtIP phosphorylation induces formation of a BRCA1-MRN-CtIP complex, which removes 53BP1. Although the complete mechanism of 53BP1 and BRCA1 interplay is unclear (71, 75).

Another process that impacts pathway choice includes chromatin compaction, which also impacts repair kinetics. Simplistically, in euchromatin or highly active/transcribed regions of DNA NHEJ is used while in HR heterochromatin is used, heterochromatin often needs remodelling or re-localisation for HR to be completed (21, 86) (Figure 11). Cell type/tissue context also impacts pathway choice. For example, differentiated cells do not re-enter the cell cycle therefore HR is not possible (82). Furthermore, disease states e.g., cancer or ageing may have different pathway choices which may cause or worsen a phenotype, typified by certain genetic deficiencies resulting in premature ageing and cancer (7). Cancer cells have dependencies on particular repair pathways and cell cycle dysregulation, therefore, resulting in abnormal pathway choice and potential therapeutic targets (22). One study found a relative decline in HR usage during replicative ageing, suggesting a reliance on other pathways such as NHEJ, although others have showed that both pathways are downregulated during ageing and result in genome instability (87, 88). It is tempting to speculate this may be a pathway of cancer formation and a reason for age associated cancer rates.

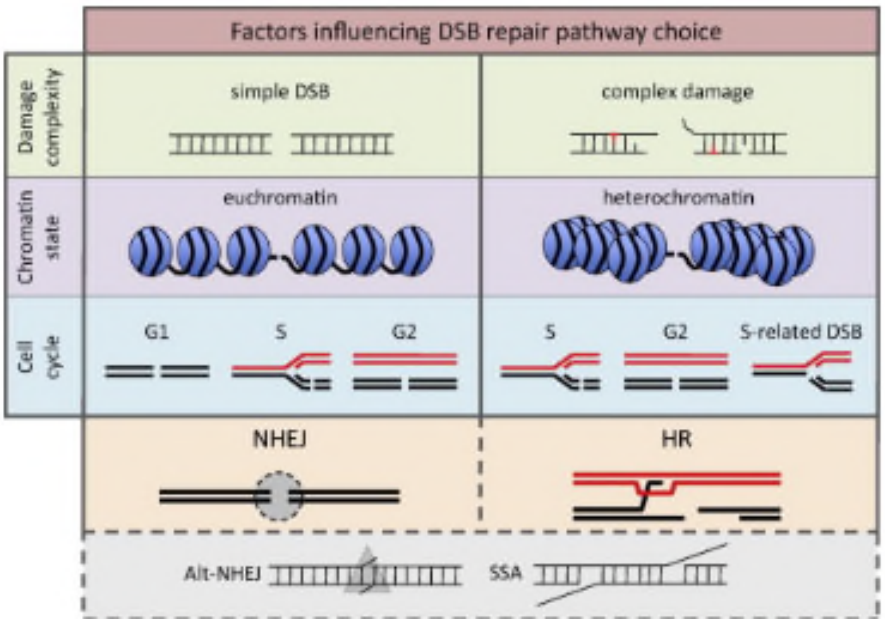


Figure 11. Factors effecting pathway choice after IR.

Damage complexity, chromatin state and cell cycle stage are thought to be the main large factors regulating pathway choice between non-homologous end joining and homologous recombination. Complex damage, heterochromatic regions, and damage in S and G2 phase are more likely to be repaired by HR whereas the opposite is true for NHEJ. Further factors influence the potential for alternative pathways such as Alternative-NHEJ and single strand annealing. Figure adapted from (13)

These outlined above are likely not complete as we still do not understand completely the intricacies of the temporal and special regulation of each pathway and how they interact with one another. For example, the simplistic model of the MRN and Ku complex symbolising HR versus NHEJ likely is not

true, a more intricate crosstalk occurs between the proteins is more feasible (89). Furthermore, other macromolecular structures have an emerging role in pathway choice for example R loops have been implicated in HR, mechanistically having been suggested to be involved in 3' overhang protection (68). Therefore, there are multiple questions that remain to untangle the DSB response and HR. Of interest to this project is how physiological resection is limited, in particular how the MRN complex is removed from DSB sites (85, 90).

1.7. HR and the MRN complex Role in Tumourigenesis and Treatment Outcomes

Given the importance of the MRN complex in a number of cellular processes it is of no surprise that issues with the MRN complex can cause disease. Genetic knockout of the MRN complex is embryonic lethal (91, 92). Conditions in human disease involving HR include ATM mutations which cause ataxia-telangiectasia (AT) disorder, MRE11 mutations cause a similar phenotype termed AT-like disorder (ATLD), NBS1 mutations cause Nijmegen breakage syndrome (NBS) and RAD50 mutations cause a similar phenotype to NBS. Other HR factors also have their respective syndromes associated with them (53). These diseases have a number of clinical features such as abnormal eye movement, growth retardation and immunodeficiency thought to be caused by HR abnormalities. Furthermore, as genome instability is a hallmark of cancer HR abnormalities such as MRN alterations are associated with multiple cancer types (30, 93). Overexpression and mutation of MRN complex subunits is often associated with poor survival, typified by their presence on a panel of breast and ovarian cancer candidate genes (30, 94, 95). Figure 12 highlights the MRN complex role in cancer formation (30).

Paradoxically HR and the MRN complex is not only involved in cancer formation but also targeted in cancer treatment. This is due to the reliance of cancer cells on certain DDR pathways. Genetic and cell cycle dysregulation as well as increased reliance on DDR pathways (caused by an increase in metabolism and growth rates damaging DNA) can sensitise cancer cells to agents targeting the DDR. For example, PARP inhibitors are used in cases of BRCA mutation positive cancers, inducing synthetic lethality. Other HR deficiencies are used as biomarkers to predict PARP inhibitor sensitivity (96). As

the MRN complex is involved in the repair of DNA induced by so many anti-cancer drugs e.g., radiotherapy, topoisomerase inhibitors, platinum agents, PARP inhibitors etc., it seems logical that it would have a role in a pathway of resistance or as a synthetically lethal agent (30). Therefore, the MRN complex has been postulated as a therapeutic target for first line and refractive cancer treatment as it seems to be upregulated in cancer and cases of radio-resistance (30, 94). Therefore, the MRN complex is important in both cancer formation and treatment.

Knowledge of viruses modulating the MRN complex' level via post-translational modifications like SUMOylation and ubiquitination (69, 94) has been used to create an oncolytic virus called Telomelysin which targets the MRN complex. Six undergoing/planned clinical trials of Telomelysin are being completed (97) as a radiosensitiser in head, neck, oesophageal and non-small cell lung cancers (98, 99) (summary website). The mechanism of action is induced by the viral protein E1B55K which binds the MRN complex and degrades the complex, therefore preventing HR and ATM activation. The use of Telomelysin aims to use PTMs to dysregulate the MRN complex and therefore the DDR, causing toxicity disproportionately to cancer cells in combination to radiotherapy.

Causing trapping on chromatin has proven to be a viable strategy for cancer treatment. For example, PARP and topoisomerase inhibitors induce trapping which inhibits their functions and causes replication stress resulting in further damage. A similar mechanism could be induced if MRN complex disassembly is inhibited, trapping the complex on chromatin. Furthermore, the excess resection and SSA upregulation phenotype could cause further toxicity.

Taken together, the study of the MRN complex is of vital academic and clinical interest. Studying the mechanism of hypothesised PTM dependent MRN complex disassembly may provide mechanistic details aiding the general understanding of MRN and DDR biology as well as drug discovery.

Cancer type	Molecules	Results
B cell lymphoma	MRE11	x MRE11 promotes tumorigenesis by facilitating resistance to replication stress.
Breast Cancer	MRN	✓ MRE11, RAD50 and NBS1 were genes with moderate penetrance.
	MRN	✓Mutations in MRN contribute to increased cancer risk.
		x MRN complex genes did not confer any appreciable risks.
	MRE11	✓ Defect in MRE11 function promotes progression of mammary hyperplasia into invasive, metastatic cancer.
		✓ MRE11 variant was associated with increased risk of breast cancer.
	MRE11, RAD50	✓ MRE11 and RAD50 were moderate-susceptibility genes for breast cancer.
	MRE11	x Variants of MRE11 gene did not constitute a risk factor.
	NBS1	✓ NBS1 variant 923T>C might be a risk factor for breast cancer development.
Burkitt lymphoma	RAD50	✓ RAD50 mutations were identified in Burkitt lymphoma.
Endometrial carcinoma	RAD50	✓ RAD50 mutation was frequently detected.
Gastric cancer	MRE11	✓ Low expression of MRE11 was associated with gastric cancer.
Glioma	MRE11, NBS1	✓ NBS1 and MRE11 variants were associated with increased risk
HBOC	MRN	✓ MRN mutations were detected in HBOC patients.
	RAD50	✓ Mutations in RAD50 was implicated in cancer predisposition.
Hepatic carcinoma	MRE11	✓ Expression of MRE11 was lower in chemical reagent induced hepatic carcinoma.
	RAD50	✓ Mutations in RAD50 lead to liver tumorigenesis.
IHC	NBS1	✓ NBS1 variants were associated with cancer susceptibility for IHC.
Lung cancer	NBS1	✓ Variants of NBS1 were related with increased risk for lung cancer.
		✓ Functional polymorphisms of NBS1 were related with increased risk for lung cancer.
Myeloid leukaemia	RAD50	✓ Alteration of RAD50 was found in myeloid leukaemia.
Neuroblastoma	MRE11	✓ Alterations in MRE11 was frequent in neuroblastoma.
NPC	NBS1	✓ Polymorphism of NBS1 is associated with development and status of NPC.
Ovarian Cancer	MRN	✓ Lack of MRN detection occurred frequently in ovarian cancer.
	MRE11, RAD50	✓ Pathogenic or likely pathogenic variants were detected in patients.

	MRE11	✓ Low expression of MRE11 was associated with cancer developments.
	RAD50	x RAD50 was ruled out as a risk factor.
Prostate cancer	NBS1	✓ Variants of NBS1 were prevalent in familial prostate cancer.
Renal cell carcinoma	NBS1	✓ Mutation in NBS1 functional domains was related with susceptibility to renal cell carcinoma.

Tabular Figure 12. Investigation of MRN complex alterations involvement in tumourigenesis and progression.

Figure adapted from (30)

1.8. DSB PTMs with a Focus on the MRN Complex

Post translational modifications are a vital control mechanism of multiple cellular processes. DSB pathways are no different, here known PTMs of the MRN complex will be outlined to review the current knowledge since MRN complex disassembly is thought to be PTM dependent.

Multiple databases and mass spectrometry analyses highlight potential PTM sites on the MRN complex, some of which have been validated which will be outlined below, although most remain to be elucidated (95, 100-104). Furthermore, a number of PTM associated proteins are reported to be within the MRN interactome from online databases and mass spectrometry studies (105-108). With the hypothesis that PTMs play a vital role in MRN complex disassembly it is important to investigate this area.

1.8.1. Phosphorylation

Phosphorylation describes the addition of a phosphate group to protein substrates catalysed by kinases. Like all PTMs phosphorylation alters the protein's structure or charge therefore modulating its function. Phosphorylation can occur on multiple different amino acid residues. Phosphate groups can be removed by dephosphorylating enzymes (109). Phosphorylation plays an important role in signal transduction within the DDR, involving the MRN complex and its interactors. CDKs, ATM and ATR are common kinases that add phosphate groups to substrates in the DDR. Each of the MRN protein subunits are substrates of ATM (34) and also induce activation of ATM (via inducing ATM dimers to form monomers) in a feedback loop (34). Phosphorylation of the MRN complex has a number of roles from promoting assembly, DNA binding and resection to facilitating MRN complex

disassembly (32, 95). For example, phosphorylation promotes disassembly of the MRC complex made of MRE11, RAD50 and C1QBP which facilitates MRNs assembly and function (39). Opposingly phosphorylation of certain residues on MRE11 promote disassembly (52). This can occur indirectly e.g., phosphorylation of UBQLN4, a proteasomal ubiquitin shuttle factor or directly via altering the affinity of the MRN complex for DNA (95). Inability of ATM to phosphorylate serine resides 676 and 678 results in MRE11 accumulation on chromatin, excess end resection, HR deficiency and SSA preference. Therefore, this mechanism is likely involved in MRN complex disassembly (52). PIKK1 phosphorylates MRE11 and impairs DNA tethering and its end resection role (62). VRK1 phosphorylation was found to protect NBS1 from ubiquitin mediated proteasomal degradation (proposed to be by RNF8) therefore promoting HR (110). ATM and CDKs also phosphorylates CtIP which marks one of the early determining steps of HR, initiating end resection via MRN-CtIP endo-nucleic digestion around the DSB site.

1.8.2. Methylation

Methylation occurs predominantly on lysine and arginine residues where a methyl group is covalently attached to nitrogen atoms by arginine/lysine methyltransferases which can be removed by demethylases (109). MRE11 is reported to be methylated on arginine in its conserved Glycine/arginine rich (GAR) motif, which if absent, decreased HR efficiency and renders cells sensitive to IR (111). This modification seems to affect the exonuclease ability of the protein but not the assembly into the MRN complex (95). Furthermore, proteins that regulate the methyltransferase PRMT1 such as USP11 (112), GFI1 (113) have been reported to regulate DNA end resection aiding in its proper initiation. The precise mechanism of how methylation regulates the MRN complex is not known.

1.8.3. Ubiquitination

Ubiquitination is a reversible process with numerous functions, generally thought to be related to protein degradation although is often part of signalling and recruitment cascades. Ubiquitin moieties can be added to lysine residues or terminal glycine residues via iso-peptide bonds, although recently

additions on other residues e.g., cysteines have been shown to be possible forming different bonds e.g., thioester (114). Chains can be formed by adding further ubiquitin molecules to lysine's on the accepting ubiquitin, termed polyubiquitination. Different chains have been associated with different biological processes e.g., K48 chains are associated with proteasomal degradation while K63 chains are associated with cellular signalling. Branched chains can also be formed with different types of linkages. Different chain types result in structural diversity which can be recognised by proteins, carrying different ubiquitin interacting domains, giving specificity and function to certain chain types. A cascade of enzymes catalyses the addition of ubiquitin with E1 enzymes activating ubiquitin, E2 enzyme conjugating ubiquitin and E3 ligating it to the substrate. There are 2 E1 enzymes, 30-50 E2 enzymes and over 600 E3 ligases (115). There are four types of E3 ligases: RING-finger, RING-in-Between-RING (RBR), U-box, and HECT type. These types have low sequence homology and have different mechanisms of action although are functionally similar. Simplistically, HECT and RBR type directly transfer the ubiquitin residue to substrates from their catalytically active cysteine residue whereas RING and U-box facilitate the addition of ubiquitin directly from the E2 enzyme (116). Furthermore, there is a class of enzymes known as E4 ligases which kinetically enhance the action of E3 ligases to upregulate their catalytic activity. For example, UBE4A is an E4 ligase that modifies the ubiquitination status at DSB and facilitates repair. Deubiquitinating enzymes (DUBs) can remove the ubiquitin residues added in these cascades (117).

Ubiquitination is shown to be vital in the DDR (104). The E3 ligases RNF8 and RNF168 must be mentioned when talking about ubiquitination in the DDR, they play an important role in the DDR chromatin signalling. RNF168 mutations can cause RIDDLE syndrome which have DDR dysregulation. Removal of these factors increase genomic instability and regulate pathway choice (118). Multiple other E3/4 ligases have been implicated in regulating multiple components of the DSB response and HR such as SKP2 and UBE4A (7, 119).

All three subunits of the MRN complex have been shown to be ubiquitinated by high throughput studies (103, 120). Although mechanistic detail has only been shown in MRE11 and NBS1 ubiquitination. There is a lack of clarity how these processes interplay with one another and the factors involved.

MRE11 is ubiquitinated by an unknown E3 ligase, subsequently a proteasomal ubiquitin shuttle factor UBQLN4 directs ubiquitinated MRE11 it to the proteasome. Without UBQLN4 excessive end resection initiation occurs therefore it is questioned whether it is involved in MRN complex disassembly. This process reduces the nuclear pool of MRE11 promoting NHEJ, rendering sensitivity to PARP inhibitors (56). UBQLN4 overexpression can lead to cisplatin (cross-linking agent) resistance in oesophageal squamous cancer by regulating MRE11 level (55).

Rad18 knockout sensitised osteosarcoma cell lines to doxorubicin (topoisomerase inhibitor), identified in a genome wide CRISPR screen. Rad18 sensitivity was shown to be mediated via its interaction with MRE11 where it promoted MRN complex formation (121), furthermore NBS1 has been shown to interact with Rad18 (122).

P97 introduced in the section 1.9 has been shown to interact with all of the components of the MRN complex (15) in a dynamic manner (Appendix 34-36). p97 interaction is bridged by a cofactor which recognises ubiquitinated or SUMOylated substrates. Without p97 MRE11 accumulates on chromatin causing excessive end resection and a switch to SSA. P97 mediated MRN disassembly does not affect the total levels of MRN indicating p97 does not direct the MRN complex for degradation in the proteosome, but just recycles and disassembles the MRN complex from chromatin. This is similar to p97s mechanism of action with other nuclear proteins (123, 124). p97 levels do not affect end resection initiation therefore ubiquitination is thought to play a role downstream of end resection. It is unknown which PTM, cofactor and E3 ligase mediate these reactions which is aimed to be identified in future work.

cIAP2 has been shown to ubiquitinate truncated MRE11 in bladder cancer after HDAC inhibition which increases its turnover (125). NBS1 has shown to be ubiquitinated by multiple E3 ligases although the spatiotemporal information of these modifications has not been completely elucidated. Skp2 adds K63 chains which enhances the NBS1-ATM interaction (126) (Figure 13). Skp2 is also associated with MRN complex disassembly in RecQL4 deficient cells, which can be rescued by Usp28 overexpression, although K48 chains are associated here, not K63 as above (127). A feedback loop between BRCA1, ATM, Skp2 and NBS1 has been suggested (128). Skp2 is phosphorylated by CK2 after IR, which induces NBS1 K63 ubiquitination. NBS1 then activates ATM highlighting one mechanism how ATM is activated by the MRN complex (126) (Figure 13). Another paper found BRCA1 phosphorylation is vital for this SKP2-NBS1 dependent ATM activation. BRCA1 interacts with SKP2 and without ATM dependent phosphorylation of BRCA1, SKP2 recruitment is not efficient to DSB sites. Therefore, neither is the NBS1-ATM interaction, highlighting a feedback mechanism to control ATM activation and end resection (128). Furthermore, elevated SKP2, ATM and NBS1 ubiquitination offers cisplatin resistance (129). Pellino1 ubiquitinates NBS1 in an ATM and γH2AX dependent manner which promotes DSB repair (130) (Figure 13). RNF8 has been shown to ubiquitinate NBS1 which promoted HR (43) although its action has also been shown to mediate the degradation of NBS1 if NBS1 is not protected by VRK1 phosphorylation. ATM activity is also modulated via PPARγ bridging an interaction with the MRN complex and E3 ligase UBR5, which in turn ubiquities ATMIN (ATM interacting protein) which de-sequesters ATM allowing activation (131, 132) (Figure 13).

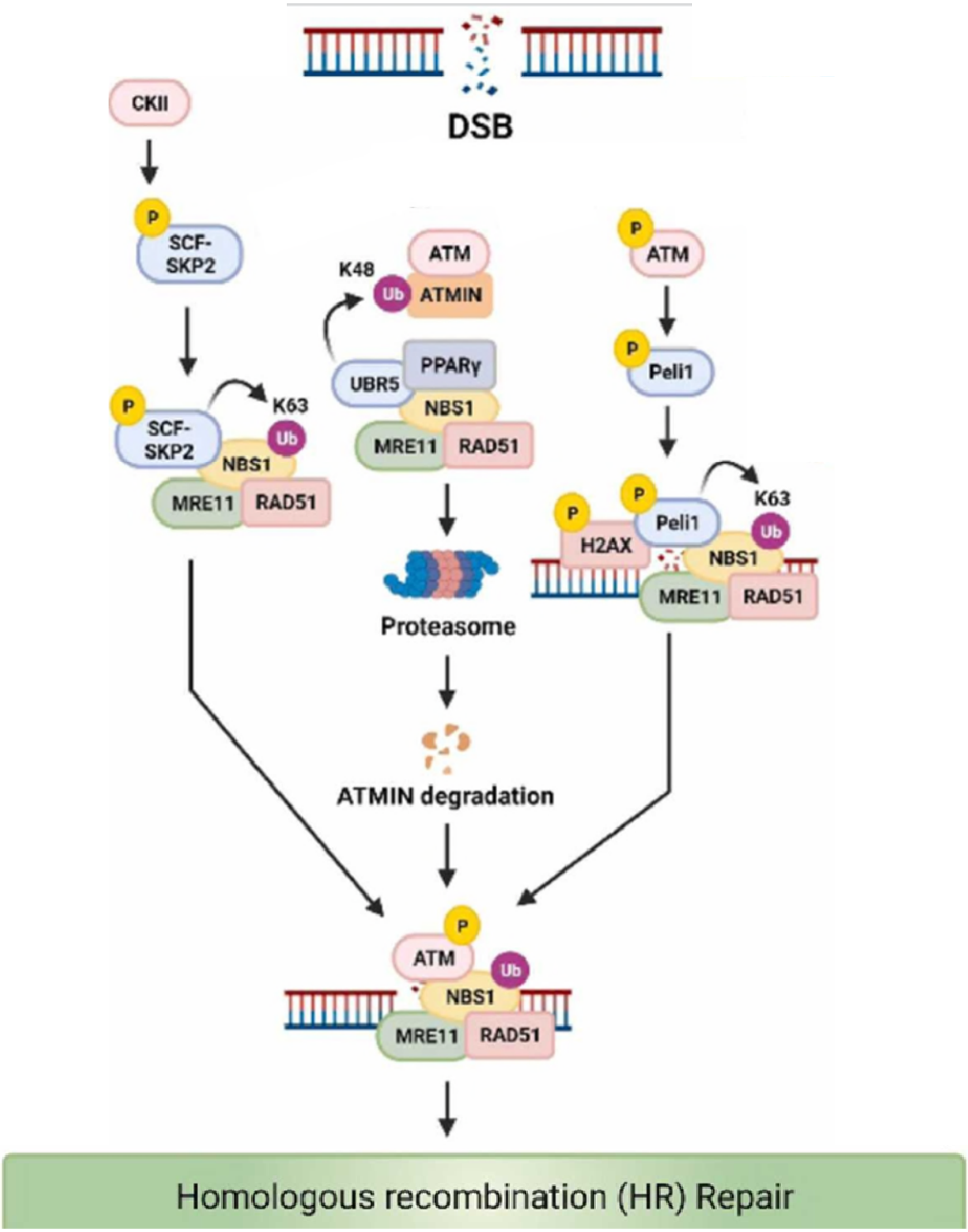


Figure 13. Schematic of known E3 ligase's role in HR.

The role of SKP2, UBR5 and Peli1 E3 ubiquitin ligases are outlined which regulate the MRN complex and therefore homologous recombination. CKII activated SKP2 adds K63 chains to NBS1 which aids in MRN complex assembly. UBR5 complexes with PPARγ and the MRN complex which results in adding K48 chains to ATMIN causing its degradation and proper ATM signalling. ATM activated Peli1 ubiquitinates NBS1 in a γH2AX dependent manner, adding K63 chains which increases MRN complex assembly. Figure adapted from (133)

Deubiquitinating enzymes such as USP4, USP7 and USP52 have also been shown to interact with the MRN complex and are thought to modulate MRN interactomics. Although these may alter the function

of MRN chromatin associated role rather than its resection role (41, 42, 117, 134, 135). USP28 was shown to protect MRN from degradation (127). USP7 was shown to be in a complex with MRN and MDC1 (135). USP7 interacts with RECQL4 to protect it from UBE20 mediated degradation (127, 136). RECQL4 is thought to protect the MRN complex from degradation therefore this could control the MRN complex concentration. Other vital proteins involved in the DDR and HR have also been shown to be ubiquitinated such as CtIP and Exo1 (117).

As previously outlined viruses seem to regulate MRN complex levels via modulating ubiquitination and SUMOylation processes, which has been exploited to therapeutic value (69, 97, 98, 137, 138).

1.8.4. SUMOylation

SUMO (Small ubiquitin like modifier)ylation, as the name indicates is a ubiquitin like modifier which attachment follows a similar pathway as ubiquitin with E1, 2 and 3 enzymes although the diversity of enzymes is smaller (139). SUMO has 4 genes SUMO 1-4, SUMO1-3 have been implicated in the DSB response (140), furthermore E3 SUMO ligases PIAS1 and PIAS4 have also been implicated as vital in the DSB response (141). SUMO 2-4 share a high degree of similarity, SUMO 1 shares about 50% sequence homology (142). SUMO 4 is missing a residue required for covalent interaction therefore is not attached to substrates (143). SUMO2/3 have similar function and are often grouped together whereas SUMO1 function is separate. Of interest SUMOylation can be completed ‘on-site’ where SUMOylation only occurs when the substrate is bound to DNA, this is of interest in the DDR response especially in the case of the MRN complex disassembly (144). All components of the MRN complex have been shown to be SUMOylated by high-throughput studies (102, 145) but only MRE11 SUMOylation has been studied in a mammalian system in the context of the DSBs.

MRX (MRN yeast homolog), long-range resection and subsequent ssDNA formation has been shown to cause a “global SUMO response”. This response induces SUMOylation of numerous DDR proteins which increases the efficiency of multiple pathways including HR (95, 104, 146, 147). MRE11 has been

shown to be one of these substrates where SUMOylation is important for MRX formation (148). MRE11 has multiple SUMO-interacting motifs which could be important for this process (149).

MRE11 and RAD50 SUMOylation increases after DSBs, while NBS1 SUMOylation decreases (58). MRE11 SUMOylation is STUbL independent and found on chromatin. PIAS1 dependent SUMOylation protects MRE11 from ubiquitin mediated degradation while deSUMOylation by SENP3 facilitates MRE11 degradation (58). Furthermore, this interaction between PIAS1 and MRE11 seemed to be increased by the presence of 3' ssDNA overhangs indicating it occurs after resection and possibility mediates disassembly. Interestingly there were opposing results for different components of the MRN complex. NBS1 SUMOylation decreases upon DSBs. RAD50 SUMOylation increased after DSB as well as upon RNF4 depletion implying that RAD50 may be regulated in a STUbL dependent manner (58). Furthermore, RNF4 interactomics via mass spectrometry also identified RAD50 as a substrate (59). P97 has been shown to act with RNF4 to extract multiple chromatin-associated proteins (150). The knowledge that independent mass spectrometry results have implicated that RNF4 and p97 are respectively associated with RAD50 could be interesting to explore in the future (15, 59, 150).

Taken together this may imply different roles and disassembly mechanisms for each protein in the MRN complex.

Multiple DDR proteins have been shown to be degraded in a STUbL mediated manner such as BRCA1, BARD1, DNA2 and CtIP, and as highlighted above potentially RAD50 (58, 59). CtIP and DNA2 SUMOylation could control the extent of DNA end resection (151).

MRE11 and NBS1 have been shown to be SUMOylated and subsequently degraded via the ubiquitin proteasome system by viral proteins (137, 138).

1.8.5. Other PTMs

NBS1 is hyperacetylated which may function in PTM competition and crosstalk as deacetylation by SIRT1 allows NBS1 to be phosphorylated (152). MRE11 has been shown to be UFMylated which

increases MRN recruitment to DSB, increases ATM interaction (153) and is involved in MRN recruitment to telomeres (154). PARP chains have been linked to initial DSB response at fast kinetics providing a scaffold for further assembly (23). Recently 'MARylation' (the addition of a single ADP-ribose due to the enzyme PARK14 unable to catalyse polymerase reactions) may be involved in MRE11 regulation as PARK14 has been shown to interact with MRE11 and regulate its activity (155). Addition of a glutathione residue to NBS1 promoted the nuclear localisation of the MRN complex and prevents its Skp-2 dependent degradation (156). The MRN complex was also shown to be modified by UBL5 (ubiquitin like protein 5) in a mass spec screen (157).

1.8.6. CtIP

CtIP is an indispensable co-factor when talking about the MRN complex and end resection. CtIP is extensively modified by numerous PTMs (32), some of which highlighted above. ATM dependent phosphorylation of CtIP results in PIAS4 SUMOylation, inducing STUbL dependent ubiquitin mediated degradation. Deregulation of this pathway results in excess end resection in a similar manner to the phenotype caused by MRN dysregulation by p97 inhibition (64).These PTMs could be a key regulation step of end resection and therefore pathway choice by regulating CtIP interaction with the MRN complex (104, 158). Although, despite CtIP regulating end resection initiation it is not clear if regulation of CtIP would also regulate end resection termination and MRN disassembly.

1.8.7. PTM Crosstalk and Overview

There is a proposed a sequential order to PTMs at DSB sites from PARylation initiating the signalling, to phosphorylation propagating the signal and SUMO and ubiquitin regulating the recruitment and turnover of later stages (109). There is also a complex network of crosstalk occurring amongst PTMs potentially regulating this proposed 'order', with examples including STUbLs and phospho-degrons/phospho-guided ubiquitination (159). Although there are rarely hard and fast rules with PTM occurring at different orders and signals having differential effects, promoting, or demoting a pathway. For example, SUMO protecting a substrate from ubiquitin mediated degradation compared

to STUbLs or phosphorylation activating proteins compared to phospho-degrons. ATM dependent phosphorylation of MRE11 may be a phospho-degron signal recruiting other factors such as E3 ligases and p97, mediating its degradation/removal from chromatin (52).

Further complexity is added to PTM regulation by branched chains and PTM residues themselves being modified e.g., phosphorylation of Ub chains (142). Therefore, fine-tuned study is needed to partition the spatiotemporal regulation of these processes as well as having a holistic view to see how these PTM may interplay.

As highlighted, there are multiple other PTMs identified by mass spec methods whose roles are yet to be completely elucidated. Furthermore, there a number of PTMs that are understudied in the DDR such as Neddylation, ISGylation and numerous others. Therefore, the study of PTMs in the context of MRN regulation is of interest and added clarity is needed.

1.9. p97 in Genome Stability

p97 (also known as VCP and Cdc48 in other taxa) is an evolutionary conserved AAA-type ATPase. It is known as a segregase or an unfoldase where it extracts proteins substrates generally from large complexes e.g., multimeric protein complexes, or difficult to access regions such as membranes for recycling or degradation. It is a vital part of the ubiquitin-proteasome system (UPS) as it recognises ubiquitinated substrates and aids in the extraction and shuttling of substrates to the proteasome for degradation (Figure 14). Most of p97 substrates are directed to the proteasome although exceptions do exist especially in the nucleus where recycling occurs (74, 160, 161). P97's role is vital to maintain cellular homeostasis as without it, proteins, and protein complexes as well as incorrectly folded proteins accumulate, this causes proteotoxic stress. p97 uses specific cofactors, 40 of which are known, these cofactors give p97 its specificity by recognising specific modified substrates, generally recognising certain residues or motifs. p97 substrates are modified by ubiquitin or ubiquitin-like molecules e.g., SUMO which cofactors recognise. P97 is found throughout subcellular locations, mainly residing in the cytoplasm (160), its role has been studied in multiple different systems including

endoplasmic reticulum associated degradation (ERAD), mitochondria-associated degradation (MAD), autophagy, endosomal trafficking and chromatin-associated degradation (CHROMAD) (162). CHROMAD is a relatively novel field as most investigation into p97s role has been studied outside of the nucleus, although it is a rapidly emerging field where p97 has been shown to regulate many chromatin-associated proteins (124, 161, 163) and those involved in DSBs (15, 54) (Figure 15). P97's role in the DDR is proposed to be vast, a global example being the p97-UFD1-NPL4 complex removing RNF8 dependant K48 chains after DNA damage. Without this complex BRCA1, 53BP1 and Rad51 signalling is affected, especially Rad51 whose activity is more reliant on this RNF8-K48-p97 pathway (74, 164). Furthermore, p97 regulates important DDR proteins such as PARP (165), MRE11 (15), Ku (166), RNF8 (118) and Rad52 (124, 167). These proteins play an important role in pathways choice and the function of said pathway. p97 often seems to act as a recycling mechanism in the nucleus, disassembling proteins but not directing them to the proteasome as it does in other subcellular locations (160).

P97 is especially important to cancer cells which are always on the brink of excess cellular, and proteotoxic stress. Increased and abnormal translation driven by oncogenes and mutational burden e.g., aneuploidy (altering the number of chromosomes) can induce proteotoxic stress. Upregulation of the UPS, including p97 is common to manage this stress, (168). UPS genes are commonly mutated, one study found that 19% of mutations in cancer cells were to proteins in the UPS system (169) (Figure 17). The UPS can be targeted in cancer (Figure 16), exemplified by inhibition of the proteasome using the drug bortezomib which prevents the functioning of the proteasome causing specific toxicity to cancer cells (170). Bortezomib is currently used to treat multiple cancers (171). By targeting other parts of the UPS, a similar phenotype could be induced but with more specificity. Therefore, p97 is also targeted therapeutically in clinical trials to potentially treat cancer (Figure 16).

1.9.1. Structure and Function

p97 contains an N domain connected to a D1 domain via the N-D1 linker with a subsequent D2 domain connected by a short D1-2 linker, ending with the C-terminus. p97 forms a homo-hexametric quaternary structure forming a barrel-like configuration (Figure 14a). D1 and D2 are ATPase domains although despite sharing large sequence homology, they have different functions. The D1 domain is vital for the hexametric structure assembly whereas the ATPase function is less important. The D2 domain is vital for the ATPase function of p97 (160).

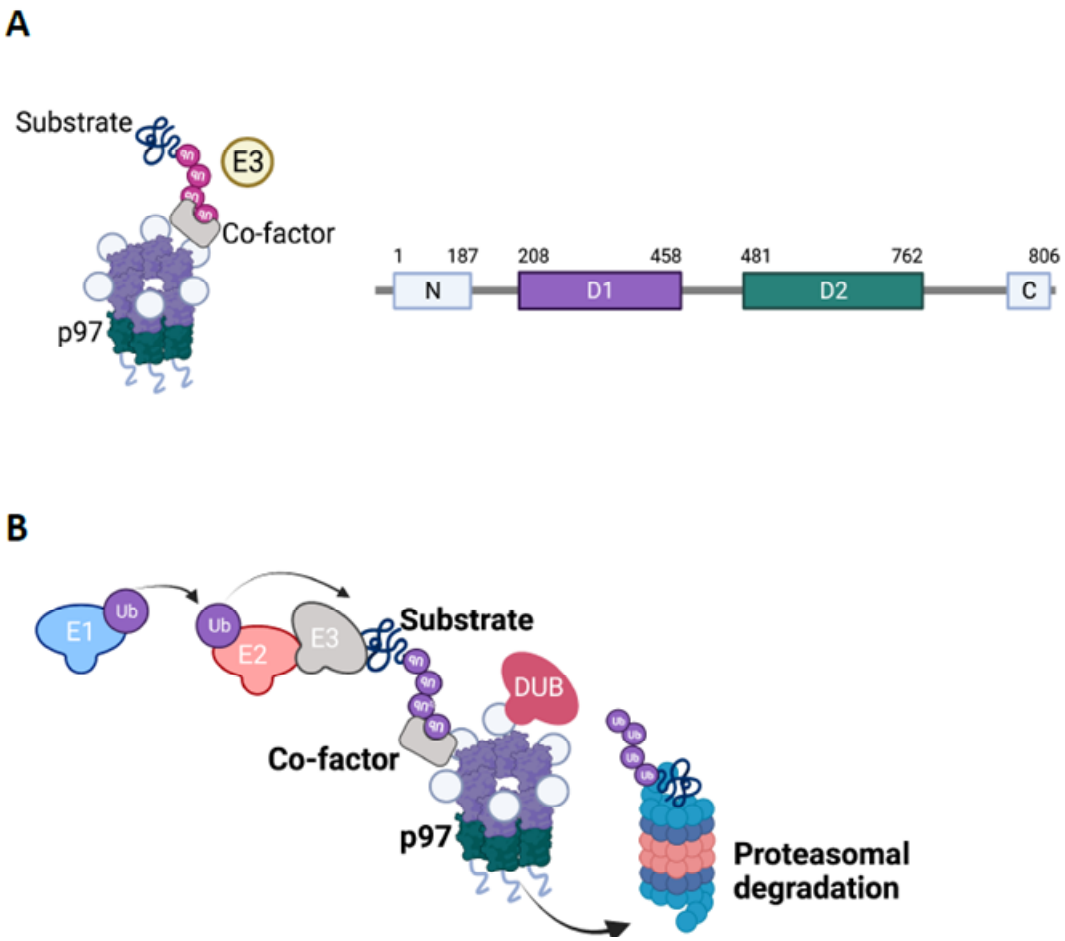


Figure 14. p97 Structure and function.

A) Highlights the homo-hexametric quaternary structure of p97 with N terminal heads present and the barrel-like structure comprised of the ATPase domains D1 and 2. The C terminal tail protrudes from the structure. Cofactor binding a ubiquitinated substrate is also shown with the E3 ligase present. Subsequent substrate processing would occur through the barrel pore. The amino acid residues of the domains are also shown. B) p97s proposed function where it uses specific cofactors to recognise ubiquitinated substrates (ubiquitin machinery E1 to 3 enzymes conjugate ubiquitin chains to these substrates while DUBs can remove these conjugates) and directs the substrate to the proteasome or recycles the substrate (not shown). Figure adapted from (26)

p97 substrate/cofactor binding mainly occurs through its N-terminal domain but it can also occur through the C-terminal tail (60). P97 also has a RecA-like domain which engages nucleotides prior to hydrolysis. ATP hydrolysis causes conformational changes resulting in an alteration of function. The central pore widens, facilitated by D1 conformational change, which allows the processing of substrates through the barrel-like core (162). p97 uses the energy from ATP hydrolysis to extract substrates, although the exact mechanism is not fully understood and may be dependent on the fate of the substrate e.g., degraded or recycled (172). p97 may also be considered a platform to assemble ubiquitin chains, associated proteins and other machinery to regulate the degradation or recycling of certain substrates (164).

p97 itself is extensively modified by numerous PTMs, even those rarer modifications, which are thought to mediate its function. The amino acids that are modified by PTMs on are similar across different types of PTM implying there may be some competition between PTMs (157, 172). Unpublished data from our lab highlight that p97 PTMs and interactions are dynamic after IR via high throughput mass spectrometry (Appendix 34-36). However, the players regulating these PTM sites, and the impact of these differential interactions are yet to be completely elucidated.

1.9.2. Cofactors

As stated previously the role of p97 is often dictated by its cofactors of which there are roughly 40 known. These cofactors generally link p97 to a specific function and subcellular space. Most cofactors known have ubiquitin regulatory X (UBX) and/or UBX-like (UBXL) domains although others contain ubiquitin-binding domain (UBD), VCP-interacting protein (VIP motifs), VCP-binding motif (VBM), SHP motif or the peptide N-glycanase/ubiquitin associated (PNGase/PUB) domain (160, 172). Most cofactors are those capable of recognising ubiquitin or ubiquitin-like conjugates although some cofactors are enzymes that can add or remove PTMs e.g., RNF4. Most cofactors bind the same hydrophobic cleft in the N terminus of p97 therefore different cofactors compete for p97 binding, the SHP motif is the exception, binding elsewhere, therefore, superseding competition (162). These

cofactors can bind p97 in different stoichiometries with most not binding to all 6 p97 proteins in the p97 hexametric complex, most likely due to steric clashes. 1 to 6 cofactors have been shown to bind the p97 complex e.g., only one ataxin versus six UBXD9 proteins can bind p97. Combinatory cofactors could also be present due the p97's hexametric structure (172). The association and disassembly of cofactor complexes are thought to be regulated by ATP hydrolysis and or PTMs of the substrate or p97 itself (162). Multiple core p97 complexes exist, of interest is the p97-UFD1-NPL4 complex, which is involved in CHROMAD and several other processes, typically associated with proteasome-dependent functions (161, 173).

1.9.3. p97's Role in DSB and HR

Despite p97 mainly residing int the cytosol, its role in the nucleus is broad and has been found to regulate DNA replication, transcription, mitosis and multiple DNA repair pathways (163). P97 also has a vital role in DSBs, where depletion of p97 radiosensitises cancer cells affecting HR, NHEJ and other repair pathways (15, 118, 161) (Figure 15). A brief outline of the confirmed roles p97 plays in the DSB response is below.

p97 dependent removal of the Ku complex promotes HR as Ku inhibits DNA end resection (166), removal of L3MBTL1 promotes NHEJ by allowing 53BP1 recruitment (174), removal of DNA-PK promotes HR by decreasing NHEJ efficiency (175), removal of Rad52 effects Rad51 loading efficiency therefore effecting HR in yeast (167) and removal of MRE11 regulates end resection controlling the balance between HR and SSA (15). P97 removal of K48 chains in the nucleus is also vital for the DDR highlighted by p97 inhibition causing K48 accumulation resulting in the dysregulation of spatiotemporal PTM dynamics causing downregulated protein signalling (164). p97 inhibition results in the failure to accumulate vital DDR proteins 53BP1, BRCA1 and Rad51 (74, 124). P97 also acts on chromatin dynamics to mediate the DDR (54). It is thought that the regulation of p97 is cell cycle dependent based on the co-factors present and the precise timings of the PTMs, suggesting p97 removes substrates in a hierarchical manner (54).

Substrates	Co-factors	E3 ligases	Associated Pathways
Aurora B	Ufd1-Npl4	Cullin-3	Mitosis
L3MBTL1	Ufd1-Npl4	Unknown	DSB repair
Ku80	Ufd1-Npl4	Unknown	DSB repair
MRN complex (MRE11 subunit)	Unknown	Unknown	DSB repair
BRCA1	BRCA1	HERC1	DSB repair
CDT1	Ufd1-Npl4	Cullin-4	DNA replication / repair
SET8	Ufd1-Npl4	Cullin-4	UV-induced lesions
WRN	Unknown	Unknown	DNA replication / repair
Rbp1	Ufd1-Npl4 UBXD7 UBXD9	Cullin-3	UV-induced lesions
Mcm7	Ufd1-Npl4	Cullin-2	DNA replication / repair
Unmodified and SUMO1-modified TOP1	TEX264	Unknown	DNA replication
Unidentified K48-linked substrates	ATX3	RNF8	DSB repair

Figure 15. p97 functions in the DNA damage response.

*List of 97 substrates in the nucleus along with the cofactor, E3 ligase and associated pathways involved with the interaction. * Unknown whether these are substrates or interacting partners. Figure adapted from (26)*

1.9.4. p97 Interaction with the MRN Complex

Two recent independent mass spectrometry screens of p97 pulldowns from our lab have identified p97 interacting with components of the MRN complex. These results show the spatiotemporal interactomics of p97 where p97 interacts with each of the components of the MRN complex at different dynamics in the two screens (Appendix 34-6). p97 appears to interact with the MRN complex solely in the nucleus as expected, although, at different rates in different nuclear fractions e.g.,

nucleosol versus chromatin. p97 interaction with the MRN complex has also been validated by co-immunoprecipitation. MRE11 and RAD50 have been shown to co-localise with p97, while p97 inhibition results in increased MRE11 and RAD50 foci, MRE11 retention on chromatin and excessive end resection (15). Furthermore, MRE11 pulldowns and subsequent mass spectrometry have identified p97 as a substrate therefore this interaction has been validated with both proteins being the 'bait' and 'prey' (appendix 33). Although the mechanisms and other regulatory factors involved in this interaction and phenotype are not completely understood, for example what PTMs, cofactors and E3 ligases are involved.

A separate finding of interest is the p97 co-factor and protease, SPRTN causes inactivation of the MRN complex by MRE11 cleavage. SPRTN positively correlates significantly with greater disease-specific survival in urinary bladder cancer patients after radiotherapy compared to those who received cystectomy (176). Thus, understanding the p97 system including the co-factors and mechanisms involved can potentially identify targets for radiosensitising cancer therapies.

1.9.5. Other Roles of p97 in the Nucleus

Outside of the DSB response, although still in the nucleus p97 has a vital function extracting multiple other substrates from chromatin (54). Interestingly disassembly of the replisome (CMG complexes) from chromatin after replication termination is p97 and K48 chain dependent (163, 177, 178). This is similar to the observations of the reliance of DDR proteins on p97 and K48 ubiquitin chains.

Therefore, it is proposed that p97 acts on the HR machinery of the MRN complex to regulate the timely removal of the MRN complex, in a similar manner to the disassembly of the replisome after termination of replication. It is proposed that this mechanism to be intricately controlled by PTMs, p97 cofactors and E3 ligases. This proposal forms the aims in chapter 2.

1.9.6. Clinical Application

As previously stated, the excess burden cancer cells have due to disrupted protein homeostasis results in proteotoxic stress. Evidence to support this mechanistic hypothesis is that p97 is upregulated in

multiple cancers and correlates with higher recurrence rate and worse disease-free periods leading to a decreased survival in p97 high expression groups (168) (Figure 17). Furthermore, p97s elevated expression has been linked to tumours with metastatic potential (168). Interestingly p97 has been shown to be excreted in many cancers therefore could be used as a biomarker as well as a therapeutic target (168). Inhibition of p97 *in-vivo* has decreased tumour size and acts as a radiosensitiser (15, 168). Multiple drugs have been used to target the UPS including proteasome, ubiquitinating and deubiquitinating enzymes (Figure 16). Several P97 inhibitors have been developed and tested in clinical trials, the first being CB-5083. Preliminary data identified CB-5083's ability to target solid

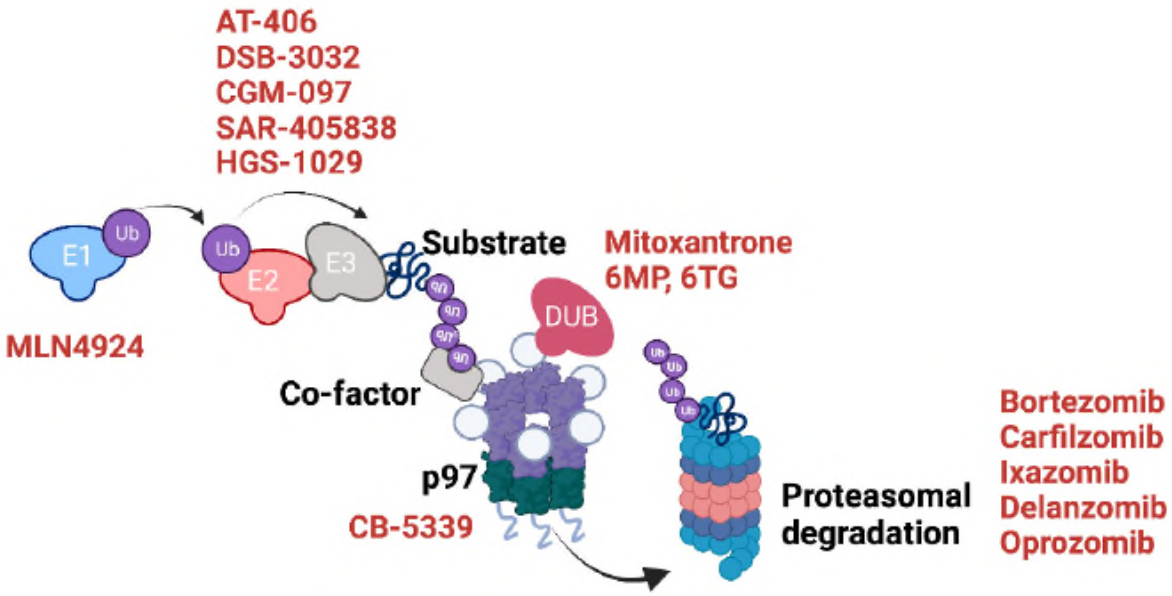


Figure 16. Small molecule inhibitors targeting different components of the ubiquitin proteasome system.

Figure adapted from (26)

tumours unlike proteasome inhibitor bortezomib (168, 179). CB-5083 is a competitive reversible ATP inhibitor targeting the D2 ATPase domain of p97. Studies showed that CB-5083 causes accumulation of K48 linked chains in the nucleus which differed to proteasome inhibitor bortezomib which targeted proteins in the cytoplasm predominately (179). This nuclear effect could be why it is effective as an anticancer agent as it impairs nuclear signalling e.g., the DDR resulting in insurmountable genome

instability and toxicity. Despite this success, CB-5083 had to be withdrawn due to unexpected eye-toxicities (NCT02243917). Therefore, an analog CB-5339 was created with 15-fold less activity on the protein which caused the eye toxicity and localised 30 times less in rat retinas but maintained a similar clinical potency. CB-5339 is now in phase one trials for treatment of solid tumours and lymphomas (NCT04402541).

Targeting specific parts of the UPS system seems to be advantageous, as evidenced by p97 inhibitors broader efficacy. Therefore, targeting p97 cofactors could result in a more specific and targeted therapy (162) as deficiencies in specific cofactors has resulted in cancer and premature ageing conditions (161).

Outside of cancer, P97 mutations have been linked to diseases such as amyotrophic lateral sclerosis (ALS), IBMPFD (Inclusion Body Myopathy associated with Paget's disease of the bone and Frontotemporal Dementia), viral infections, Parkinson's and Alzheimer's (180).

Cancer Type	**Features with which Higher VCP/p97 Levels Correlated**
Colorectal	greater invasion depth (T3–4), presence of venous invasion, higher tumour stage (III and IV), and higher recurrence rate
	CEA diagnostic marker
	carcinogenesis and metastasis development in a xenograft model
	USP11 levels influence colon cancer drug resistance
Pancreatic	lymph node metastasis and disease-free and overall survival
	low levels of miR-198 and poor patient outcomes
	high levels of Ki-67 and a malignant prognosis
Liver	shorter disease-free and overall survival
	low levels of miR-129-5p and HCC development and progression
	high levels of Neat1 and HCC diagnosis and treatment
	sorafenib response in HCC cells
	PTPRO levels
Gastric	greater tumour size, presence of vascular and lymphatic invasion, lymph node metastasis, and shorter overall and disease-free survival

	cell survival, degradation of cellular regulators, and gastric carcinogenesis
	low levels of CHOP and DR5
Esophageal	higher frequencies of lymph node metastasis, deeper invasion, metastasis, and shorter disease free and overall survival
	shorter overall survival
Breast	shorter overall survival
	poor outcomes of triple-negative patients receiving chemotherapy
	lower survival rates
	expression of the SOX2 protein
Prostate	poor prognosis and increased metastatic potential
	high levels of IL-6
	maintenance of mitochondrial activity
Lung	shorter disease-free and overall survival
	NSCLC development, progression, and metastasis
	low levels of miR-129 and NSCLC development and progression
	increased levels of ER stress and EMT markers, chemoresistance and shorter patient survival
Bone	higher metastatic potential (LM8)
	expression of the Aurora B protein
	low levels of miR-129-5p and osteosarcoma development and progression
	autophagy, anoikis resistance and osteosarcoma metastasis
	apoptotic response modulated by SAP
	cellular transformation and tumorigenesis
Head and neck	tumour stages, lymph node metastasis and shorter overall survival
	development of carcinoma in situ lesions and invasivity
	better 5-year disease-free survival rates for HPV-negative patients
	clinical outcomes of chemo-radiotherapy
Thyroid	disease recurrence in patients with follicular thyroid carcinoma
	BPA exposure
	shorter disease-free survival and an increased risk of recurrence in patients with papillary thyroid cancer subjected to ablative radioiodine treatment
Hematological	tumour grade, stage, histological subtype, recurrence, and shorter overall and disease-free survival of patients with B-cell lymphoma
	multiple myeloma development and progression

	poor prednisone responders in paediatric patients with acute lymphoblastic leukaemia exosome generation and secretion in Jurkat tumour cells
Melanoma	advanced radiotherapy immune escape
Glioblastoma	radiosensitivity of glioblastoma cells, and survival time of xenografted mice with radiation treatment HDAC6 levels and temozolomide resistance therapy
Ovarian	chemotherapy response in patients receiving the platinum-taxane combination
Testicular	development of different types of human testicular tumours
Bladder	shorter survival following bladder removal by cystectomy
Squamous cell carcinoma	development of squamous cell carcinoma

Tabular Figure 17. p97 alteration's role in tumourigenesis, progression or treatment resistance.

Figure adapted from (168).

2. Aims

Multiple mass spectrometry screens have identified components of the MRN complex interacting with p97 (15, 26, 181) (Figures 33-36). MRE11 accumulation and excessive end resection occurs upon p97 inhibition and p97 is known to regulate the activity of other key proteins and complexes activity on chromatin. Therefore, creating the overarching aim, to elucidate the mechanism of **how p97 directs the disassembly of the MRN complex from DNA after DSBs** (Figure 18).

Aims more specific to this thesis include 1) generation and validation of the tools needed to answer the above broad research questions, 2) development of expertise in experimental methods and 3) collection preliminary data such as the PTMs status of the MRN complex after ionising radiation.

2.1. Specific Objectives

- **Create and validate synthetic GOI-pcDNA5 / C\N terminally tagged APEX2 plasmids.**
- **Validate synthetic plasmids expression and subsequent function of the expressed protein via assessing protein-protein interactions in a mammalian system.**
- **Create HEK293 and HeLa stable cell lines expressing fusion proteins.**
- **Identify post translational modifications (PTMs) on the MRN complex.**

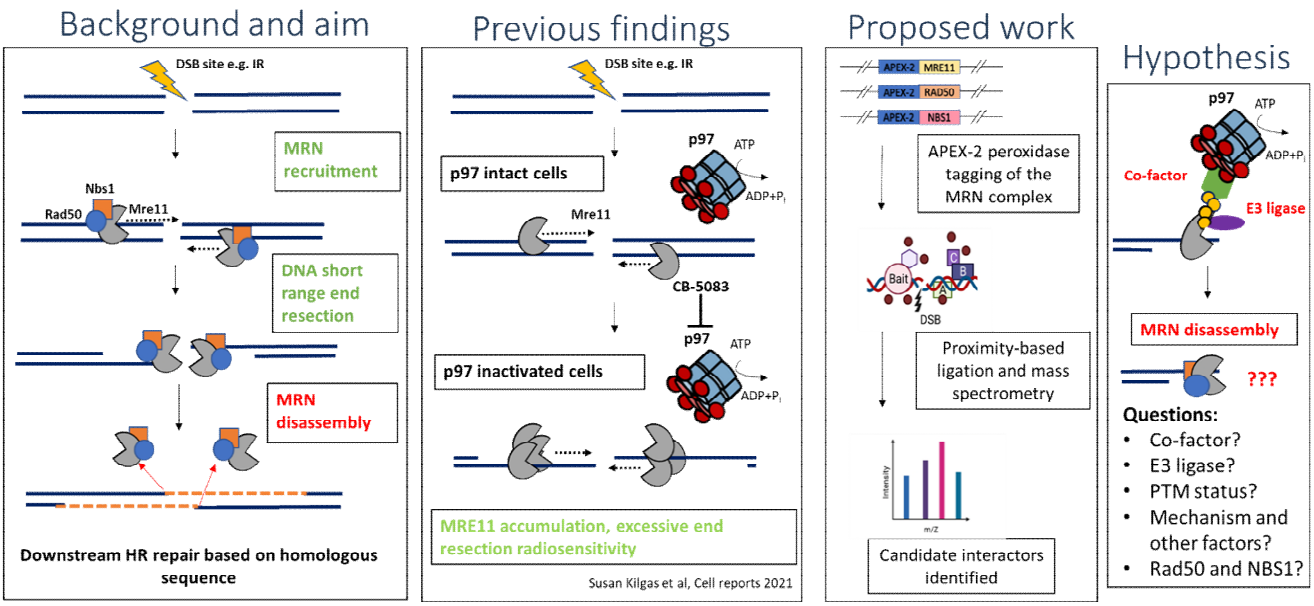


Figure 18. Schematic overview of project.

The role of the MRN complex after double-strand breaks highlighting what is known (green) and is not known (Red). Previous findings show p97 inactivation results in MRE11 accumulation, excessive end resection and radiosensitivity. Highlighted is our proposed work enabling us to investigate the hypothesis.

3.Methods

3.1. Tissue Culture

HEK293 and HeLa cells were obtained from the American Type Culture Collection (ATCC). Cell lines were grown in Dulbecco's Modified Eagle's Medium (DMEM), supplemented with 10% FBS and 1X penicillin/streptomycin antibiotics. Cells were maintained between 10-90% confluency, splitting cells when they reached 90% by washing, trypsinising, quenching and diluting. Cells were kept at 37°C, 5% CO2, in a humidified incubator. Cells were regularly tested for mycoplasma using biochemical tests to ensure only negative cells were used. Briefly, the MycoAlert biochemical mycoplasma detection kit was used where luminescence is used as a readout for the conversion of ADP to ATP by a mycoplasma specific enzyme. 1ml of media from cultured cells (at 80% confluency or higher) was collected and spun at 200 x g for 5 minutes to collect a cleared supernatant free of mammalian cells. 100µL of supernatant was collected and added to 100 µL of MycoAlert reagent. The sample was incubated for 5 minutes before measuring read 'A' using a spectrophotometer. Subsequently 100 µL of the

Mycoalert substrate was added and incubated for 10 minutes before taking reading 'B'. If the ratio of B/A was greater than 1.2 the sample was assumed contaminated with mycoplasma and was not used. Further samples would be tested and if positive thrown away to thraw new cell lines which were tested before use.

3.2. Plasmid Transfections

Cells were seeded to 70% confluency at the time of transfection. Cells were transfected using Polyethyleneimine (PEI) or Fugene according to the manufacturer's instructions. Depending on the transfection wanted and the plate size different concentrations were used. Briefly, for a 10cm plate transfections using PEI: Solution A) 480µL PBS was mixed with 20µL PEI and solution B) 480µL PBS was mixed with 21.7µL plasmid DNA. Solutions A and B were mixed, gently vortexed and incubated for 15 minutes at RT.

Fugene transfection is similar. For fugene transfections in 10cm plates a solution of 5.4µL of DNA was added to 325µL of optimem, which was briefly vortexed then 24µL of fugene was added and vortexed once more. This solution was left incubate for 10-15 minutes.

In both cases the transfection mixes were both added dropwise to the cells and then mixed. For PEI, before transfection the media was replaced with DMEM only media, and then replaced with supplemented media 2-4 hours after transfection. For Fugene, media volume was halved.

If co-transfections were completed the DNA volumes would increase to account for lost efficiency. Cells were then incubated a 37°C for 48-72 hours until harvesting and downstream analysis.

3.3. Molecular Cloning

An overview of molecular cloning and the DNA assembly process using the NEB HiFi system is shown in figure 20. This system uses primers with overhangs complementary for one another which are used to amplify specific DNA amplicons via polymerase chain reaction (PCR). This then allows multiple amplicons to be assembled based on primer complementarity, creating a synthetic plasmid.

Primer's design is therefore important. Optimum primers are around 20 nucleotides long, have a GC content between 40 to 60% and are not prone to form secondary structures such as hairpins, and primer-dimers. Online primer design tools were also used to ensure the formation of secondary structures was minimised and to ensure the complementary region was valid. The primer Melting Temperature (Tm) defines the annealing temperature used during the PCR. An example of the primers used for DNA assembly reactions are shown in figures 21, 22 and 37.

3.3.1. PCR Amplification

PCR amplification was completed to generate amplified sequences with overhangs to allow downstream ligation. Appropriate template DNA was sourced and 0.5 µL added into a 200µL tube along with other PCR reagents of 0.5 µL Q5 polymerase (high fidelity heat stable polymerase), 1.25 µL of designed forward and reverse primers, 1 µL of dNTPs and 5 µL of Q5 PCR buffer (containing $MgCl_2$). The tube was then added to the thermocycler where an initial extended denaturation was completed of 5 minutes at 95°C, subsequently 35 cycles of a 3-step process was completed. 1) denaturation at 95 °C for 30 seconds, 2) annealing at -5 °C of the primers Tm for 30 seconds and 3) extension at 72 °C for a variable time period dependent on the size of the sequence to be amplified (generally 1 minute per kilobase), then after the 35 cycles a long extension time at 72 °C of 7 minutes was completed to ensure all the sequences were completely elongated. Samples were then maintained at 4 °C until collection.

DpnI, a restriction enzyme was then added to the PCR mixture and incubated at 37 °C for an hour. DpnI digests methylated DNA which occurs in bacteria therefore digesting the template bacterial DNA.

The PCR mixture was then loaded along with GelRed (which intercalates with DNA) into a self-casted 1% agarose gel where 1% by weight of agarose was dissolved in TAE (40mM Tris base, 20mM Acetic acid and 1mM EDTA) and set with a comb. Electrophoresis was then completed for 1 hour at 100 volts to sperate the DNA sample based on size.

Images were taken on a spectrophotometer using the iBright system.

3.3.2. Band Extraction

Band extraction was then completed to purify the PCR amplicon at the correct molecular weight from the agarose gel. This was completed by excising the band with a scalpel by visualising the band under UV light (due to the GelRed fluorescence), careful to trim excess agarose. NEB gel extraction kit was then used to purify the PCR amplicon. Briefly, the excised gel piece was weighed and 4 volumes by weight of gel dissolving buffer was added and incubated for 5-10 minutes at 50°C until the gel was completely dissolved. The dissolved sample was then added to the column and centrifuged at 16,000 x g for 1 minute, the flow through was discarded. The column was then washed twice with 200 µL of DNA wash buffer and centrifuged as above, disregarding the flow though once again. The column was then transferred to a clean 1.5ml tube and 10µL of elution buffer was added to the column and incubated for 1 minute and centrifuged as above to elute the DNA.

The DNA was then quantified using the Nanodrop system. Previously the Nanodrop was equilibrated using elution buffer.

3.3.3. DNA Assembly and Ligation

Based on the DNA concentration and type of assembly (2/3 amplicon or 4+ amplicon) different volumes of purified DNA were mixed during ligation. For 2-3 amplicon ligations a ratio of 1:2, vector: insert was completed, where between 0.03 and 0.02 pmols of DNA were mixed, while 4+ amplicon assembly requires a ratio of 1:1, vector: insert at 0.2-0.5 pmols of DNA. Moles of DNA were calculated based on the DNA mass, length of sequence and molecular weight of DNA (650 Daltons) using the formula below.

$$pmols = \frac{DNA\ mass\ in\ ng\ x\ 1{,}000}{no.of\ base\ pairs\ x\ 650\ daltons}$$

Amplicons to be assembled were incubated together at the correct ratio and mass as highlighted above, with 10µL of HiFi DNA assembly master mix for 15-60 minutes. The length of incubation

depends on DNA concentration and number of amplicons assembled. Lower concentration and/or a higher number of DNA amplicons need longer incubation times and are generally less efficient.

3.3.4. Transformation

50 µL of DH5α chemically competent *Escherichia coli* slurry was thawed on ice. The desired ligation product being a synthetic plasmid (made above) was then added and gently mixed with the bacterial slurry by flicking the tube and incubated on ice for 30 minutes. Heat shock was then completed in a 42°C water bath for 30 seconds, inducing transformation. Transformed bacteria were recovered on ice for 5 minutes and transferred to a bacterial shaker tube where 950 µL SOC outgrowth medium in ampicillin (50µg/ml) was added and incubated at 37°C and 250 rpm for 1 hour. Bacteria were then centrifuged at 500 x g for 5 mins where subsequently most of the supernatant was removed. The remaining media was used to resuspend the pellet which was then plated onto agar plates containing ampicillin (50µg/ml) and grown overnight in a bacterial incubator at 37°C. If there were significantly more colonies than the negative control plate, then the ligation was assumed successful and progresses onto the next step of colony PCR validation.

3.3.5. Colony PCR

Single colonies on selection plates were picked and added to a similar PCR mixture as in section 3.3.1 although the Q5 polymerase was replaced with a comparatively lower fidelity polymerase – Taq, as fidelity was not as important here. The extension temperature was lowered to 68°C due to differences in optimum temperature between the DNA polymerases used. Transformed colonies contains the plasmid of interest therefore acts as the DNA template for the PCR reaction. Primers used were specific for sequences in respective assembled amplicons e.g., backbone and insert, therefore validating if the ligation had occurred by amplifying a sequence only present if both the backbone and insert were ligated.

Concurrently the colonies picked were also transferred and labelled to a fresh plate for growth, forming a patch plate.

After the PCR reaction, amplicons were loaded into a 1% agarose gel and analysed via gel electrophoresis at 100 volts for 1 hour. If a species at the correct molecular weight were amplified, it progresses to be analysed by sequencing.

3.3.6. DNA Sequencing

Colonies on patch plates from successful colony PCR results were expanded in 5 mL of Luria-Bertani medium with appropriate antibiotics (ampicillin at 50µg/ml) and incubated in a bacterial shaker (37°C, 250 rpm) overnight. The next day part of the sample was frozen at -80°C after supplemented with equal volume 20% glycerol. The remaining sample was centrifuged at 500 x g for 5 minutes. The bacterial pellet was then used for DNA purification via miniprep (process highlighted in section 3.4).

Once purified DNA was obtained and quantified it was diluted to a concentration of 100ng/µl for the sequencing reaction. Primer solutions were also diluted to 3.2pmol/µl. Template DNA and primers where then sent, outsourced for sequencing. Initially one primer would be sent as an initial validation followed by enough primers to cover the whole insert and bridge region if positive.

Sanger sequencing works by completing an altered *in vitro* DNA replication reaction. Primers are used as start sites for the DNA polymerase which then continues to replicate the DNA. The reaction contains a small concentration of fluorescently labelled ddNTPs (dideoxynucleosides), which when incorporated into the DNA chain terminates the polymerisation reaction. This occurs as the 3' hydroxyl group is removed from the nucleotide which is required for the DNA polymerase phosphodiester reaction to occur.

Traditionally 4 separate ddNTP reactions occur, one for each nucleotide base. The lengths of the sequences are then analysed by gel electrophoresis on an agarose gel. Since the identity of the ddNTP is known in each reaction, and the size is known of each amplicon on the gel one can uncover the base identity and order, revealing the DNA sequence. Modern methods use fluorescently or other differentially tagged ddNTPs allowing the reaction to occur in one tube and are analysed via gel

capillaries or other methods with laser fluorescence detectors. A chromatogram is then generated where multiple Sanger sequences are overlapped to increase validity, revealing the DNA sequence.

Raw sequencing data would be returned days later, where the chromatogram would be assessed and if reliable, the sequence would be aligned to assure accurate PCR amplification and DNA amplicon ligation. Alignment using specific software e.g., Clustal omega and Jalview were used. The full insert and bridge area was sequenced to ensure no variants were present which could affect downstream analysis (Figure 27).

3.4. DNA Purification

Maxiprep was performed as per manufacturer's instructions (QIAGEN; cat#12162). 200ml of overnight bacterial culture was centrifuged at 6000xg for 15 minutes at 4°C. Bacterial pellets were resuspended in P1 Buffer 10 mL (50 mM Tris-HCl, 10 mM EDTA, 100 µg/mL RNase A, pH 8.0). Resuspended bacteria were lysed using Buffer P2 10 mL (200 mM NaOH, 1% SDS w/v) and gently mixed via inverting 4-6 times prior to incubation for 5 minutes at RT. Subsequently 10 mL of chilled Buffer P3 (3.0 M potassium acetate, pH 5.5) was added, mixed 4-6 times by vigorous inversion, and incubated for 20 minutes on ice. Concurrently, buffer QBT (750 mM NaCl; 50 mM MOPS, pH 7.0; 15% isopropanol (v/v); 0.15% Triton X-100 (v/v)) was added to a QIAGEN-tip 500 to equilibrate the column by gravity flow. The cell lysate was then clarified via centrifuged at 20,000 x g for 30 mins at 4°C, the supernatant was then re-centrifuged at 20,000 x g for 15 mins at 4°C. The subsequent supernatant was then added to the equilibrated QIAGEN-tip 500 and allowed to enter the resin by gravity flow. QIAGEN-tip 500 then was washed with 2 x 30 mL Buffer QC (1.0 M NaCl; 50 mM MOPS, pH 7.0; 15% isopropanol (v/v)). DNA was then eluted from the QIAGEN-tip with 15 mL buffer QF (1.25 M NaCl; 50 mM Tris-HCl, pH 8.5; 15% isopropanol). DNA was then precipitated by adding 10.5 mL RT isopropanol and centrifuged at 15,000 x g for 30 mins at 4°C. The supernatant was then carefully decanted, and the remaining DNA pellet was washed with 5 mL of RT 70% ethanol and centrifuged at 6000 x g for 20 minutes at 4°C. Supernatant was then decanted, leaving the DNA pellet which was air-dried until no liquid was left.

The pellet was subsequently dissolved in a suitable volume of TE buffer (10 mM Tris-HCl pH 8.0; 1 mM EDTA). Plasmid yield and contaminants were measured using a NanoDrop Spectrophotometer. DNA concentration was measured using wavelengths at 260nm, whereas contaminants were measured at wavelengths of 280 and 230 nm for protein and other organic compounds e.g., phenols respectively. If concentrations were too large more TE buffer would be added to achieve around 1mg/ml of DNA.

The miniprep DNA purification protocol was similar to that of the maxiprep protocol above. Briefly, expanded bacteria was pelleted and resuspended in P1 buffer equivalent and vortexed. P2 lysis buffer equivalent was then added, inverted, and incubated for 1 minute. Neutralising buffer was then added and left to incubate for 2 minutes. Centrifugation at 16,000 x g for 2-5 minutes was then completed, the supernatant was then transferred to the column and flow through was discarded. Wash buffer 1 and then 2 were then added to the column and centrifuged as above for 1 minute and flow through discarded. The column was then moved to a fresh tube and elution buffer was added, left incubate for 1 minute then centrifugated as above for 1 minute, eluting the DNA.

3.5. Stable Cell Line Generation

An overview of the process can be seen in Figure 32. Briefly host cell lines were co-transfected, grown in selective media and expanded to two 10cm before freezing and validation.

HEK293 and HeLa FRT Flp-In host cell lines were seeded at 30% confluency in a 10cm plate of DMEM supplemented media as in section 3.1 as well as including zeocin (100µg/ml) and blasticidin (15 µg/ml) to maintain host cell lines only and prevent contamination. Mycoplasma testing was completed prior to transfection as outlined in section 3.1.

The FRT recombinase-containing plasmid pOG44 was transfected alone in the negative control and co-transfected along with the experimental plasmids in both Hek293 and HeLa cell lines. Fugene transfection was used with a slight alteration to that described in the section 3.2 due to the co-transfection reduced efficiency. To 1.2ml of optimem, a ratio of 9:1 of pOG44:pcDNA5 (synthesised plasmid) was added (20µg of pOG44 and 2.3µg of synthesised plasmid) and vortexed. 60µL of fugene

was added to this and again vortexed, then left to incubate for 15 minutes. In the meantime, media was replaced with supplemented DMEM with blasticidin (15 µg/ml) alone. The DNA containing mixture was then added dropwise to the plate and mixed.

The plate was left for 2 days to integrate the plasmid into the genome. Cells were then split into a range of dilutions on 15cm plates along with selection antibiotic of hygromycin (200 µg/ml for HeLa and 100 µg/ml for Hek293 cells). Concentrations of selection antibiotic were outlined via creating a kill curve ensuring the concentration kills 95%+ of the cellular population by 7 days but not too quickly (as that concentration may also affect resistant cells). Transfected cells were trypsinised and diluted to 1:1.25, 1:5 and 1:25 concentrations and plated on 15cm dishes. Media was changed every 3 days ensuring the hygromycin concentration was correct. This was completed until colonies formed which took around 3-4 weeks.

Single colonies were picked using pipette tips and placed on a 96 well plate. 16+ colonies were picked per transfection. These colonies were expanded to larger surface area plates until they were 100% confluent on 2x10cm plates where freezing occurred ready for downstream validation.

3.6. Protein Analysis

3.6.1. Western Blotting

Cells were harvested on ice by scrapping or trypsinising to detach cells from the dish. Detached cells were then washed with PBS and centrifuged at 500 x g for 5 mins at 4°C. Supernatant was then removed and cells were rewashed 2 times with PBS. 50-100 µL of RIPA lysis buffer supplemented with freshly added protease and phosphatase inhibitors (aprotinin (10 µg/mL), leupeptin (10 µg/mL), chymostatin (10µg/mL), sodium pyrophosphate (4 mM), sodium orthovanadate (2.5 mM), sodium fluoride (20 mM), phenylmethylsulphonyl fluoride (2mM), N-Ethylmaleimide (20mM)) was added to the pellet and left on ice for 10 minutes. Sonification was then completed for 10-15 cycles of 30 seconds on and 30 seconds off in a 4°C water bath. Samples were then centrifuged at 20,000 x g for 15 minutes at 4°C. The supernatant was then removed, and protein was quantified using the BCA assay

and Omega software. Briefly, the BCA assay is a two-step copper based colorimetric assay to quantify protein. In a 96 well plate a standard curve in triplicate was created by performing a serial dilution of dissolved bovine serum albumin at known concentrations. Lysed samples were also measured in triplicate and added to the plate. Reagent A (carbonate buffer with bicinchoninic acid at high pH) and reagent B (Cupric sulphate) were added at 50:1 to these samples. Samples were then incubated in dark for 5 minutes and absorbance at 560 nm was quantified using the Omega spectrophotometer. The concentration of the experimental samples could then be calculated based on the standard curve. Protein samples were normalised to contain the same amount of protein by diluting with water. Generally, 30 µg of protein was prepared per sample. Laemmli buffer was added, and the sample boiled at 95°C for 5 minutes. Protein samples were then loaded into lanes and ran via electrophoresis on varied acrylamide percentage SDS-PAGE self-casted gels in 1X Running Buffer at 100 V for approximately 1.5 hours.

Self-casted gels were made using the mini-PROTEAN Tetra Handcast System (Biorad). Varying volumes of 4X separating buffer (1.5M Tris, 4% SDS, pH8.8), water and acrylamide were mixed depending on the percentage gel. An example of the ratios for a 9% seprating gel used can be seen below:

Reagents	**Volume (µl)**
30% Acrylamide	3600
4x Separating Buffer	3000
H_2O	5300
10% APS	60
TEMED	8

Acrylamide and water volumes were adjusted for different percentage gels. Subsequently TEMED and APS was added to induce polymerisation. The solution was then poured into a mould, isopropanol was

then added to ensure the top of the gel is level. The mould was then left to set for 1 hour, once set, the isopropanol was washed out and stacking buffer was added to the mould along with a comb to create the wells. Stacking buffer was a lower percentage of acrylamide and made of similar reagents, the difference being using the lower pH stacking buffer (pH 6.8) instead of separating buffer. After 20-30 minutes the gels were set and are used or stored in running buffer to prevent drying out.

Samples running in SDS-PAGE were then transferred to a nitrocellulose or PVDF membrane using a Mini Trans-Blot Electrophoretic Transfer Cell. Briefly, a gel sandwich was assembled as per manufacturer's instructions and inserted into the tank with ice-cold transfer buffer (1x Tris/Glycine buffer; 20 % methanol; 0.025 % SDS) and an ice pack, transfer was then performed at 100 V for 1 hour. Membranes were then blocked in 5% skimmed milk in TBST for 1 hour at RT. Membranes were then washed 3 times for 5 minutes in TBST before appropriate primary antibody (1:500-5000 concentration) was added in dilution buffer (3% BSA/TBS-T) and incubated overnight at 4 °C or at room temperature for 2+ hours. After incubation, membranes were washed again, 3 times for 5 minutes each. Membranes were then incubated in a suitable secondary antibody (1:50,000 concentration) in diluent (2.5% skimmed milk), specific to the species of primary antibody for 1 hour at RT on a rocker. The membrane was then washed as above, developed, and imaged and analysed using the iBright system. Bands were detected using chemiluminescence and a spectrophotometer. Chemiluminescence was induced in development via the action of a horseradish peroxidase (HRP) reaction. The secondary antibody was conjugated with a HRP enzyme which catalyses an oxidisation reaction producing a chemiluminescent signal via the conversion of a chromogenic substrate to an active form e.g., luminol. Membranes were developed by exposing them for varying times to ensure the signal was clear and imaged by a spectrophotometer.

3.6.2. Co-Immunoprecipitation

Cells were trypsinised, washed twice with ice-cold PBS and centrifuged at 500 x g for 5 minutes at 4°C as above to create a cell pellet. Co-IP lysis buffer (50 mM Tris-HCl, 150 mM NaCl, 1 mM EDTA, 0.5-1% Triton X-100, pH 8.0) along with inhibitors as with RIPA buffer above were added and incubated on a rotating wheel for 10 mins at 10-15 revolutions per minute at 4°C. IP lysis buffer was used instead of RIPA buffer as RIPA disrupts protein-protein interactions (via the detergent effecting hydrophobic interactions an the salt effecting ionic interactions) which would affect Co-IP results. Lysate was centrifugated at 1000 x g for 5 mins at 4°C. The supernatant was then removed and stored on ice, the remaining DNA pellet was washed with 200µL benzonase buffer (50 mM Tris-HCl, 150 mM NaCl, 2 mM $MgCl_2$). The was the sample was inverted to ensure the pellet was dislodged and then centrifuged at the same setting as above. The supernatant was collected and added to the previous supernatant. Benzonase enzyme was added to the benzonase buffer and 200µL of this solution was added to the remaining DNA pellet. The sample was then vortexed and incubated on the rotation wheel for 1 hour or longer at 10-15 rotations per minute at 4°C. During this time all of the digestible pellet should have been digested, if a pellet is still visible, incubation time was increased. The sample was centrifuged as above, and the supernatant was collected and added to the pooled sample. The remaining pellet was disregarded and is thought to contain indigestible DNA e.g., heterochromatin and other debris. 10% of the pooled sample was collected as input and stored at -80°C.

Antibody tagged beads (anti-tag immunoglobulin e.g., HA magnetic or agarose bead) were washed with IP wash buffer (50 mM Tris-HCl, 150 mM NaCl). Wash was completed 3 times for 5 minutes on a rotating wheel at 10-15 rpm at 4°C, centrifuging after each time and removing the supernatant using a magnetic rack or centrifugation. Beads were then decanted into low-binding tubes. 5µL of Ethidium Bromide (50µg/ml) was added to the IP lysates which were subsequently loaded onto the washed beads and incubated at 4°C on a rotating wheel at 15 rpm for at least 2 hours. Samples were collected and washed three times as above, using IP wash buffer, the rotating wheel, centrifugation, and the magnetic rack. During the last wash, thinner tipped pipettes were used to ensure beads were

completely dry. Proteins were eluted by addition of 2X Laemmli buffer and boiling samples for 10 minutes at 95°C. Input samples underwent the same treatment. Proteins were then analysed by Western Blotting as in section 3.6.1.

3.6.3. Denaturing IP

Cells were trypsinised, washed twice with ice-cold PBS and centrifuged at 500 x g for 5 minutes at 4°C as above to create a cell pellet. 250µL of Denaturing IP lysis buffer (50 mM Tris-HCl, 150 mM NaCl, 2 mM $MgCl_2$, 0.3% Triton X-100, 1X Benzonase) was added to the pellet and incubated for 30 minutes at 4°C on a rotating wheel at 15 rpm. Centrifugation of the sample was then completed at 20,000 x g for 15 minutes at 4°C. Supernatant was removed and put in a 15ml tube. 12µL of 20% SDS was added to create a final concentration of 1% SDS, vortexed and left incubating on ice for 10-15 minutes. This was completed as SDS affects benzonase activity by denaturing proteins therefore has to be added after lysis to denature the proteins post DNA digestion. Once the solution was colourless 10% input was then collected (if cloudy the sample was heated, incubation time increased and more SDS may be added). 10 volumes of triton buffer (20 mM Tris-HCl, 137 mM NaCl, 1 mM EDTA, 1% Triton X-100) was then added to quench the SDS and incubated on roller for 15-30 minutes. SDS has to be quenched to prevent it denaturing the antibody on the beads. Meanwhile the beads were washed 3 times using IP wash buffer, rotation, centrifugation, and the magnetic rack as outlined in the Co-IP section. The beads were decanted into 5ml low bind tubes, to which the lysates were added and incubated at 4°C on a rotating wheel at 15 rpm for at least 2 hours. Beads were then washed as above and eluted with Laemmli buffer and boiled at 95 for 5 minutes. Input samples were treated the same. Proteins were then analysed by Western Blotting.

3.7. Ionising Radiation Treatment

Cells were irradiated in complete medium at 1.5 Gy/min using a Gamma-Service Medical GmbH GSR D1 irradiator.

3.8. Solutions and Reagents

3.8.1. Antibodies

Protein	Working Dilution	Source	Species	Catalogue number
MRE11	1:1000	Calbiochem	Rabbit	SAB4501912
RAD50	1:1000	Abcam	Mouse	AB89
NBS1	1:1000	Abcam	BD Biosciences	611871
RNF8	1:1000	Abcam	Rabbit	Ab4183
Ubiquitin	1:500	Chemicon	Mouse	Mab1510
SUMO1	1:1000	Santa Cruz	Mouse	sc-9060
HA	1:2000	Roche	Rat	11867423001
Flag	1:2000	Sigma	Mouse	F3165
GAPDH	1:2000	Invitrogen	Mouse	MA5-15738
Vinculin	1:2000	Abcam	Mouse	ab130007
B-actin	1:2000	Invitrogen	Mouse	AM4302
Mouse-HRP	1:50,000	Sigma	Rabbit	A9044
Rabbit-HRP	1:50,000	Sigma	Goat	A9169
Rat-HRP	1:50,000	Sigma	Goat	A9037

3.8.2. Buffers

1x Phosphate Buffered Saline Buffer (PBS buffer)

10x PBS - 80.0 g NaCl, 2.0 g KCl, 14.4 g Na_2HPO_4 and 2.4 g KH_2PO_4 dissolved in 800 mL ddH_2O. Solution was increased to 1 L with ddH2O, and the pH was adjusted to 7.4. 1X working concentration (137 mM NaCl; 2.7 mM KCl,pH 7.4; 12 mM phosphate) with ddH_2O.

Lysis Buffer: radioimmunoprecipitation assay buffer (RIPA buffer)

2x RIPA buffer was prepared - 100 mM Tris-HCl, 300 mM NaCl and 3 mM EDTA and diluted with ddH_2O to 1x working concentration.

5x Laemmli Buffer (LB)

5x LB - 0.25 % bromophenol blue (SLS), 50 % glycerol (Fisher Scientific), 10 % SDS and 0.25 M Tris-HCl (pH 6.8). 1X working concentration (50 mM Tris-HCl, pH 6.8; 2 % SDS; 10% glycerol; 0.05 % bromophenol blue) with ddH_2O and supplemented with 15 % β-mercaptoethanol.

Running Buffer: Tris/Glycine/SDS

10x - 30.0 g of Tris base and 144.0 g of glycine dissolved in 1 L of ddH_2O. 1X working concentration (25 mM Tris; 190mM glycine) with ddH_2O and supplemented with 0.1 % SDS.

Transfer Buffer

1x Tris/Glycine buffer as above supplemented with 20 % methanol and 0.025w/v SDS.

Tris-buffered saline with Tween 20 (TBS-T) buffer

10x TBS buffer - dissolving 88.0 g of NaCl and 24.0 g of Tris base in 800mL ddH_2O. The final volume was adjusted to 1 L with ddH2O, and the pH adjusted to 7.6. 1X working concentration (20 mM Tris, pH 7.5; 150 mM NaCl) with ddH_2O and supplemented with 0.1 % Tween 20 (Sigma).

4. Results

4.1. Introduction

An overview of the work completed is presented below in figure 19. The aim was to develop and validate tools to answer the broader research question of understanding how the MRN complex is disassembled from DNA. Initiated by generating synthetic plasmids using molecular cloning. Subsequent validation of the expression of the plasmids made via western blotting was completed followed by investigation of the protein-protein interaction as a proxy for functionality via co-immunoprecipitation (Co-IP), both of which in mammalian cell lines. Investigation of the PTM status of the MRN complex via denaturing immunoprecipitation was completed. After validation, stable cell lines expressing the tagged fusion proteins were created.

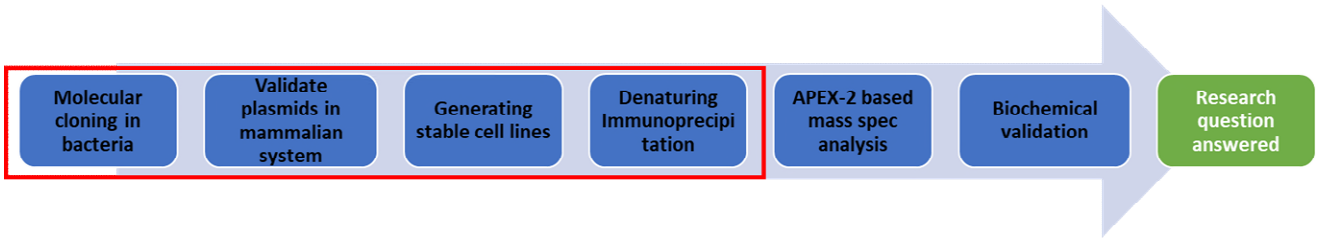


Figure 19. Research project plan and progression to answer research questions.

Outlined in red is work completed in my masters, prospective work is outlined in the non-highlighted boxes.

4.2. Molecular Cloning

Cloning was performed generating three plasmids for each component of the MRN complex. Three different backbones were used, a pcDNA5 vector containing a streptavidin-streptavidin-HA tag and two APEX2 containing vectors (Figure 21). As the APEX2 tag might disturb protein function, folding or interaction, the tag was either added at the C or N terminus of the protein studied. Therefore, in total creating 9 plasmids. In this section the general flow of the cloning process as well as issues that arose and how they were overcame will be outlined.

Molecular cloning traditionally relies on the use of restriction enzymes and ligases. Due to the efficiency, lab expertise and ease of the method, the HiFi DNA assembly kit was used. This process

uses specifically designed primers with overhangs and use the polymerase chain reaction (PCR) to create DNA amplicons with regions of complementarity allowing annealing and subsequent ligation of said amplicons. These ligated amplicons create a synthetic plasmid which can be transformed into bacteria, amplified further, and validated by colony PCR and Sanger sequencing (Figure 20).

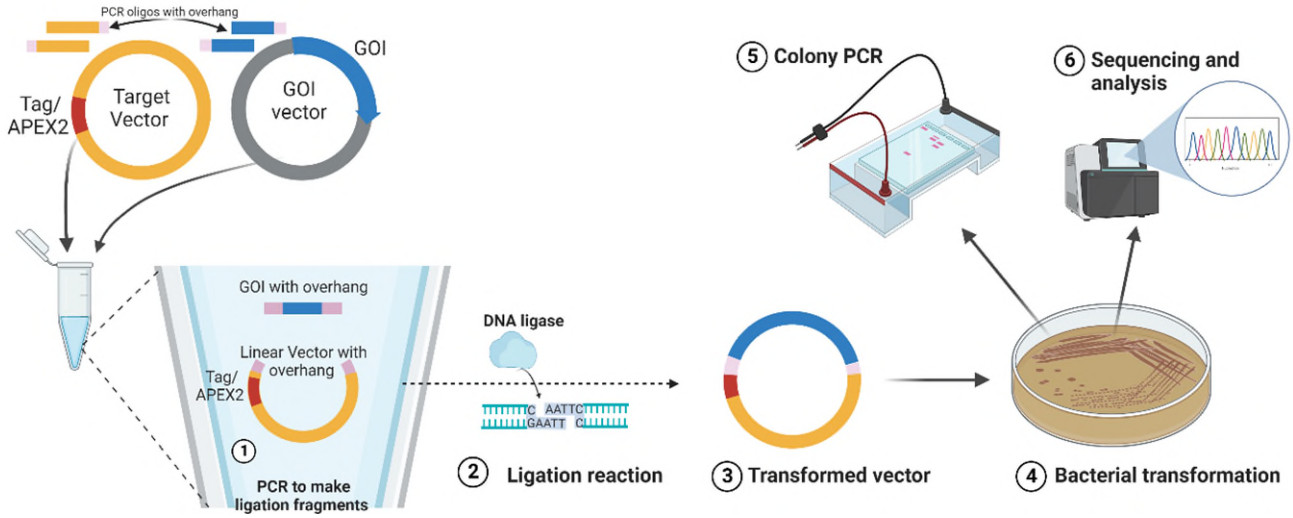


Figure 20. Molecular cloning overview.

1) PCR reaction to create and amplify the target vector and gene of interest (GOI) both with specific overhangs based on the primer design which allows for a ligation reaction in 2) catalysed by DNA ligase. Here amplicons are ligated together to create the transformed vector in 3). Chemically competent NEB 5-alpha E. coli are then transformed and validated in 5) via colony PCR and subsequent candidates are further validated via Sanger sequencing in 6). Figure created with BioRender.com.

4.3. Primer Design

Using the HiFi assembly kit the annealing and ligation of DNA amplicons are dependent on the overhangs created by the primers. Overhangs on the PCR amplicons are complementary therefore allow annealing, forming a synthetic sequence. Figure 22 shows an example of the primer design for a 3-amplicon assembly using the *rad50* gene and pGL35 backbone, these primers can also be visualised on the plasmid map, highlighting which fragments are amplified and where the annealing occurs (Figure 21). In the case of the APEX2 vector, the insert could be either be tagged on its C or N terminus. C and N terminally tagged APEX2 vectors required different primers to ensure the presence of an ATG (start codon) and a STOP codon in the correct reading frame for the fusion protein. Primers for the C terminally tagged APEX2 vector are shown in figure 22. In the case of N terminally tagged APEX2 vector

the stop sequence would not be at the end of the insert sequence but after the APEX2 sequence and the start codon of the insert would be the first start codon after the promoter.

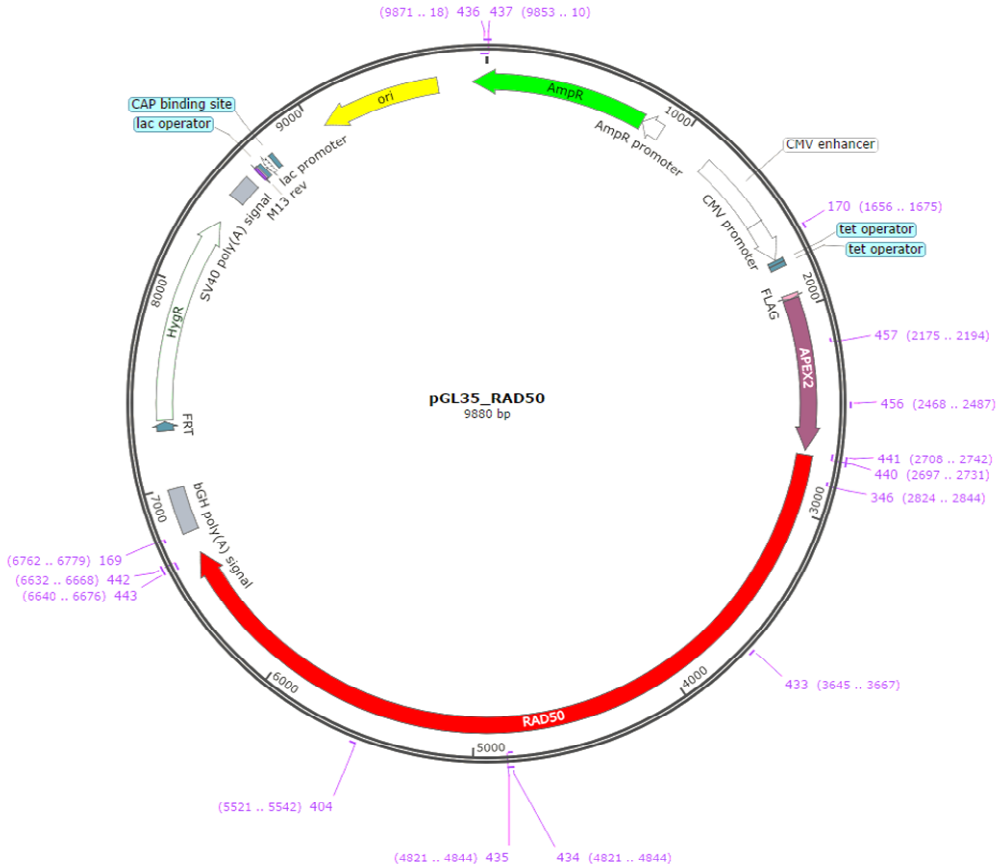


Figure 21. Plasmid map example of the construct synthesised.

In this case rad50 was the insert with FLAG_APEX2 tagged in the C-terminal using the pGL35 vector backbone. Also shown are primer sites used for PCR amplification and subsequent ligation as well as for downstream colony PCR and sequencing. Other sites include a CMV promoter with a tet operon, a AmpR promoter inducing expression of an ampicillin resistance gene, origin of replication and a FRT site and hygromycin resistance gene for downstream stable cell line generation.

	In PGL35				
#	**Name**	**Primer 5' (overlap/spacer/ANNEAL) 3'**	**Len.**	**3' %GC**	**3' Tm**
436	PGL35_Frag1_fw	catagttgcctgactccccgTCGTGTAG	18	61	58
440	PGL35_Frag1_RAD_rv	cgatccgggacattccacttccacTTCCACTTCCG	22	55	60
441	RAD50_35_fw	gtggaagtggaatgtcccggatcgaAAAGATGAGC	24	50	61
442	RAD50_35_rv	gagctcggtacttaatgaacattgaatccCAGGGAGC	23	48	59
443	PGL35_Frag2_RAD_fw	ggattcaatgttcattaagtaccgagctcGGATCCAC	22	55	60
437	PGL35_Frag2_rv	cggggagtcaggcaactatgGATGAACGAAATAGACAG	28	43	59

Figure 22. Primer design table.

The oligonucleotide names and the assigned number are shown which can be visualised in Figure 4 of the plasmid map. The length, GC content and melting temperature of each oligonucleotide is also shown. Shading regions show sequences specific to rad50, red and blue highlight sequences complementary to the backbone (Amplicon 'a' or amplicon 'b'), start and stop

codons are highlighted in yellow and pink respectively and the case of the sequence indicates if it anneals with another amplicon, highlighting how the annealing and ligation works.

4.4. DNA Amplification and Extraction

PCR was performed using the primers designed and a high fidelity (proofreading capabilities), heat stable DNA polymerase (Q5). 35 cycles of PCR were used to amplify the target sequences using the pool of nucleotides present. The amplicon mixture is then loaded on a 1% agarose gel where electrophoresis is used to separate DNA based on weight. This results in a band containing the amplicons at their expected weight/length (Figures 23 and 24). Figure 23 shows a gel after the PCR amplification where bands are close to the expected length for a 3-amplicon assembly using *mre11* and *nbn* (gene of NBS1) i.e., the insert and the 2 backbone amplicons. Figure 24 shows a similar result although for rad50 with a 2-4 amplicon assembly (completed due to problems downstream of ligation highlighted in sections 4.5-6). Band excision (appendix 39) and gel extraction of the correct bands was performed to reduce contaminates, an example of which can be seen at the bottom of the gel where 'primer-dimers' appear to have formed (figure 24). The primers used to amplify the amplicons in figures 23 and 24 are found in appendix 37.

4.4.1. Overcoming Limitations

Initially the PCR reaction was not efficient (appendix 38). To overcome this the annealing temperature was altered and the extension time extended. Furthermore, the PCR volume was doubled hence multiple loading lanes in figures 23 and 24. Although due to changing too many variables nonspecific banding occurred (appendix 38). The original conditions were returned to with increasing the PCR volume. This alteration along with gained experimental experience resulted in more intense and specific bands of the amplicons of interest, indicating increased yield, with less contaminants.

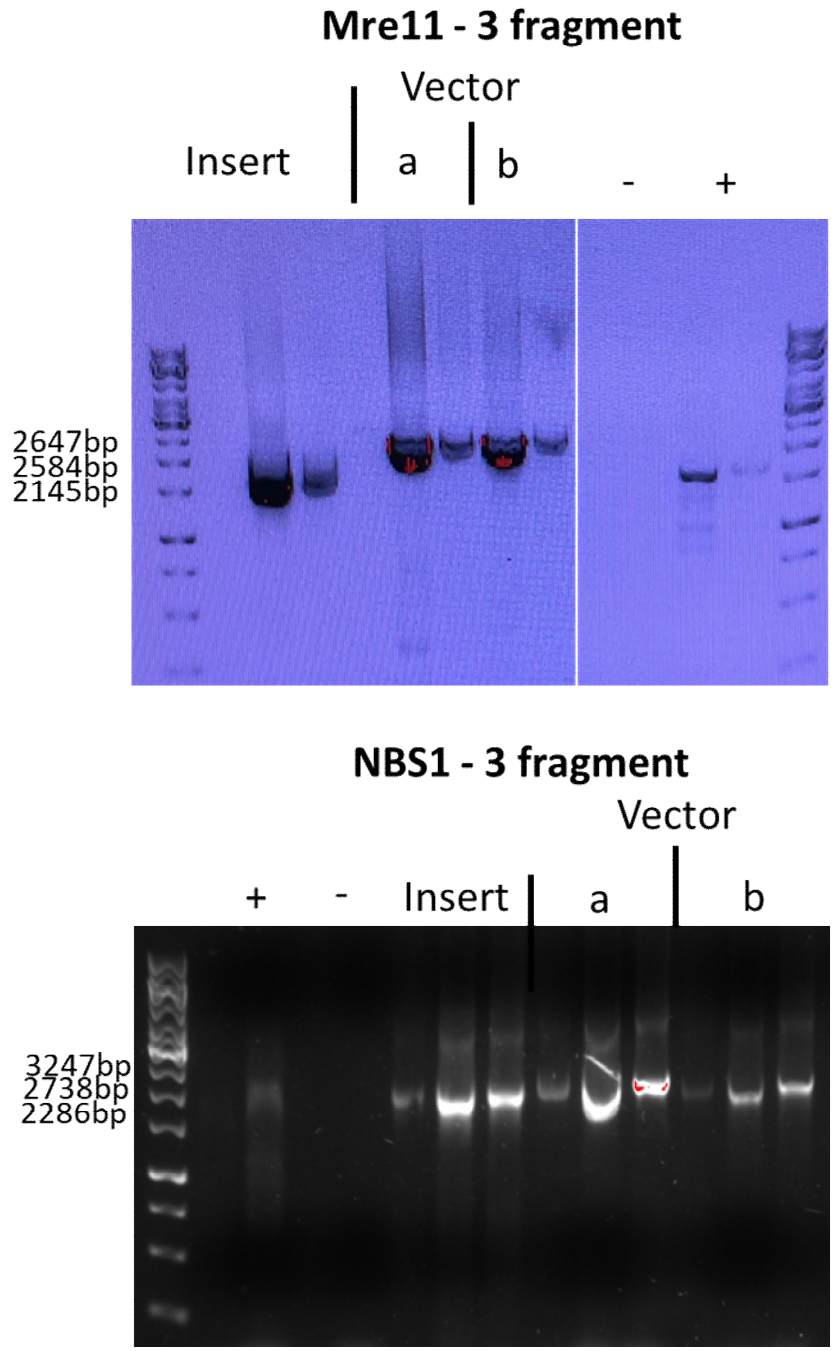


Figure 23. PCR amplicon run on a 1% agarose electrophoresis gel.

Amplification of mre11 and nbn inserts and pcDNA5 and pGL35 vector amplicons (a and b) and their respective base pair length. Positive control of a known rad50 containing plasmid and negative control of no oligonucleotides in the PCR mixture are also loaded.

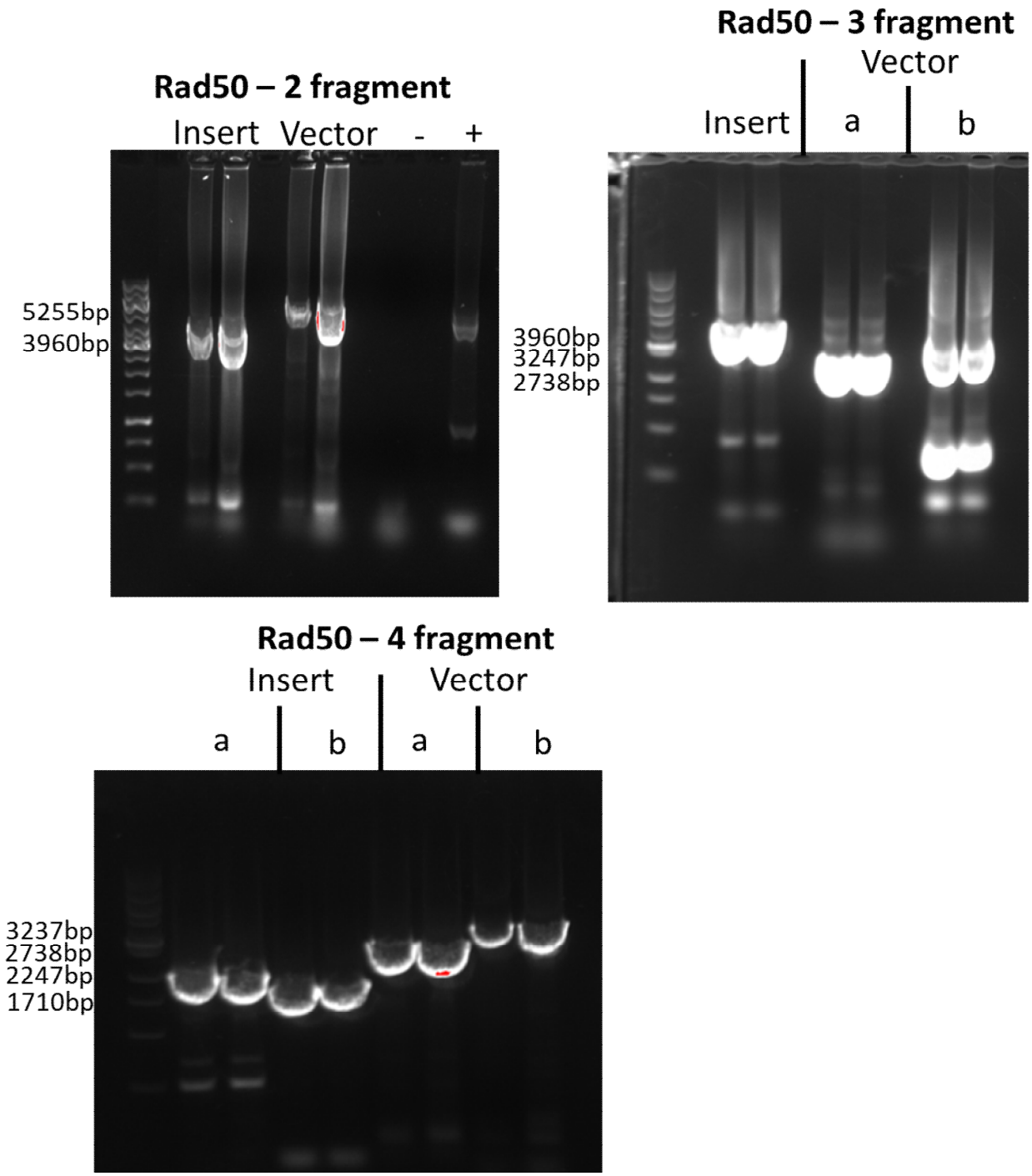


Figure 24. PCR amplicons run on 1% agarose electrophoresis gels from various rad50 amplification strategies.

Showing 2, 3 and 4 amplicon amplification. 2 amplicon amplification shows the whole rad50 cDNA sequence and the whole pcDNA5 vector being amplified, 3 amplicon shows the vector (in this case pGL35) split into two amplicons and 4 amplicon shows both the vector and rad50 sequence split into two amplicons. Negative control without oligonucleotides and positive control of a known rad50 containing plasmid are shown in the 2-amplicon amplification. The expected length of the DNA sequences is also highlighted.

4.5. Ligation and Transfection

The bands on the electrophoresis gels at the correct molecular weight were excised (appendix 39, using UV light to visualise the bands) and gel extraction was performed to purify the amplicons. The concentration of the purified DNA was then measured (appendix 40) and converted to total mass.

The DNA amplicons (using at least 50-100ng) are then ligated together using at a ratio of 1:2 or 1:1 vector: insert depending on the number of amplicons ligating. A mixture containing DNA ligase was added to the mixture of amplicons and incubated at 50 degrees Celsius for 15-60 minutes depending on the number and length of the amplicons, dictating the efficiency of ligation.

The ligated mixture was then used to transform competent bacteria via heat shock and grown for 1 hour in LB broth with ampicillin (50 µg/ml) and then plated on LB agar with ampicillin overnight.

Positively transformed bacteria will form colonies on the plates as can be seen in figure 25 due to the presence of an ampicillin resistance gene (Figure 21) in the synthetic plasmid. Figure 25 shows examples of positively transformed colonies for *mre11*, *rad50* and *nbn* in different vectors along with appropriate controls.

4.5.1. Overcoming Limitations

Initially the ligation was not efficient. This was concluded as the experimental plate had less colonies than the negative control plate and the ligation and transfection positive controls were working as expected. Therefore, the negative result was caused by the experimental reagents or conditions (appendix 41). These negative results were thought to be caused by low concentrations of PCR amplicons therefore the PCR volume was doubled, and band excision efficiency was increased due to increase experience, although this did not affect results. Therefore, the inefficient ligation was estimated to be due to the large size of the backbone aiming to be ligated (5000+ base pairs) therefore the backbone was split into 2 smaller amplicons using different primers. Furthermore, the ligating reaction was incubated for longer and an increased DNA mass was added which increased the DNA ligation efficiency.

These adaptations induced successful ligation of mre11 and nbn into vectors (Figure 25 left) but did not work efficiently for *rad50* (appendix 41). Despite this there were a few of the colonies on the rad50 plate were tested. During testing (section 4.6.1) false positive results were highlighted. Therefore, similar to the backbone the *rad50* was split into two amplicons making a 4-amplicon assembly which worked (Figure 25 right).

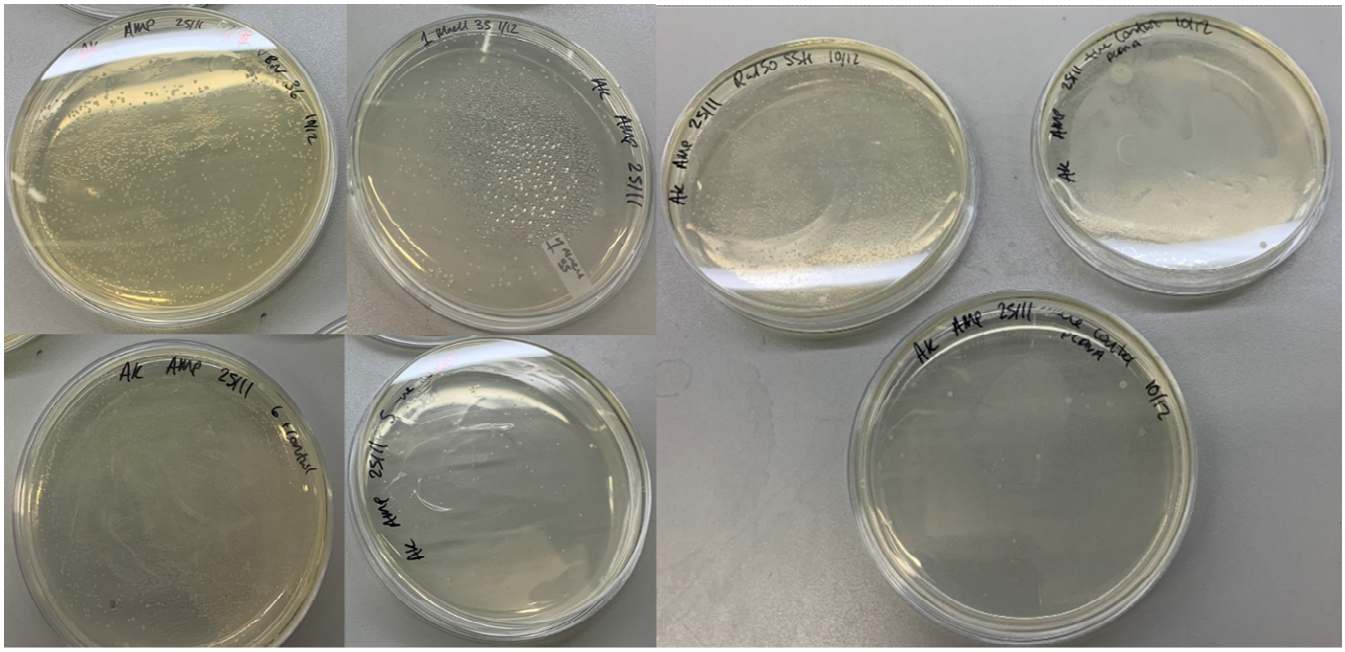


Figure 25. Transformed bacteria post ligation.

Agar plates containing ampicillin (50µg/ml) showing colonies transformed with synthetic DNA constructs after ligation occurred. NBN insert in a pGL36 vector, mre11 insert in a pGL35 vector and RAD50 in a pcDNA5 vector are shown along with appropriate controls, positive being a validated insert and vector from the manufacturer and negative control, missing the insert.

4.6. Cloning Validation – Colony PCR and Sanger Sequencing

Colony PCR was used to validate the transformed colonies to ensure the insertion had occurred (screening for false positives). Specific primers annealing on both the insert and vector were used, therefore amplifying an amplicon only present if ligation had occurred (e.g., primers 456 and 346 in figure 21). Taq - a lower fidelity DNA polymerase was used here at a PCR elongation temperature of 68 degrees. Plasmid DNA present in the bacterial colonies from the agar plates highlighted in figure 25 were used as template DNA. Patch plates as highlighted in appendix 43 were used to organise tested colonies for downstream expansion. Agarose gel electrophoresis was then completed to

visualise the results. Successful colony PCR can be visualised in figure 26 where a fragment from the ligation of *mre11*-APEX2 plasmids (C and N terminally tagged) has been amplified using specific primers generating amplicons of different lengths.

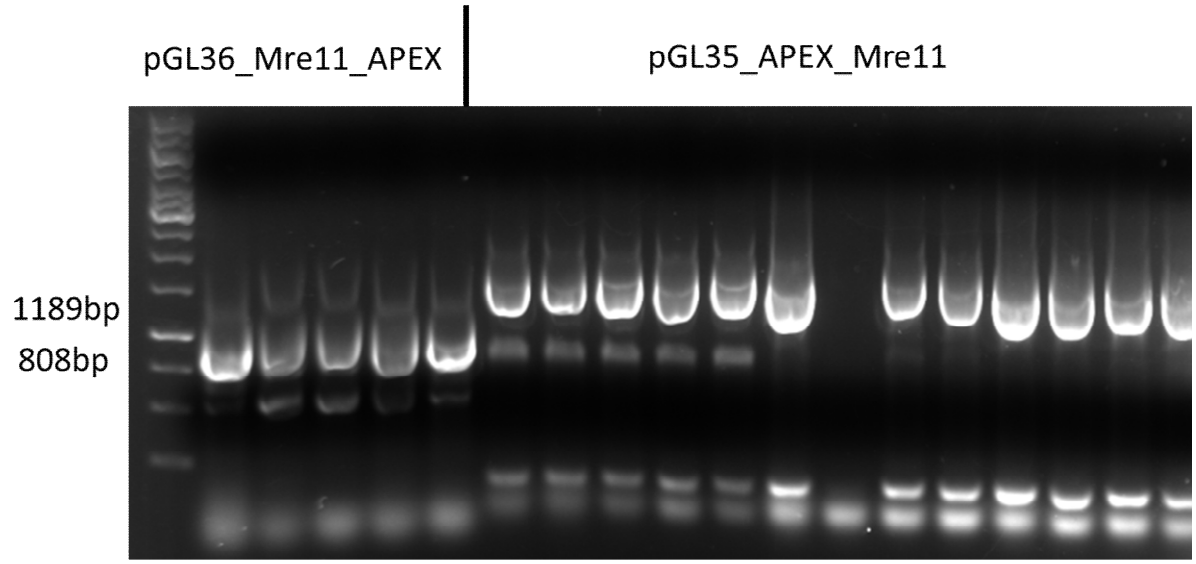


Figure 26. Candidate colony PCR result of 1% agarose electrophoresis gel.

Showing amplicons of those only possible if ligation has taken place based on the oligonucleotides used. Highlighted are a N-terminally APEX2 tagged mre11 pGL36 and a C-terminally APEX2 tagged mre11 pGL35 amplicon. Expected length of the amplicons was highlighted.

Plasmid DNA of positive colonies was purified via miniprep and sent for Sanger sequencing to confirm 100% accuracy in case of fidelity or ligation issues by sequencing the complete insert along with the 'bridge' areas (appendix 44 and 47). Sequencing products are then aligned to a reference sequence e.g., that outlined in the plasmid map (Figure 21). Complete coverage was achieved by using primers at regularly spaced intervals (Figure 21).

An example of alignment data can be visualised in figure 27 of pGL36_*mre11*_APEX2 where the ligation/bridge regions are shown at the beginning and end of the insert along with two sequencing results that perfectly align with the reference sequence. The total sequence similarity between sequencing reactions and the reference sequence is shown in figure 28.

If the sequencing validation was complete the positive colony would then be expanded in a substantial volume for DNA purification via 'maxi-prep' to obtain large amounts of purified DNA for downstream validation and analysis (Appendix 48).

4.6.1. Overcoming Limitations

Initially, there were not many positive results during colony PCR and those with bands were false positives (appendix 42), although after making changes highlighted in section 4.5.1 to the PCR and ligation reactions the results were more consistent and specific which were backed-up by Sanger sequencing (Figures 27 and 28).

An interesting result was the initial rad50 colony during 3 amplicon assembly which was tested despite there not being a large number of colonies on the ligation plate as highlighted in section 4.5.1. The colony PCR resulted in an amplification of a species at the correct molecular weight. Although the alignment results showed large portions of *rad50* sequence which were missing (appendix 44 and 45). This seemed to be due to the long length of the *rad50* sequence and the increased ligation incubation time. A false positive arose where the primer annealed to the start of *rad50*, then to a complementary sequence 1000s of bp downstream (appendix 44 and 45). This could have occurred due to the *rad50* sequence folding into a secondary structure. Based on this finding a 4-amplicon assembly for *rad50* was completed (Figures 24 and 25). This highlights the importance of Sanger sequence confirmation since the colony PCR returned a false positive (Appendix 44 and 45).

```
pGL36 Mre11_APEX start sequence alignment

mre11cmvfw      ACACCGGGACCGATCCAGCCTCCGGACTCTAGCGTTTAAACTTAAGCTTG
mre11ref        --------------------------------------------------
promoterref     ACACCGGGACCGATCCAGCCTCCGGACTCTAGCGTTTAAACTTAAGCTTG


mre11cmvfw      GTACCCACCATGGACTACAAGGATGACGACGATAAGATGAGTACTGCAGA
mre11ref        ----------------------------------ATGAGTACTGCAGA
promoterref     GTACCCACCATGGACTACAAGGATGACGACGATAAG--------------


mre11cmvfw      TGCACTTGATGATGAAAACACATTTAAAATATTAGTTGCAACAGATATTC
mre11ref        TGCACTTGATGATGAAAACACATTTAAAATATTAGTTGCAACAGATATTC
promoterref     --------------------------------------------------



pGL36 Mre11_APEX End sequence alignment

apexref         --------------------------------------------------
mre11457rv      AGTGAGGATGATGATGATGATCCTTTTATGAACACTAGTTCTTTAAGAAG
mre11ref        AGTGAGGATGATGATGATGATCCTTTTATGAACACTAGTTCTTTAAGAAG


apexref         -------------------------------GGAAAGTCTTACCCAACTG
mre11457rv      AAATAGAAGAGGAAGTGGAAGTGGAAGTGGAGGAAAGTCTTACCCAACTG
mre11ref        AAATAGAAGATAA-------------------------------------


apexref         TGAGTGCTGATTACCAGGACGCCGTTGAGAAGGCGAAGAAGAAGCTCAGA
mre11457rv      TGAGTGCTGATTACCAGGACGCCGTTGAGAAGGCGAAGAAGAAGCTCAGA
mre11ref        --------------------------------------------------
```

Figure 27. Candidate multiple sequence alignment result.

Showing the 'bridge' regions of the synthetic plasmid contrasted. The beginning and end of the insert (mre11in this case) is shown along with the portion of the vector it was inserted into. The name of the sequence is labelled on the left, with those labelled as 'ref' being reference sequences that the Sanger sequencing result is aligned to. The sequencing results are labelled as mre11cmvfw and mre11457rv indicating the oligonucleotide used to initiate the sequencing reaction.

Seq name	**Identity no.**	1	2	3	4	5	6	7
APEX2ref	1	100	95.35	N/A	100	N/A	N/A	N/A
***mre11*457rv**	2		100	100	98.28	N/A	99.8	N/A
***mre11*750fw**	3			100	98.28	85.77	95.65	N/A
***mre11*bghrv**	4				100	N/A	99.14	N/A
***mre11*cmvfw**	5					100	99.51	94.66
***mre11*ref**	6						100	N/A
promoterref	7							100

Figure 28. Alignment similarity table.

Highlighting a matrix showing the percentage identity of the Sanger sequences (those without 'ref' in the seq name) results with reference sequences of mre11, APEX2 and the promoter region.

Sanger sequencing of the NBS1 plasmids found that each plasmid obtained for *nbn* contained 3 non-synonymous variants (NM_002485.5:c.G102A - RCV000242759.9, NM_002485.5:c.T1197C -

RCV000173761.14, NM_002485.5:c.A2016G - RCV000243757.1) and one synonymous variant (NM_002485.5:c.G553C (p.E184Q) - RCV000162358.4) mutation. Therefore, the original insert sequence likely contains these variants. Non-synonymous mutations are unlikely to be deleterious as there is no change to the amino acid sequence. Synonymous mutations could be deleterious as the amino acid change could influence the structure and function of the final protein. Therefore, investigation into the potential impact of the synonymous variant was investigated.

The variant is in the BRC1 domain of *nbn* therefore could impact the structure and function of the protein (Figure 5) although it is of similar structural properties (glutamic acid to glutamine), with the difference being an amine group compared to a hydroxyl group. Furthermore, two human sequences are in GenBank (AF058696.2 and AK312410.1) and both are labelled as benign/normal sequences therefore are likely a natural human or a benign variant. Furthermore, other animals have variation in amino acid position 184 with multiple containing glutamine at that position (appendix 46). All evidence taken together this variant is unlikely to have functional significance.

Similar analysis was completed on all inserts. One *mre11* sequence contained multiple variants, one of which identified as a potential clinical variant (RCV001030637.1) and another, a deletion at nucleotides 2083 (NM_005591.4:2083_2085del). Therefore, a wild-type plasmid sequence was sourced and used for cloning.

4.7. Validation of Plasmids in a Mammalian System

Positive synthesised plasmids where then validated in a mammalian system, as this is the system, they are intended to be used in. This was important as downstream stable cell line formation was planned therefore it is vital to ensure that the plasmids were expressed and functional. Overexpression of the plasmids was completed via transient transfection in HEK293 cells. Subsequently, western blotting and co-Immunoprecipitation was completed to validate the expression and functionality of the plasmids.

4.8. Western Blotting

HEK293 cells were grown in 10cm plates in DMEM FBS/PS media then subsequently transfected with the validated plasmids at 70% confluency using cationic lipid-based transfection using the agent PEI. The transfected cells were then left for 48 hours and subsequently lysed for analysis.

Results of the western blotting can be seen in figure 29 where all the plasmids were expressed, albeit at different levels, likely to be due to varying transfection efficiencies. In figure 29 A) and B) antibodies for the tags introduced in the synthetic plasmids were used, highlighting only protein expressed from exogenous sources. Anti-HA and anti-FLAG allowed visualisation of the overexpressed protein. Initially, all apart from MRE11 in the pcDNA5 vector was observed (red box in figure 29b). MRE11 overexpression from the pcDNA5 vector was repeated and observed in figure 29c, human error was likely to be the cause of the initial issue. Figure 29 part D and E shows the use of antibodies specific to the protein of interest that was overexpressed, therefore enabling visualisation of the endogenous protein as well as the exogenous sourced protein. Here, all the proteins are successfully overexpressed as the band was more intense and generally at a higher molecular weight due to the tags added, as expected. Anti-GAPDH was used as a loading control to ensure the same amount of protein was loaded in each sample. GAPDH band intensity was relatively consistent implying the BCA protein quantification was successful.

Overall, these results shows that all 9 synthetic plasmids made by DNA assembly during molecular cloning were successfully expressed in a mammalian system.

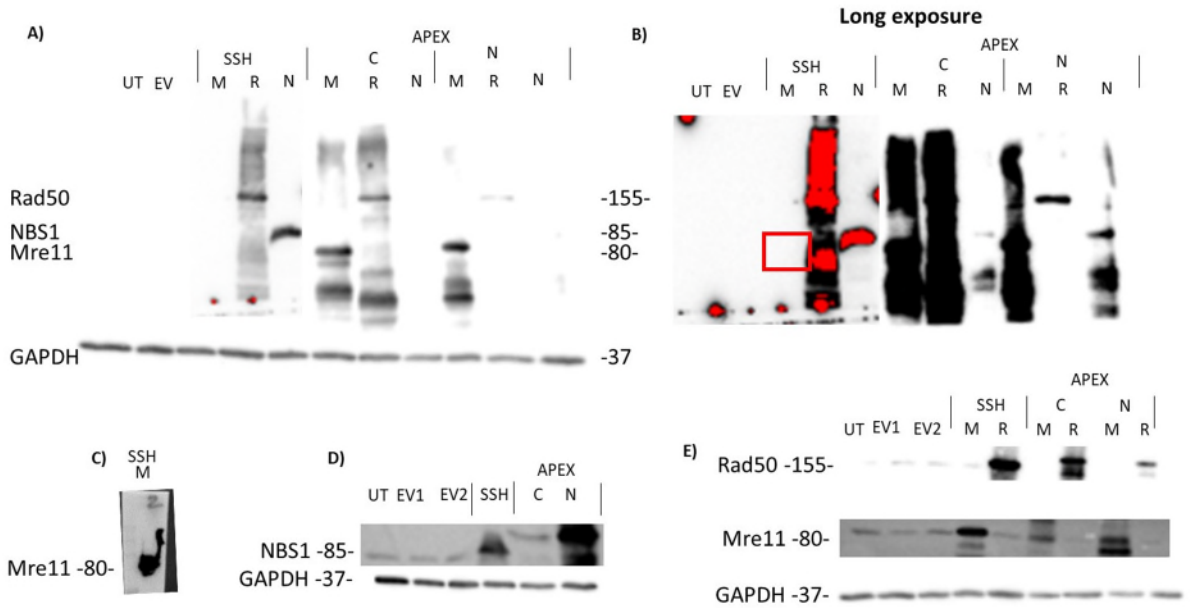


Figure 29. Western blot validation of SSH and FLAG/APEX2 tagged synthetic plasmids in mammalian cells.

A) Western blot of overexpressed HEK293 cells blotted with anti-HA (SSH tagged samples), anti-FLAG (APEX2 tagged samples) and anti-GAPDH as loading control. It shows the differential expression of most of the POI. B) Same western blot as in A) with longer exposure showing the expression of all but one of the POI highlighted in the red box. C) Re-running of the MRE11-SSH tagged plasmid showing expression of the plasmid not observed in A) and B). D) Western blot of overexpressed HEK293 cells with NBS1 containing plasmids blotted with anti-NBS1 and anti-GAPDH as loading control. Shows the expression of both endogenous and exogenous NBS1. E) Western blot of overexpressed HEK293 cells with MRE11 and RAD50 containing plasmids blotted with anti-MRE11, anti_RAD50 and anti-GAPDH as loading control. Shows the expression of both endogenous and exogenous MRE11 and RAD50.
UT – Un-transfected, EV – Empty Vector, SSH – streptavidin-streptavidin-hemagglutinin tag, M – MRE11, R – RAD50, N- NBS1, POI – protein/s of interest.

4.9. Co-Immunoprecipitation Validation

Plasmid functionality was also tested as a validation measure. This was only completed for the APEX2 containing vectors as this validation was used to ensure plasmids were functional, not only expressed, prior to generating stable cell lines. Furthermore, differences between C and N terminally tagged APEX2 vectors were assessed.

Functionality was assessed via a proxy of measuring the protein of interests expected protein-protein interactions (other MRN binding partners), assuming that if the protein interacted with MRN complex partners, that it was acting functionally in the system. There are obvious flaws with this method as the protein could interact with other components of the MRN complex but not functionally carry out its physiological role although due to technical and time constraints this method was chosen.

Protein-protein interactions can be measured by several methods, one of the main methods is Co-IP, which describes a process of capturing and pulling down a specific protein based on an antibody-tagged bead which is specific for your protein of interest. Since the synthesised proteins contain tags, those tags can be used to pulldown the proteins of interest.

The results for the Co-IP of the APEX2 plasmids can be seen in figure 30. In part A, expression of the *mre11* plasmids was shown in the input along with the successful specific pulldown of the MRE11. RAD50 and NBS1 expression levels are similar in the input. RAD50 interacts with both C and N terminally APEX2 tagged MRE11 protein whereas NBS1 interacts with N terminally tagged only. In part B, expression of the *rad50* plasmids were shown in the input along with the successful specific pulldown of the RAD50 containing plasmids. NBS1 expression levels were similar in the input, although MRE11 levels were not clearly visible. MRE11 and NBS1 seem to interact with only the C-terminus APEX2 tagged RAD50 plasmid but not the N-terminally APEX2 tagged plasmid. In part C expression of the NBS1 plasmids was shown in the input along with the successful specific pulldown of the NBS1 containing plasmids. MRE11 expression levels were similar in the input although RAD50 expression was variable. MRE11 interacts with both C and N tagged NBS1 proteins whereas RAD50 faintly interacts only with N terminally tagged.

These results imply that the N-tagged *mre11* vector, C-tagged *rad50* vector and N-tagged *nbn* vector should be used for downstream stable line generation as they interacted with the expected proteins that form the MRN complex and are assumed to be functional proteins. This may imply that the APEX2 tagging interferes with the proteins function as it is a 27kDa protein therefore may alter the structure, function and interacting partners of the protein. Although the western blot or the co-immunoprecipitation (co-IPs) experiments were not repeated as these results were expected and mainly used for validation, furthermore downstream experiments e.g., further co-IPs and denaturing immunoprecipitation would also give similar results. Although to

confidently conclude that APEX2 effected the structure and function of the proteins, this experiment would need to be repeated.

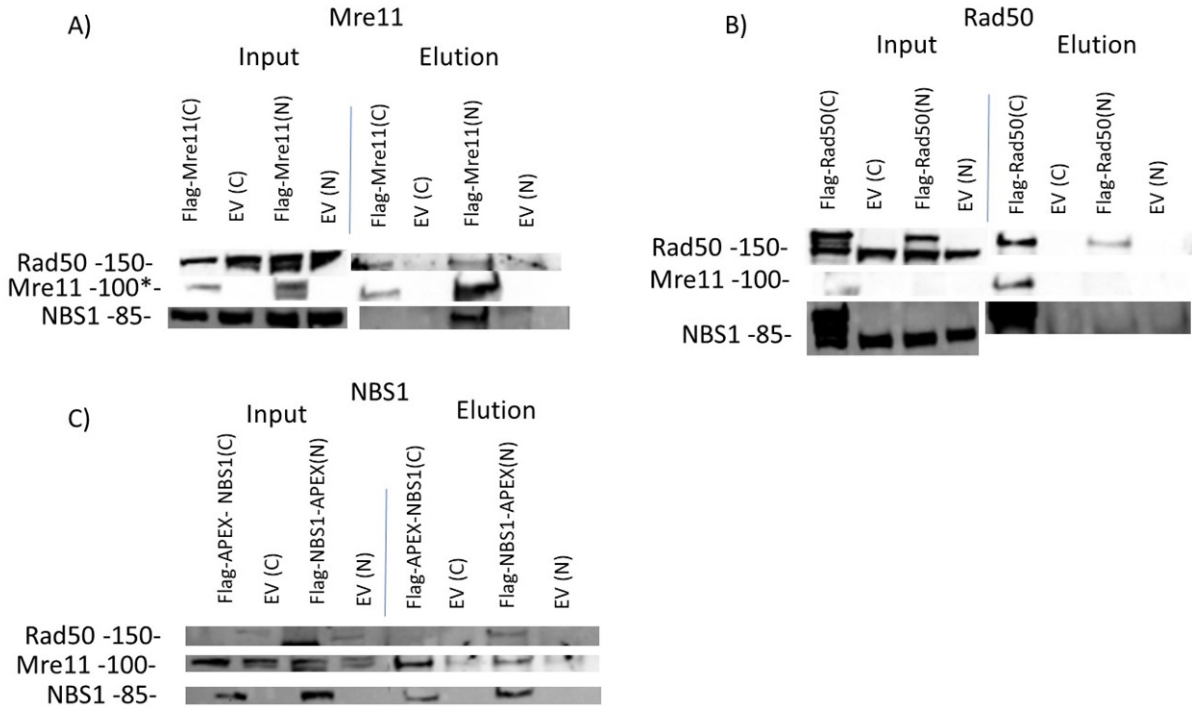


Figure 30. Co-Immunoprecipitation (Co-IP) testing of functionality of APEX2 synthetic plasmids.

*A-C) Western blot of Co-IP on 9% acrylamide gels. Cells have been transfected with FLAG tagged GOI (M, R, N) with APEX2 on the C or N terminus of the protein inducing overexpression. A) Overexpression of MRE11 APEX2 proteins. Blotting using anti-RAD50, anti-FLAG and anti-NBS1 were completed. Expression of the MRE11 plasmids is shown in the input along with the successful specific pulldown of the MRE11 containing plasmids. RAD50 and NBS1 expression levels are similar in the input. RAD50 interacts with both C and N terminally APEX2 tagged MRE11 plasmids whereas NBS1 interacts with N terminally tagged only. B) Overexpression of RAD50 APEX2 proteins. Blotting using anti-RAD50, anti-MRE11 and anti-NBS1 were completed. Expression of the RAD50 plasmids is shown in the input along with the successful specific pulldown of the RAD50 containing plasmids. NBS1 expression levels are similar in the input, although MRE11 levels are not clearly visible. MRE11 and NBS1 seem to interact with only the C-terminus APEX2 tagged RAD50 plasmid but not the N-terminally APEX2 tagged plasmid. C) Overexpression of NBS1 APEX2 proteins. Blotting using anti-RAD50, anti-MRE11 and anti-FLAG were completed. Expression of the NBS1 plasmids is shown in the input along with the successful specific pulldown of the NBS1 containing plasmids. MRE11 expression levels are similar in the input although RAD50 expression is variable. MRE11 interacts with both C and N tagged NBS1 plasmids whereas RAD50 interacts with N terminally tagged only. POI protein/s of interest, EV – Empty Vector, SSH – streptavidin-streptavidin-hemagglutinin tag, M – MRE11, R – RAD50, N-NBS1, (C) - C terminally tagged POI, (N) - N terminally tagged POI. *MRE11 running higher than expected – different percentage gel used.*

4.10. Post-translational Modification Investigation

4.10.1. Denaturing Immunoprecipitation

To investigate the post-translational landscape of the MRN complex multiple denaturing immunoprecipitation assays focussing on ubiquitination and SUMOylation due to their role in p97

interactomics were initially completed (representative figures in appendix 49 for MRE11 and appendix 51 for NBS1, data not shown for RAD50). Other lab members also attempted a similar assay (appendix 50) although in all cases ubiquitination, SUMO1 and SUMO2/3 was not observed. DIP describes a method where a specific protein is pulled down similar to CO-IP although all the interactions are washed off and the protein denatured, leaving only covalently bound residues on the protein of interest.

Initially no positive control was used therefore it was unclear if the lack of PTMs was a true negative result (appendix 49 and 50). RNF8 overexpression which is an E3 ubiquitin ligase which auto-ubiquitinates itself, would act as a positive control to ensure ubiquitination could be observed using DIP (118). Appendix 51 shows preliminary results of RNF8 ubiquitination, although due to human error the anti-RNF8/FLAG blot did not work therefore it was not certain that the RNF8-FLAG protein was overexpressed and specifically pulled down. This indicated that the DIP worked as the positive control of RNF8 identified ubiquitination.

A separate observation that may have affected the results was that the anti-ubiquitin antibody was not that sensitive, and that tagged ubiquitin overexpression was likely required to observe ubiquitination via the more sensitive anti-HA antibody. This was checked and confirmed in figure 31 via Co-IP where only the anti-HA antibody was sensitive enough to visualise ubiquitin chains, as even with ubiquitin overexpression the ubiquitin antibody was not sensitive enough. As a result, a new antibody was ordered from a recent paper that observed MRN ubiquitin and SUMOylation (58).

Further denaturing IP attempts by myself and others found that MRE11 was not observed to be ubiquitinated or SUMOylated even with tagged ubiquitin overexpression (data not shown and appendix 50). This is contradictory to the literature which have found each component of the MRN complex to be ubiquitinated by both high-throughput (101) and mechanistic studies (58, 95, 182).

4.10.2. Co-Immunoprecipitation

Using ‘native’ or Co-IP where the solvent concentrations are not as harsh has been seen to increase PTM signal observation in our lab for an unknown reason. Therefore, due to the difficulties of performing DIP and the uncertainty of the ubiquitination status of the MRN complex, a Co-IP was performed where MRE11 was overexpressed and pulled down (figure 31). This would investigate if any of the proteins interacting with MRE11 are ubiquitinated.

The Co-IP identified successful MRE11 overexpression and specific pulldown, as well as pulling down RAD50 in the elution highlighting interacting proteins are present in the eluate. The vinculin blot shows that a similar amount of protein was loaded in each well and identifies the pulldown was specific as it was not present in the elution. There are two species which seem to be ubiquitinated at around 100 and 150 Kilodaltons in the HA (ubiquitin) blot. This is a similar weight to both MRE11 and NBS1 (around 100) and RAD50 (around 150), although this cannot be confirmed as the eluate was a homogeneous mixture of proteins that interact with MRE11. Despite the uncertainty it does represent progress to observing the PTMs of the MRN complex which will be explored in more detail in future.

In future other methods such as mass spectrometry using ‘di-gly’ sites, native and re-attempting denaturing IP with a different bait specific for the PTM investigated could be used to visualise MRN ubiquitination. Furthermore, increased protease inhibitors and potentially DUB inhibitors can be used to ensure the protein of interest is not modified after cell lysis.

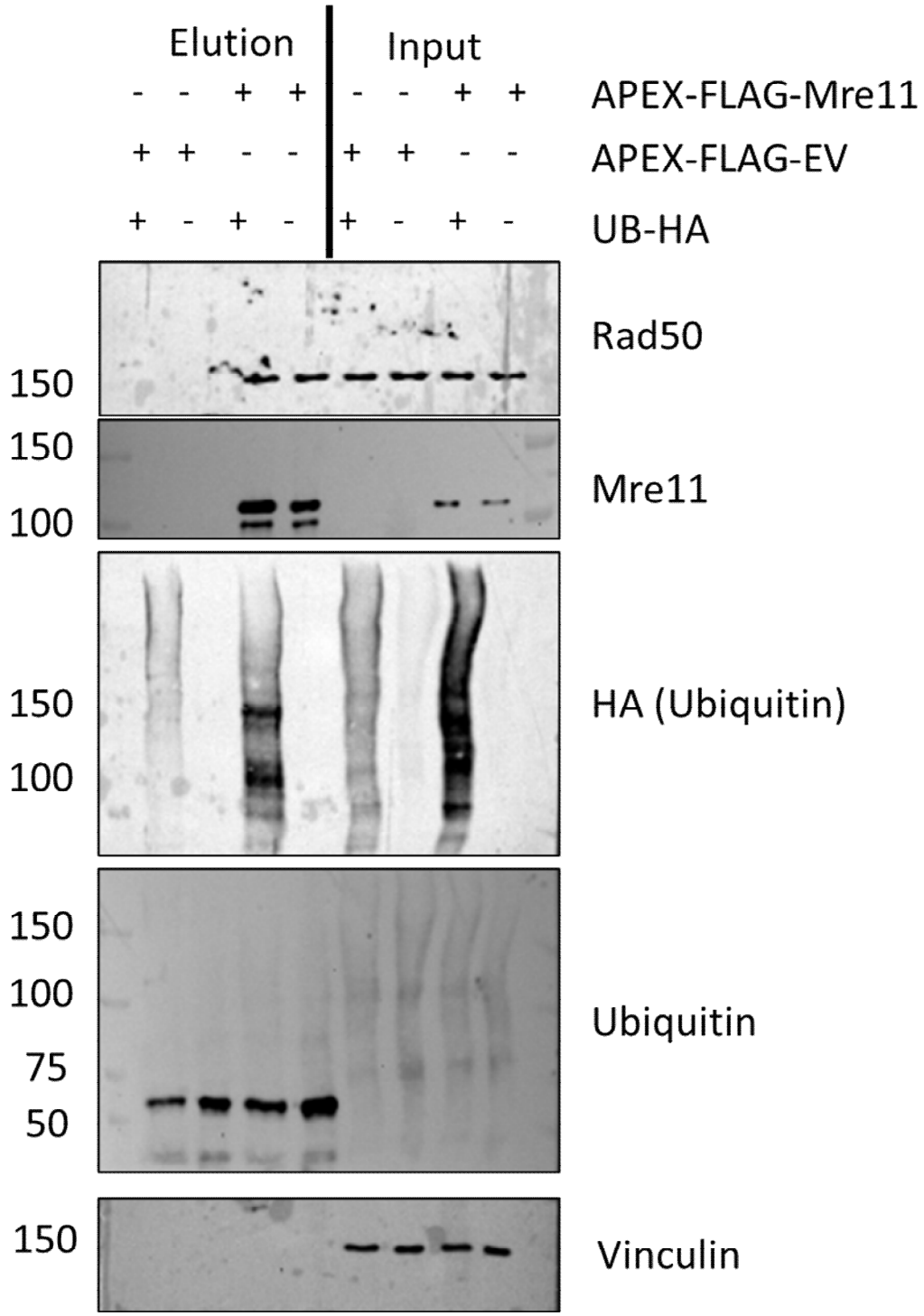


Figure 31. Co-immunoprecipitation of MRE11 to identify ubiquitination status of the MRN complex

The POI was expressed for 2 days where subsequent lysis and chromatin digestion via benzonase was completed to study the whole cell fraction. Flagged-tagged MRE11 is pulldown using magnetic flag beads and the elution is blotted along with the input (prior to bead capture) on 9% acrylamide gels. Blotting for anti- RAD50, MRE11, HA (ubiquitin), ubiquitin and vinculin is shown. It shows MRE11 over expressed and specifically pulled down in the elution, RAD50 was present in the elution only when FLAG_MRE11 is overexpressed and pulled down highlighting the co-IP was successful. Anti-ubiquitin Ig was shown to not be effective in recognising ubiquitin as Anti-HA shows a greater signal. Species at the molecular weight of MRE11 and

RAD50 (100 and 150 respectively) appear to be modified by ubiquitin in the elution. Anti-vinculin shows the specificity of the pulldown due to its appearance only in the input. Molecular weight markers are highlighted on the left in kilodaltons.

4.11. Stable Cell Line Generation

Using the plasmids made during the DNA assembly HiFi molecular cloning and validated downstream by western blotting and Co-IP, stable cell lines were made. These were made using the 'Flp-In' system where a FRT site was used along with the Flp recombinase to stably integrate a plasmid into the genome of a host cell line. An overview of this process can be seen below in figure 32. Generation of the stable cell lines was important prior to mass spectrometry so transient transfection efficiency is not a variable that could affect difference between conditions. It was also useful for biochemical experimentation due to the same reason.

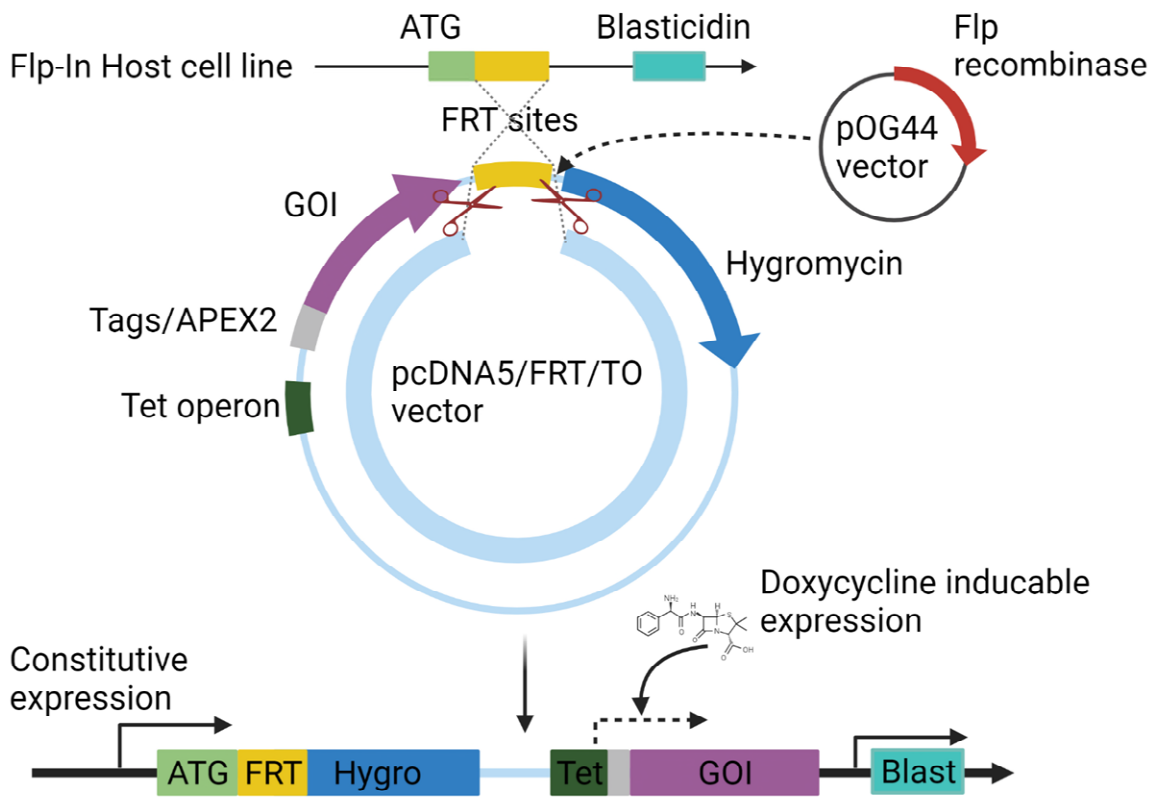


Figure 32. Schematic of the Flp-In system used to create stable cell lines.

Co-transfection of the pcDNA5 vector (containing the Tet operon, tags, APEX2, GOI and hygromycin resistance sequences) and the pOG44 vector containing the Flp recombinase allows for site directed insertion via homologous recombination of the pcDNA5 vector into the host cell line. Hygromycin and Blasticidin are constitutively expressed and used to select for stably transfected cells. Expression of the POI is induced with the addition of doxycycline due to the presence of tet-operon where doxycycline can bind and activate expression. Figure created with BioRender.com.

Stable cell line generation was completed by co-transfecting a Flp recombinase containing plasmid and the FRT containing plasmid of interest into a host FRT cell line. This host FRT cell line already contains a FRT site at a specific locus that is known to be expressed in the genome. HEK293 and HeLa FRT cell lines were used to generate these cell lines, resulting in 8 cell lines made (MRE11, NBS1, RAD50 and APEX2 alone in HEK293 and HeLa cell lines). The Flp recombinase containing plasmid gets expressed due to constitutive CMV promoter. This protein then catalyses a homologous recombination event between the FRT sites in the plasmid of interest and the host cell line at the FRT site in the genome (figure 32). This recombination event allows the plasmid to get stably integrated into the genome. This recombination causes the hygromycin gene to be expressed as insertion occurs at a start codon that is present prior to the FRT site. Without this insertion hygromycin does not contain a start codon therefore cannot be expressed (figure 32). Therefore, selection using hygromycin can be completed to select those clones which have stably integrated the plasmid. The expression of the protein of interest is controlled by an inducible promoter due to the presence of the tet operon. Doxycycline addition engages the tet operon and induces the expression of the protein of interest.

Selection occurs over multiple weeks. Subsequent expansion of positive clones was then completed where 10+ clones per construct are expanded to 10cm dishes, collected and frozen down.

5. Discussion

This thesis has outlined the work completed to create the necessary molecular tools to answer an important biological question of **how is p97 directed to disassemble the MRN complex from DNA after DSBs**. This question is based on the finding that p97 extracts MRE11 from chromatin and interacts with the MRN complex.

To answer this broad question several smaller questions are brought to light including which subunits of the MRN complex are required for disassembly, which residues are modified and by what type of

PTM, what E3 ligase/enzyme acts on the MRN complex, which PTM is recognised by p97 cofactors and by which co-factors, and why does dysregulation of the MRN complex disassembly result in excess end resection. Answering these questions will help us understand how MRN complex disassembly is regulated and identify enzymatic targets in the pathway. An ongoing collaboration was initiated during this MRes work between Professor Kristijan Ramadan and Professor Benedikt Kessler to answer these questions via APEX based proximity ligation assay followed by mass spectrometry, which will continue during my DPhil work.

Initial steps to answer these questions were completed where synthetic plasmids were made using the NEB HiFi DNA assembly system. The MRN complex proteins were cloned into C and N terminally tagged APEX2 and SSH tag containing vectors, creating 9 plasmids in total. These plasmids were validated using colony PCR and Sanger sequencing. The fusion proteins were then assessed in a mammalian system using western blotting and co-immunoprecipitation techniques to verify expression and functionality respectively. It was found that all 9 plasmids were adequately expressed and most of the fusion proteins interacted with the other components of the MRN complex. APEX2 seemed to disrupt the interaction of some of the tagged proteins, this finding was not repeated therefore this issue will be address in future work. Validated plasmids were then used to create stable cell lines in Hek293 and HeLa FRT cells, creating 8 stable cell lines in total. These cell lines will be validated via western blot assays of the protein of interest in the future, preceding APEX2 based mass spectrometry screening. Frozen stable cell line samples will be validated to ensure stable integration and the protein of interest expressed in doxycycline present and not in absent conditions.

In parallel to molecular cloning and stable cell line generation, the post-translational modification status of the MRN complex was investigated using immunoprecipitation assays. Despite some technical difficulties, ubiquitinylation events were observed at MRE11/NBS1 and RAD50 molecular weights using Co-IP, which concurs with the literature (32, 95). Interestingly after multiple attempts by myself and others, ubiquitination of the MRN complex could not be observed using DIP.

Furthermore, ubiquitination was observed of RNF8 using DIP and of the MRN complex using Co-IP. This suggests that the strong denaturing conditions used in DIP modified the ubiquitination status of the MRN complex. This is unexpected as after lysis, protease inhibitors e.g., MEM should prevent DUB action and ubiquitination is a covalent interaction therefore is not thought to be lost. Interestingly, despite consensus that ubiquitination occurs on lysine residues there is evidence that other types of linkages can be formed with different types of bonds. The bonds formed on lysine residues are iso-peptide bonds which have a half-life of 400 years, whereas the bonds formed on other residues e.g., cystines form a thioester bond which are much more transient and could be affected by the denaturing conditions (114). This could be a mechanism explaining why the MRN complex ubiquitination status cannot be elucidated using DIP but can be using Co-IP. This work will be directly followed up by further co, denaturing and native IPs under different conditions to confirm the PTM status of the MRN complex.

It is unknown which E3 ubiquitin ligase(s) and p97 cofactor(s) modify and recognise the MRN complex, mediating the p97 interaction and end resection. Although preliminary work from our lab (appendix 52) highlights that knockdown of the E3 ligase UBE4A and p97 cofactor UBXD8 has the same effect on MRE11 and γH2AX foci as p97 inhibition. This indicates that these factors are involved in the p97 dependent removal of the MRN complex. Although further investigation is required to elucidate if these factors play a role in p97 and MRN complex crosstalk and if they are the sole players. To answer this question APEX2 mass spectrometry will be completed, a brief overview of which is below.

The stable cell lines will be irradiated and treated with biotin-phenol and H_2O_2 to induce biotin-phenoxyl radicals, inducing the biotinylation of nearby amino acids by the tagged APEX2 enzyme on the protein of interest (in a radius of roughly 20nm). The biotinylated proteins will then be isolated using a streptavidin-based purification from varying nuclear factions and analysed by non-labelled quantitative mass spectrometry (183). This technique will allow the creation of a dynamic interactome map of the MRN complex identifying both stably and transiently interacting partners, before and after

irradiation induced DNA damage. This will allow the elucidation of interacting partners that could be involved in the p97 dependent extraction of MRE11 e.g., cofactors and E3 ligases.

Advantages APEX2 has over other proximity-based methods are its smaller size and speed of labelling, although other methods like turbo-ID have been adapted to reduce this difference. Proximity based ligation assays have preference over immunoprecipitation purification techniques prior to mass spectrometry as all weak, strong, transient, and stable interactions can be elucidated. This allows better resolution of the interactome and limits background and negative signals.

Further mass spectrometry analysis may also be completed in parallel to identify dynamic PTMs sites of the MRN complex after treatment using 'digly' sites. This could be completed under depletion of the candidate hits, with and without IR, to observe the PTM difference in each condition. Allowing identification of E3 ligase(s) and p97 cofactor(s) that affect the PTM status of the MRN complex and whether these interactions are IR-inducible.

An alternative approach to mass spectrometry-based screening would be a functional genomic CRISPR-Cas9 screen to determine potential E3 ligases for the MRN complex relevant in cancer. Our lab has recently obtained a ubiquitin associated CRISPR screen which could be used. The effect of the CRISPR screen on MRN complex foci could be measured via immunofluorescence.

The candidate MRN/p97 interactors identified by the APEX2 mass spec screen will be followed up by numerous other methods such as immunoprecipitation, immunofluorescence, proximity-based labelling and cycloheximide chase experiments, in different conditions e.g., with and without IR, E3 ligase etc. Together this will allow validation of the APEX2 hits and potential discovery of new targetable enzymes in specific p97-coordinated pathways.

Investigation of how identified MRN/p97 interactors and PTM site's affect DNA end resection could be assessed by ssDNA assays such as the quantitative single molecule analysis of resection tracks (SMART) assay and the semi-quantitative BrdU assay under non-denaturing conditions (184). Similarly,

identified candidates and PTM site's role in DSB repair pathway choice and cell survival could be studied. Numerous assays such as FACS-based reporter assays and clonogenics/fluorescent-based cell survival assays using the incucyte, could be completed respectively. Furthermore, how the inactivation of candidates affects synthetic lethality and radiosensitisation across a panel of cancer cell lines could be studied. Together this would determine to what extent potential candidates are involved in the regulation of MRN-mediated DNA end resection, and how this affects DSB choice, and cell survival. Therefore, highlighting the impact to cancer formation and therapy.

Separate but related topics could also be explored such as how MRN complex phosphorylation is mechanistically involved with downstream disassembly from DNA and if this is connected to p97. ATM-dependent MRE11 phosphorylation at specific residues is required for MRE11 removal from DNA after DSBs. When this process is inhibited, it causes a similar phenotype to p97 inhibition (52). Since both inhibition of ATM dependent phosphorylation and p97 have similar phenotypes and proposed mechanisms it within reason to suggest that ATM phosphorylation of the MRN complex is involved in p97 dependent removal of MRE11. Speculatively, the phosphorylation could act as a phospho-degron signal, recruiting other factors e.g., E3 ligases and p97 cofactors aiding p97 in its function of removing MRE11. This could be studied by chemically inhibiting ATM after IR treatment to observe the effects on: p97 recruitment and interaction with the MRN complex, downstream E3 ligase and p97 co-factor recruitment and the ubiquitination/PTM status of the MRN complex. This could elucidate how MRN phosphorylation interplays with p97 involved processes after DSBs.

A further topic includes the investigation of how SUMOylation and UBQLN4 interplay with p97 dependent MRN complex disassembly. UBQLN4 facilitates the degradation of MRE11, (56) whilst SUMOylation protects MRE11 from ubiquitination and subsequent degradation (58). Despite these processes being proteasome dependent, it could be investigated if these actions are dependent on the p97 pathway. Furthermore, RAD50 interacts with RNF4 (59, 150) and is SUMOylated, which induces its degradation (58). Therefore, it would also be interesting to investigate if SUMOylation of

RAD50 after DSBs induces RNF4, a cofactor of p97, to ubiquitinate and degrade RAD50 in a STUbL, p97 dependent manner.

The MRN complex and p97 are both targets of drugs in development e.g., Telomelysin and CB-5339 (NCT04402541, (97), (Figure 16) and their inhibition have been postulated as radiosensitisers (15, 94, 168, 175). HR and the UPS are dysregulated and involved in progressive cancer along with key players in those pathways - the MRN complex and p97 (Figures 12 and 17) (94, 180). Therefore, understanding how these systems interact could aid in cancer prevention, diagnosis, and treatment. For example, characterising the E3 ligases or the p97 cofactors that regulate MRN complex disassembly could provide novel and more specific targets for drug development, potentially increasing efficacy and reducing side effects of current therapy.

The phenotype observed in many MRN dysregulations is excess end resection and ssDNA, enhanced reliance on SSA, genome instability, and cell death. Inducing this phenotype has been shown to shrink mouse xenografts and specifically target cancer cells (15, 56). Therefore, targeting MRN complex disassembly can lead to cancer specific toxicity.

Trapping of substrates on chromatin is a proposed mechanism of action of numerous drugs e.g., PARP and topoisomerase inhibitors. Therefore, uncovering how the MRN complex is disassembled could allow its manipulation to trap is on chromatin, inducing cancer toxicity.

6. Conclusion

This thesis outlines the generation and validation of plasmids which were used to generate stable cell lines. The stable cell lines are to be used as the model system to generate downstream ‘big data’ via the APEX2 based proximity ligation assay of the MRN complex followed by mass spectrometry in conditions with/without ionising radiation (IR). This will create interatomic data that can inform downstream analysis and unbiased conclusions, allowing elucidation of the overarching research aims of how the MRN complex is disassembled from DSB after IR. In parallel to generation of the model

system, investigation of the post translation modifications (PTMs) of the MRN complex has been completed by various immunoprecipitation methods. This investigation outlines the difficultly in observing PTMs although despite this, components of the MRN complex are possibly ubiquitinated. As a result of this work experimental and intellectual expertise have been developed which will continue to be honed during the continuation of this project during my DPhil.

Word count – 27,143 including figure legends, titles, and in-text citations.

7.References

1. Chan K-F, Koukouravas S, Yeo JY, Koh DW-S, Gan SK-E. Probability of change in life: Amino acid changes in single nucleotide substitutions. Biosystems. 2020;193-194:104135.
2. Hanahan D, Weinberg RA. The hallmarks of cancer. cell. 2000;100(1):57-70.
3. Hanahan D, Weinberg Robert A. Hallmarks of Cancer: The Next Generation. Cell. 2011;144(5):646-74.
4. Hanahan D. Hallmarks of Cancer: New Dimensions. Cancer Discovery. 2022;12(1):31-46.
5. Hao D, Wang L, Di L-j. Distinct mutation accumulation rates among tissues determine the variation in cancer risk. Scientific Reports. 2016;6(1):19458.
6. Maxwell KN, Wubbenhorst B, Wenz BM, De Sloover D, Pluta J, Emery L, et al. BRCA locus-specific loss of heterozygosity in germline BRCA1 and BRCA2 carriers. Nat Commun. 2017;8(1):319.
7. Ciccia A, Elledge SJ. The DNA damage response: making it safe to play with knives. Mol Cell. 2010;40(2):179-204.
8. Jackson SP, Bartek J. The DNA-damage response in human biology and disease. Nature. 2009;461(7267):1071-8.
9. Su Y, Meador JA, Geard CR, Balajee AS. Analysis of ionizing radiation-induced DNA damage and repair in three-dimensional human skin model system. Exp Dermatol. 2010;19(8):e16-22.
10. Lomax ME, Folkes LK, O'Neill P. Biological Consequences of Radiation-induced DNA Damage: Relevance to Radiotherapy. Clinical Oncology. 2013;25(10):578-85.
11. Nickoloff JA, Sharma N, Allen CP, Taylor L, Allen SJ, Jaiswal AS, et al. Roles of homologous recombination in response to ionizing radiation-induced DNA damage. International Journal of Radiation Biology. 2021:1-12.
12. van de Kamp G, Heemskerk T, Kanaar R, Essers J. DNA Double Strand Break Repair Pathways in Response to Different Types of Ionizing Radiation. Front Genet. 2021;12:738230.
13. Vignard J, Mirey G, Salles B. Ionizing-radiation induced DNA double-strand breaks: A direct and indirect lighting up. Radiotherapy and Oncology. 2013;108(3):362-9.
14. Steel GG, McMillan TJ, Peacock J. The 5Rs of radiobiology. International journal of radiation biology. 1989;56(6):1045-8.
15. Kilgas S, Singh AN, Paillas S, Then CK, Torrecilla I, Nicholson J, et al. p97/VCP inhibition causes excessive MRE11-dependent DNA end resection promoting cell killing after ionizing radiation. Cell Rep. 2021;35(8):109153.
16. Zeng Y, Jie X, Wu B, Wu G, Liu L, Xu S. IQGAP3 interacts with Rad17 to recruit the Mre11-Rad50-Nbs1 complex and contributes to radioresistance in lung cancer. Cancer Letters. 2020;493:254-65.
17. Chen C, Wang Y, Mei JF, Li SS, Xu HX, Xiong HP, et al. Targeting RAD50 increases sensitivity to radiotherapy in colorectal cancer cells. Neoplasma. 2018;65(1):75-80.

18. Liu C, Liao K, Gross N, Wang Z, Li G, Zuo W, et al. Homologous recombination enhances radioresistance in hypopharyngeal cancer cell line by targeting DNA damage response. Oral Oncology. 2020;100:104469.
19. Wang Z, Zuo W, Zeng Q, Li Y, Lu T, Bu Y, et al. The Homologous Recombination Repair Pathway is Associated with Resistance to Radiotherapy in Nasopharyngeal Carcinoma. Int J Biol Sci. 2020;16(3):408-19.
20. Lim YC, Roberts TL, Day BW, Harding A, Kozlov S, Kijas AW, et al. A role for homologous recombination and abnormal cell-cycle progression in radioresistance of glioma-initiating cells. Mol Cancer Ther. 2012;11(9):1863-72.
21. Krenning L, van den Berg J, Medema RH. Life or Death after a Break: What Determines the Choice? Molecular Cell. 2019;76(2):346-58.
22. Ceccaldi R, Rondinelli B, D'Andrea AD. Repair Pathway Choices and Consequences at the Double-Strand Break. Trends in Cell Biology. 2016;26(1):52-64.
23. Kochan JA, Desclos ECB, Bosch R, Meister L, Vriend LEM, van Attikum H, et al. Meta-analysis of DNA double-strand break response kinetics. Nucleic Acids Res. 2017;45(22):12625-37.
24. Blackford AN, Jackson SP. ATM, ATR, and DNA-PK: The Trinity at the Heart of the DNA Damage Response. Molecular Cell. 2017;66(6):801-17.
25. Wilson J, Loizou JI. Exploring the genetic space of the DNA damage response for cancer therapy through CRISPR-based screens. Molecular Oncology. 2022;n/a(n/a).
26. Kilgas S. p97/VCP regulates MRE11-dependent DNA and resection and alters cellular toxicity of ionising radiation: University of Oxford; 2022.
27. Syed A, Tainer JA. The MRE11-RAD50-NBS1 Complex Conducts the Orchestration of Damage Signaling and Outcomes to Stress in DNA Replication and Repair. Annu Rev Biochem. 2018;87:263-94.
28. Oh J, Symington LS. Role of the Mre11 Complex in Preserving Genome Integrity. Genes. 2018;9(12):589.
29. Whelan DR, Rothenberg E. Super-resolution mapping of cellular double-strand break resection complexes during homologous recombination. Proceedings of the National Academy of Sciences. 2021;118(11):e2021963118.
30. Bian L, Meng Y, Zhang M, Li D. MRE11-RAD50-NBS1 complex alterations and DNA damage response: implications for cancer treatment. Molecular Cancer. 2019;18(1):169.
31. Marsella A, Cassani C, Casari E, Tisi R, Longhese MP. Structure-function relationships of the Mre11 protein in the control of DNA end bridging and processing. Curr Genet. 2019;65(1):11-6.
32. Zhang T, Zhou Z, Yang H, Wang W. MRE11-RAD50-NBS1-CtIP: one key nuclease ensemble functions in the maintenance of genome stability. Genome Instability & Disease. 2022;3(3):123-35.
33. Schiller CB, Seifert FU, Linke-Winnebeck C, Hopfner K-P. Structural studies of DNA end detection and resection in homologous recombination. Cold Spring Harb Perspect Biol. 2014;6(10):a017962-a.
34. Lavin MF, Kozlov SV, Gatei M, Kijas AW. ATM-Dependent Phosphorylation of All Three Members of the MRN Complex: From Sensor to Adaptor. Biomolecules. 2015;5:2877 - 902.
35. Myler LR, Gallardo IF, Soniat MM, Deshpande RA, Gonzalez XB, Kim Y, et al. Single-molecule imaging reveals how Mre11-Rad50-Nbs1 initiates DNA break repair. Molecular cell. 2017;67(5):891-8. e4.
36. Cejka P, Symington LS. DNA End Resection: Mechanism and Control. Annual Review of Genetics. 2021;55(1):285-307.
37. von Morgen P, Burdova K, Flower TG, O'Reilly NJ, Boulton SJ, Smerdon SJ, et al. MRE11 stability is regulated by CK2-dependent interaction with R2TP complex. Oncogene. 2017;36(34):4943-50.
38. Zeng X, Zhao F, Cui G, Zhang Y, Deshpande RA, Chen Y, et al. METTL16 antagonizes MRE11-mediated DNA end resection and confers synthetic lethality to PARP inhibition in pancreatic ductal adenocarcinoma. Nature Cancer. 2022;3(9):1088-104.

39. Bai Y, Wang W, Li S, Zhan J, Li H, Zhao M, et al. C1QBP Promotes Homologous Recombination by Stabilizing MRE11 and Controlling the Assembly and Activation of MRE11/RAD50/NBS1 Complex. Mol Cell. 2019;75(6):1299-314.e6.
40. He YJ, Meghani K, Caron MC, Yang C, Ronato DA, Bian J, et al. DYNLL1 binds to MRE11 to limit DNA end resection in BRCA1-deficient cells. Nature. 2018;563(7732):522-6.
41. Liu H, Zhang H, Wang X, Tian Q, Hu Z, Peng C, et al. The Deubiquitylating Enzyme USP4 Cooperates with CtIP in DNA Double-Strand Break End Resection. Cell Rep. 2015;13(1):93-107.
42. Wijnhoven P, Konietzny R, Blackford AN, Travers J, Kessler BM, Nishi R, et al. USP4 Auto-Deubiquitylation Promotes Homologous Recombination. Mol Cell. 2015;60(3):362-73.
43. Lu CS, Truong LN, Aslanian A, Shi LZ, Li Y, Hwang PY, et al. The RING finger protein RNF8 ubiquitinates Nbs1 to promote DNA double-strand break repair by homologous recombination. J Biol Chem. 2012;287(52):43984-94.
44. Wang Y-L, Zhao W-W, Bai S-M, Feng L-L, Bie S-Y, Gong L, et al. MRNIP condensates promote DNA double-strand break sensing and end resection. Nat Commun. 2022;13(1):2638.
45. Gobbini E, Casari E, Colombo CV, Bonetti D, Longhese MP. The 9-1-1 Complex Controls Mre11 Nuclease and Checkpoint Activation during Short-Range Resection of DNA Double-Strand Breaks. Cell Reports. 2020;33(3):108287.
46. Gut F, Käshammer L, Lammens K, Bartho JD, Boggusch A-M, van de Logt E, et al. Structural mechanism of endonucleolytic processing of blocked DNA ends and hairpins by Mre11-Rad50. Molecular Cell. 2022.
47. Ranjha L, Howard SM, Cejka P. Main steps in DNA double-strand break repair: an introduction to homologous recombination and related processes. Chromosoma. 2018;127(2):187-214.
48. Reginato G, Cejka P. The MRE11 complex: A versatile toolkit for the repair of broken DNA. DNA Repair. 2020;91-92:102869.
49. Anand R, Jasrotia A, Bundschuh D, Howard SM, Ranjha L, Stucki M, et al. NBS1 promotes the endonuclease activity of the MRE11-RAD50 complex by sensing CtIP phosphorylation. The EMBO journal. 2019;38(7):e101005.
50. Paull TT. 20 Years of Mre11 Biology: No End in Sight. Molecular Cell. 2018;71(3):419-27.
51. Shibata A, Moiani D, Arvai AS, Perry J, Harding SM, Genois MM, et al. DNA double-strand break repair pathway choice is directed by distinct MRE11 nuclease activities. Mol Cell. 2014;53(1):7-18.
52. Kijas AW, Lim YC, Bolderson E, Cerosaletti K, Gatei M, Jakob B, et al. ATM-dependent phosphorylation of MRE11 controls extent of resection during homology directed repair by signalling through Exonuclease 1. Nucleic Acids Res. 2015;43(17):8352-67.
53. Paudyal SC, You Z. Sharpening the ends for repair: mechanisms and regulation of DNA resection. Acta biochimica et biophysica Sinica. 2016;48 7:647-57.
54. Torrecilla I, Oehler J, Ramadan K. The role of ubiquitin-dependent segregase p97 (VCP or Cdc48) in chromatin dynamics after DNA double strand breaks. Philos Trans R Soc Lond B Biol Sci. 2017;372(1731).
55. Murakami T, Shoji Y, Nishi T, Chang SC, Jachimowicz RD, Hoshimoto S, et al. Regulation of MRE11A by UBQLN4 leads to cisplatin resistance in patients with esophageal squamous cell carcinoma. Mol Oncol. 2021;15(4):1069-87.
56. Jachimowicz RD, Beleggia F, Isensee J, Velpula BB, Goergens J, Bustos MA, et al. UBQLN4 Represses Homologous Recombination and Is Overexpressed in Aggressive Tumors. Cell. 2019;176(3):505-19 e22.
57. Jachimowicz RD, Reinhardt HC. UBQLN4 promotes non-homologous end joining by repressing DNA end-resection. Molecular & Cellular Oncology. 2019;6(2):1-3.
58. Zhang T, Yang H, Zhou Z, Bai Y, Wang J, Wang W. Crosstalk between SUMOylation and ubiquitylation controls DNA end resection by maintaining MRE11 homeostasis on chromatin. Nat Commun. 2022;13(1):5133.

59. Kumar R, González-Prieto R, Xiao Z, Verlaan-de Vries M, Vertegaal ACO. The STUbL RNF4 regulates protein group SUMOylation by targeting the SUMO conjugation machinery. Nat Commun. 2017;8(1):1809.
60. Buchberger A, Schindelin H, Hänzelmann P. Control of p97 function by cofactor binding. FEBS Lett. 2015;589(19 Pt A):2578-89.
61. Li Z, Li J, Kong Y, Yan S, Ahmad N, Liu X. Plk1 Phosphorylation of Mre11 Antagonizes the DNA Damage Response. Cancer Res. 2017;77(12):3169-80.
62. Di Virgilio M, Ying CY, Gautier J. PIKK-dependent phosphorylation of Mre11 induces MRN complex inactivation by disassembly from chromatin. DNA Repair (Amst). 2009;8(11):1311-20.
63. Langerak P, Mejia-Ramirez E, Limbo O, Russell P. Release of Ku and MRN from DNA Ends by Mre11 Nuclease Activity and Ctp1 Is Required for Homologous Recombination Repair of Double-Strand Breaks. PLOS Genetics. 2011;7(9):e1002271.
64. Han J, Wan L, Jiang G, Cao L, Xia F, Tian T, et al. ATM controls the extent of DNA end resection by eliciting sequential posttranslational modifications of CtIP. Proceedings of the National Academy of Sciences. 2021;118(12):e2022600118.
65. Nimonkar AV, Genschel J, Kinoshita E, Polaczek P, Campbell JL, Wyman C, et al. BLM-DNA2-RPA-MRN and EXO1-BLM-RPA-MRN constitute two DNA end resection machineries for human DNA break repair. Genes Dev. 2011;25(4):350-62.
66. van de Kooij B, Kruswick A, van Attikum H, Yaffe MB. Multi-pathway DNA-repair reporters reveal competition between end-joining, single-strand annealing and homologous recombination at Cas9-induced DNA double-strand breaks. Nat Commun. 2022;13(1):5295.
67. Ouyang J, Yadav T, Zhang JM, Yang H, Rheinbay E, Guo H, et al. RNA transcripts stimulate homologous recombination by forming DR-loops. Nature. 2021;594(7862):283-8.
68. Liu S, Hua Y, Wang J, Li L, Yuan J, Zhang B, et al. RNA polymerase III is required for the repair of DNA double-strand breaks by homologous recombination. Cell. 2021;184(5):1314-29.e10.
69. Kleinberger T. En Guard! The Interactions between Adenoviruses and the DNA Damage Response. Viruses. 2020;12(9).
70. Kieffer SR, Lowndes NF. Immediate-Early, Early, and Late Responses to DNA Double Stranded Breaks. Front Genet. 2022;13:793884.
71. Daley JM, Sung P. 53BP1, BRCA1, and the choice between recombination and end joining at DNA double-strand breaks. Mol Cell Biol. 2014;34(8):1380-8.
72. Ochs F, Somyajit K, Altmeyer M, Rask MB, Lukas J, Lukas C. 53BP1 fosters fidelity of homology-directed DNA repair. Nat Struct Mol Biol. 2016;23(8):714-21.
73. Nakada S. Opposing roles of RNF8/RNF168 and deubiquitinating enzymes in ubiquitination-dependent DNA double-strand break response signaling and DNA-repair pathway choice. J Radiat Res. 2016;57 Suppl 1(Suppl 1):i33-i40.
74. Meerang M, Ritz D, Paliwal S, Garajova Z, Bosshard M, Mailand N, et al. The ubiquitin-selective segregase VCP/p97 orchestrates the response to DNA double-strand breaks. Nat Cell Biol. 2011;13(11):1376-82.
75. Xu Y, Xu D. Repair pathway choice for double-strand breaks. Essays in Biochemistry. 2020;64(5):765-77.
76. Gnügge R, Symington LS. DNA end resection during homologous recombination. Current Opinion in Genetics & Development. 2021;71:99-105.
77. Zou L, Elledge SJ. Sensing DNA damage through ATRIP recognition of RPA-ssDNA complexes. Science. 2003;300(5625):1542-8.
78. Wright WD, Shah SS, Heyer W-D. Homologous recombination and the repair of DNA double-strand breaks. Journal of Biological Chemistry. 2018;293(27):10524-35.
79. Elbakry A, Löbrich M. Homologous Recombination Subpathways: A Tangle to Resolve. Front Genet. 2021;12:723847.
80. Guirouilh-Barbat J, Lambert S, Bertrand P, Lopez BS. Is homologous recombination really an error-free process? Frontiers in Genetics. 2014;5.

81. Kraus E, Leung W-Y, Haber JE. Break-induced replication: A review and an example in budding yeast. Proceedings of the National Academy of Sciences. 2001;98(15):8255-62.
82. Meyenberg M, Ferreira da Silva J, Loizou JI. Tissue Specific DNA Repair Outcomes Shape the Landscape of Genome Editing. Frontiers in Genetics. 2021;12.
83. Chiruvella KK, Liang Z, Wilson TE. Repair of double-strand breaks by end joining. Cold Spring Harb Perspect Biol. 2013;5(5):a012757.
84. Zhao X, Wei C, Li J, Xing P, Li J, Zheng S, et al. Cell cycle-dependent control of homologous recombination. Acta Biochimica et Biophysica Sinica. 2017;49(1672-9145):655.
85. Symington LS, Gautier J. Double-strand break end resection and repair pathway choice. Annu Rev Genet. 2011;45:247-71.
86. Caron P, Pobega E, Polo SE. DNA Double-Strand Break Repair: All Roads Lead to HeterochROMAtin Marks. Frontiers in Genetics. 2021;12.
87. Delabaere L, Ertl HA, Massey DJ, Hofley CM, Sohail F, Bienenstock EJ, et al. Aging impairs double-strand break repair by homologous recombination in Drosophila germ cells. Aging Cell. 2017;16(2):320-8.
88. Li Z, Zhang W, Chen Y, Guo W, Zhang J, Tang H, et al. Impaired DNA double-strand break repair contributes to the age-associated rise of genomic instability in humans. Cell Death & Differentiation. 2016;23(11):1765-77.
89. Ingram SP, Warmenhoven JW, Henthorn NT, Smith EAK, Chadwick AL, Burnet NG, et al. Mechanistic modelling supports entwined rather than exclusively competitive DNA double-strand break repair pathway. Scientific Reports. 2019;9(1):6359.
90. Ronato DA, Mersaoui SY, Busatto FF, Affar EB, Richard S, Masson J-Y. Limiting the DNA Double-Strand Break Resectosome for Genome Protection. Trends in Biochemical Sciences. 2020;45(9):779-93.
91. Zhu J, Petersen S, Tessarollo L, Nussenzweig A. Targeted disruption of the Nijmegen breakage syndrome gene NBS1 leads to early embryonic lethality in mice. Curr Biol. 2001;11(2):105-9.
92. Luo G, Yao MS, Bender CF, Mills M, Bladl AR, Bradley A, et al. Disruption of mRad50 causes embryonic stem cell lethality, abnormal embryonic development, and sensitivity to ionizing radiation. Proc Natl Acad Sci U S A. 1999;96(13):7376-81.
93. Wu S, Zhang Y, Zhang Y, Chen L-h, Ouyang H-f, Xu X, et al. Mutational landscape of homologous recombination-related genes in small-cell lung cancer. Cancer Medicine. 2022;n/a(n/a).
94. Wang YY, Hung AC, Lo S, Hsieh YC, Yuan SF. MRE11 as a molecular signature and therapeutic target for cancer treatment with radiotherapy. Cancer Lett. 2021;514:1-11.
95. Lu R, Zhang H, Jiang YN, Wang ZQ, Sun L, Zhou ZW. Post-Translational Modification of MRE11: Its Implication in DDR and Diseases. Genes (Basel). 2021;12(8).
96. Setton J, Zinda M, Riaz N, Durocher D, Zimmermann M, Koehler M, et al. Synthetic Lethality in Cancer Therapeutics: The Next Generation. Cancer Discovery. 2021;11(7):1626-35.
97. Taguchi S, Fukuhara H, Todo T. Oncolytic virus therapy in Japan: progress in clinical trials and future perspectives. Jpn J Clin Oncol. 2019;49(3):201-9.
98. Rajecki M, af Hällström T, Hakkarainen T, Nokisalmi P, Hautaniemi S, Nieminen AI, et al. Mre11 inhibition by oncolytic adenovirus associates with autophagy and underlies synergy with ionizing radiation. Int J Cancer. 2009;125(10):2441-9.
99. Kuroda S, Fujiwara T, Shirakawa Y, Yamasaki Y, Yano S, Uno F, et al. Telomerase-dependent oncolytic adenovirus sensitizes human cancer cells to ionizing radiation via inhibition of DNA repair machinery. Cancer Res. 2010;70(22):9339-48.
100. Sanford EJ, Smolka MB. A field guide to the proteomics of post-translational modifications in DNA repair. Proteomics. 2022:e2200064.
101. Akimov V, Barrio-Hernandez I, Hansen SVF, Hallenborg P, Pedersen A-K, Bekker-Jensen DB, et al. UbiSite approach for comprehensive mapping of lysine and N-terminal ubiquitination sites. Nature Structural & Molecular Biology. 2018;25(7):631-40.

102. Hendriks IA, Vertegaal ACO. A comprehensive compilation of SUMO proteomics. Nature Reviews Molecular Cell Biology. 2016;17(9):581-95.
103. Elia Andrew EH, Boardman Alexander P, Wang David C, Huttlin Edward L, Everley Robert A, Dephoure N, et al. Quantitative Proteomic Atlas of Ubiquitination and Acetylation in the DNA Damage Response. Molecular Cell. 2015;59(5):867-81.
104. Himmels S-F, Sartori AA. Controlling DNA-End Resection: An Emerging Task for Ubiquitin and SUMO. Frontiers in Genetics. 2016;7.
105. Trulsson F, Akimov V, Robu M, van Overbeek N, Berrocal DAP, Shah RG, et al. Deubiquitinating enzymes and the proteasome regulate preferential sets of ubiquitin substrates. Nat Commun. 2022;13(1):2736.
106. Huttlin EL, Bruckner RJ, Navarrete-Perea J, Cannon JR, Baltier K, Gebreab F, et al. Dual proteome-scale networks reveal cell-specific remodeling of the human interactome. Cell. 2021;184(11):3022-40.e28.
107. Huttlin EL, Ting L, Bruckner RJ, Gebreab F, Gygi MP, Szpyt J, et al. The BioPlex Network: A Systematic Exploration of the Human Interactome. Cell. 2015;162(2):425-40.
108. Oughtred R, Rust J, Chang C, Breitkreutz BJ, Stark C, Willems A, et al. The BioGRID database: A comprehensive biomedical resource of curated protein, genetic, and chemical interactions. Protein Sci. 2021;30(1):187-200.
109. Bai M, Ti D, Mei Q, Liu J, Yan X, Chen D, et al. The Role of Posttranslational Modifications in DNA Repair. BioMed Research International. 2020;2020:7493902.
110. Monsalve DM, Campillo-Marcos I, Salzano M, Sanz-García M, Cantarero L, Lazo PA. VRK1 phosphorylates and protects NBS1 from ubiquitination and proteasomal degradation in response to DNA damage. Biochim Biophys Acta. 2016;1863(4):760-9.
111. Boisvert FM, Déry U, Masson JY, Richard S. Arginine methylation of MRE11 by PRMT1 is required for DNA damage checkpoint control. Genes Dev. 2005;19(6):671-6.
112. Sanchez-Bailon MP, Choi S-Y, Dufficy ER, Sharma K, McNee GS, Gunnell E, et al. Arginine methylation and ubiquitylation crosstalk controls DNA end-resection and homologous recombination repair. Nat Commun. 2021;12(1):6313.
113. Vadnais C, Chen R, Fraszczak J, Yu Z, Boulais J, Pinder J, et al. GFI1 facilitates efficient DNA repair by regulating PRMT1 dependent methylation of MRE11 and 53BP1. Nat Commun. 2018;9(1):1418.
114. Squair DR, Virdee S. A new dawn beyond lysine ubiquitination. Nature Chemical Biology. 2022;18(8):802-11.
115. George AJ, Hoffiz YC, Charles AJ, Zhu Y, Mabb AM. A Comprehensive Atlas of E3 Ubiquitin Ligase Mutations in Neurological Disorders. Frontiers in Genetics. 2018;9.
116. Yang Q, Zhao J, Chen D, Wang Y. E3 ubiquitin ligases: styles, structures and functions. Molecular Biomedicine. 2021;2(1):23.
117. Borsos BN, Majoros H, Pankotai T. Ubiquitylation-Mediated Fine-Tuning of DNA Double-Strand Break Repair. Cancers (Basel). 2020;12(6).
118. Singh AN, Oehler J, Torrecilla I, Kilgas S, Li S, Vaz B, et al. The p97-Ataxin 3 complex regulates homeostasis of the DNA damage response E3 ubiquitin ligase RNF8. EMBO J. 2019;38(21):e102361.
119. Baranes-Bachar K, Levy-Barda A, Oehler J, Reid DA, Soria-Bretones I, Voss TC, et al. The Ubiquitin E3/E4 Ligase UBE4A Adjusts Protein Ubiquitylation and Accumulation at Sites of DNA Damage, Facilitating Double-Strand Break Repair. Mol Cell. 2018;69(5):866-78.e7.
120. Wagner SA, Beli P, Weinert BT, Nielsen ML, Cox J, Mann M, et al. A Proteome-wide, Quantitative Survey of In Vivo Ubiquitylation Sites Reveals Widespread Regulatory Roles*. Molecular & Cellular Proteomics. 2011;10(10):M111.013284.
121. Du M, Gu J, Liu C, Liu N, Yu Z, Zhou C, et al. Genome-wide CRISPR screen identified Rad18 as a determinant of doxorubicin sensitivity in osteosarcoma. J Exp Clin Cancer Res. 2022;41(1):154.

122. Lee NS, Kim S, Jung YW, Kim H. Eukaryotic DNA damage responses: Homologous recombination factors and ubiquitin modification. Mutation Research/Fundamental and Molecular Mechanisms of Mutagenesis. 2018;809:88-98.
123. Rodríguez-Acebes S, Martín-Rufo R, Fernández-Llorente A, de la Vega-Barranco G, Oroz PB, Martín-Doncel E, et al. VCP/p97 extracts DNA polymerase α/Primase from chromatin to limit the activation of the replication stress response. bioRxiv. 2022.
124. Dantuma NP, Acs K, Luijsterburg MS. Should I stay or should I go: VCP/p97-mediated chromatin extraction in the DNA damage response. Exp Cell Res. 2014;329(1):9-17.
125. Nicholson J, Jevons SJ, Groselj B, Ellermann S, Konietzny R, Kerr M, et al. E3 Ligase cIAP2 Mediates Downregulation of MRE11 and Radiosensitization in Response to HDAC Inhibition in Bladder Cancer. Cancer Res. 2017;77(11):3027-39.
126. Wu J, Zhang X, Zhang L, Wu CY, Rezaeian AH, Chan CH, et al. Skp2 E3 ligase integrates ATM activation and homologous recombination repair by ubiquitinating NBS1. Mol Cell. 2012;46(3):351-61.
127. Kim H, Choi H, Im J-S, Park S-Y, Shin G, Yoo J-H, et al. Stable maintenance of the Mre11-Rad50-Nbs1 complex is sufficient to restore the DNA double-strand break response in cells lacking RecQL4 helicase activity. Journal of Biological Chemistry. 2021;297(4).
128. Qi L, Chakravarthy R, Li MM, Deng C-X, Li R, Hu Y. Phosphorylation of BRCA1 by ATM upon Double-Strand Breaks Impacts ATM Function in End-Resection: A Potential Feedback Loop. iScience. 2022:104944.
129. Yan W, Yang Y, Yang W. Inhibition of SKP2 activity impaired ATM-mediated DNA repair and enhanced sensitivity of cisplatin-resistant mantle cell lymphoma cells. Cancer Biotherapy and Radiopharmaceuticals. 2019;34(7):451-8.
130. Ha GH, Ji JH, Chae S, Park J, Kim S, Lee JK, et al. Pellino1 regulates reversible ATM activation via NBS1 ubiquitination at DNA double-strand breaks. Nat Commun. 2019;10(1):1577.
131. Zhang T, Cronshaw J, Kanu N, Snijders AP, Behrens A. UBR5-mediated ubiquitination of ATMIN is required for ionizing radiation-induced ATM signaling and function. Proc Natl Acad Sci U S A. 2014;111(33):12091-6.
132. Li CG, Mahon C, Sweeney NM, Verschueren E, Kantamani V, Li D, et al. PPARγ Interaction with UBR5/ATMIN Promotes DNA Repair to Maintain Endothelial Homeostasis. Cell Rep. 2019;26(5):1333-43.e7.
133. Sahay O, Barik GK, Sharma T, Pillai AD, Rapole S, Santra MK. Damsel in distress calling on her knights: Illuminating the pioneering role of E3 ubiquitin ligases in guarding the genome integrity. DNA Repair. 2022;109:103261.
134. Gao M, Guo G, Huang J, Kloeber JA, Zhao F, Deng M, et al. USP52 regulates DNA end resection and chemosensitivity through removing inhibitory ubiquitination from CtIP. Nat Commun. 2020;11(1):5362.
135. Su D, Ma S, Shan L, Wang Y, Wang Y, Cao C, et al. Ubiquitin-specific protease 7 sustains DNA damage response and promotes cervical carcinogenesis. J Clin Invest. 2018;128(10):4280-96.
136. Huang Q, Qin D, Pei D, Vermeulen M, Zhang X. UBE2O and USP7 co-regulate RECQL4 ubiquitinylation and homologous recombination-mediated DNA repair. Faseb j. 2022;36(1):e22112.
137. Castillo-Villanueva E, Ballesteros G, Schmid M, Hidalgo P, Schreiner S, Dobner T, et al. The Mre11 Cellular Protein Is Modified by Conjugation of Both SUMO-1 and SUMO-2/3 during Adenovirus Infection. ISRN Virology. 2014;2014:989160.
138. Sohn SY, Hearing P. Adenovirus regulates sumoylation of Mre11-Rad50-Nbs1 components through a paralog-specific mechanism. J Virol. 2012;86(18):9656-65.
139. Salas-Lloret D, González-Prieto R. Insights in Post-Translational Modifications: Ubiquitin and SUMO. Int J Mol Sci. 2022;23(6):3281.
140. Zhao Y, Brickner JR, Majid MC, Mosammaparast N. Crosstalk between ubiquitin and other post-translational modifications on chromatin during double-strand break repair. Trends in Cell Biology. 2014;24(7):426-34.

141. Galanty Y, Belotserkovskaya R, Coates J, Polo S, Miller KM, Jackson SP. Mammalian SUMO E3-ligases PIAS1 and PIAS4 promote responses to DNA double-strand breaks. Nature. 2009;462(7275):935-9.
142. Yu J, Qin B, Lou Z. Ubiquitin and ubiquitin-like molecules in DNA double strand break repair. Cell & Bioscience. 2020;10(1):13.
143. Owerbach D, McKay EM, Yeh ET, Gabbay KH, Bohren KM. A proline-90 residue unique to SUMO-4 prevents maturation and sumoylation. Biochem Biophys Res Commun. 2005;337(2):517-20.
144. Sarangi P, Zhao X. SUMO-mediated regulation of DNA damage repair and responses. Trends Biochem Sci. 2015;40(4):233-42.
145. Hendriks IA, Lyon D, Young C, Jensen LJ, Vertegaal ACO, Nielsen ML. Site-specific mapping of the human SUMO proteome reveals co-modification with phosphorylation. Nature Structural & Molecular Biology. 2017;24(3):325-36.
146. Cremona CA, Sarangi P, Yang Y, Hang LE, Rahman S, Zhao X. Extensive DNA damage-induced sumoylation contributes to replication and repair and acts in addition to the mec1 checkpoint. Mol Cell. 2012;45(3):422-32.
147. Psakhye I, Jentsch S. Protein group modification and synergy in the SUMO pathway as exemplified in DNA repair. Cell. 2012;151(4):807-20.
148. Chen Y-J, Chuang Y-C, Chuang C-N, Cheng Y-H, Chang C-R, Leng C-H, et al. S. cerevisiae Mre11 recruits conjugated SUMO moieties to facilitate the assembly and function of the Mre11-Rad50-Xrs2 complex. Nucleic Acids Res. 2016;44(5):2199-213.
149. Dhingra N, Zhao X. Intricate SUMO-based control of the homologous recombination machinery. Genes Dev. 2019;33(19-20):1346-54.
150. Kuo CY, Li X, Stark JM, Shih HM, Ann DK. RNF4 regulates DNA double-strand break repair in a cell cycle-dependent manner. Cell Cycle. 2016;15(6):787-98.
151. Dhingra N, Zhao X. Advances in SUMO-based regulation of homologous recombination. Current Opinion in Genetics & Development. 2021;71:114-9.
152. Yuan Z, Zhang X, Sengupta N, Lane WS, Seto E. SIRT1 regulates the function of the Nijmegen breakage syndrome protein. Mol Cell. 2007;27(1):149-62.
153. Wang Z, Gong Y, Peng B, Shi R, Fan D, Zhao H, et al. MRE11 UFMylation promotes ATM activation. Nucleic Acids Res. 2019;47(8):4124-35.
154. Lee L, Perez Oliva AB, Martinez-Balsalobre E, Churikov D, Peter J, Rahmouni D, et al. UFMylation of MRE11 is essential for telomere length maintenance and hematopoietic stem cell survival. Sci Adv. 2021;7(39):eabc7371.
155. Dhoonmoon A, Nicolae CM, Moldovan G-L. The KU-PARP14 axis differentially regulates DNA resection at stalled replication forks by MRE11 and EXO1. Nat Commun. 2022;13(1):5063.
156. Zhou J, Gu L, Shi Y, Huang T, Fan X, Bi X, et al. GSTpi reduces DNA damage and cell death by regulating the ubiquitination and nuclear translocation of NBS1. Cell Mol Life Sci. 2021;79(1):54.
157. Da Costa IC, Schmidt CK. Ubiquitin-like proteins in the DNA damage response: the next generation. Essays Biochem. 2020;64(5):737-52.
158. Tang M, Li S, Chen J. Ubiquitylation in DNA double-strand break repair. DNA Repair. 2021;103:103129.
159. Dantuma NP, van Attikum H. Spatiotemporal regulation of posttranslational modifications in the DNA damage response. The EMBO Journal. 2016;35(1):6-23.
160. Ye Y, Tang WK, Zhang T, Xia D. A Mighty “Protein Extractor” of the Cell: Structure and Function of the p97/CDC48 ATPase. Frontiers in Molecular Biosciences. 2017;4(39).
161. Vaz B, Halder S, Ramadan K. Role of p97/VCP (Cdc48) in genome stability. Frontiers in Genetics. 2013;4.
162. Hänzelmann P, Galgenmüller C, Schindelin H. Structure and Function of the AAA+ ATPase p97, a Key Player in Protein Homeostasis. Subcell Biochem. 2019;93:221-72.
163. Franz A, Ackermann L, Hoppe T. Ring of Change: CDC48/p97 Drives Protein Dynamics at Chromatin. Front Genet. 2016;7:73.

164. Ramadan K. p97/VCP- and Lys48-linked polyubiquitination form a new signaling pathway in DNA damage response. Cell Cycle. 2012;11(6):1062-9.
165. Krastev DB, Li S, Sun Y, Wicks AJ, Hoslett G, Weekes D, et al. The ubiquitin-dependent ATPase p97 removes cytotoxic trapped PARP1 from chromatin. Nature Cell Biology. 2022;24(1):62-73.
166. van den Boom J, Wolf M, Weimann L, Schulze N, Li F, Kaschani F, et al. VCP/p97 Extracts Sterically Trapped Ku70/80 Rings from DNA in Double-Strand Break Repair. Mol Cell. 2016;64(1):189-98.
167. Bergink S, Ammon T, Kern M, Schermelleh L, Leonhardt H, Jentsch S. Role of Cdc48/p97 as a SUMO-targeted segregase curbing Rad51-Rad52 interaction. Nat Cell Biol. 2013;15(5):526-32.
168. Costantini S, Capone F, Polo A, Bagnara P, Budillon A. Valosin-Containing Protein (VCP)/p97: A Prognostic Biomarker and Therapeutic Target in Cancer. Int J Mol Sci. 2021;22.
169. Tokheim C, Wang X, Timms RT, Zhang B, Mena EL, Wang B, et al. Systematic characterization of mutations altering protein degradation in human cancers. Mol Cell. 2021;81(6):1292-308.e11.
170. Shen M, Schmitt S, Buac D, Dou QP. Targeting the ubiquitin-proteasome system for cancer therapy. Expert Opin Ther Targets. 2013;17(9):1091-108.
171. Chen D, Frezza M, Schmitt S, Kanwar JSS, Dou QP. Bortezomib as the first proteasome inhibitor anticancer drug: current status and future perspectives. Current cancer drug targets. 2011;11 3:239-53.
172. Hänzelmann P, Schindelin H. The Interplay of Cofactor Interactions and Post-translational Modifications in the Regulation of the AAA+ ATPase p97. Front Mol Biosci. 2017;4:21.
173. van den Boom J, Meyer H. VCP/p97-Mediated Unfolding as a Principle in Protein Homeostasis and Signaling. Mol Cell. 2018;69(2):182-94.
174. Acs K, Luijsterburg MS, Ackermann L, Salomons FA, Hoppe T, Dantuma NP. The AAA-ATPase VCP/p97 promotes 53BP1 recruitment by removing L3MBTL1 from DNA double-strand breaks. Nature Structural & Molecular Biology. 2011;18(12):1345-50.
175. Jiang N, Shen Y, Fei X, Sheng K, Sun P, Qiu Y, et al. Valosin-containing protein regulates the proteasome-mediated degradation of DNA-PKcs in glioma cells. Cell Death & Disease. 2013;4(5):e647-e.
176. Na J, Newman JA, Then CK, Syed J, Vendrell I, Torrecilla I, et al. SPRTN protease-cleaved MRE11 decreases DNA repair and radiosensitises cancer cells. Cell Death & Disease. 2021;12(2):165.
177. Jones RM, Ruiz JH, Scaramuzza S, Nath S, Henklewska M, Natsume T, et al. Characterising replisome disassembly in human cells. bioRxiv. 2022.
178. Ramadan K, Halder S, Wiseman K, Vaz B. Strategic role of the ubiquitin-dependent segregase p97 (VCP or Cdc48) in DNA replication. Chromosoma. 2016;126:17-32.
179. Anderson DJ, Le Moigne R, Djakovic S, Kumar B, Rice J, Wong S, et al. Targeting the AAA ATPase p97 as an Approach to Treat Cancer through Disruption of Protein Homeostasis. Cancer Cell. 2015;28(5):653-65.
180. Huryn DM, Kornfilt DJP, Wipf P. p97: An Emerging Target for Cancer, Neurodegenerative Diseases, and Viral Infections. J Med Chem. 2020;63(5):1892-907.
181. Heidelberger JB, Voigt A, Borisova ME, Petrosino G, Ruf S, Wagner SA, et al. Proteomic profiling of VCP substrates links VCP to K6-linked ubiquitylation and c-Myc function. EMBO reports. 2018;19(4):e44754.
182. Su S, Zhang Y, Liu P. Roles of Ubiquitination and SUMOylation in DNA Damage Response. Curr Issues Mol Biol. 2020;35:59-84.
183. Trinkle-Mulcahy L. Recent advances in proximity-based labeling methods for interactome mapping. F1000Res. 2019;8.
184. Kilgas S, Kiltie AE, Ramadan K. Immunofluorescence microscopy-based detection of ssDNA foci by BrdU in mammalian cells. STAR protocols. 2021;2(4):100978.

8. Appendix

MRE11-HA pull down			
Mascot output (1% FDR)			
Description	Score	No. of significant sequences	emPAI
MRE11	419	9	0.59
RAD50	269	10	0.28
NBS1	247	5	0.25
VCP/p97	228	5	0.23

Figure 33. Mass spectrometry results from a MRE11 pulldown.

Highlighted are components of the MRN complex along with p97 showing the no. of significant sequences found, score indicating the match of the mass spectra to the reference mass and emPAI (exponentially modified protein abundance index) which estimates the abundance of peptides.

	SILAC RATIO					
	MRE11			RAD50		
	0.5h	8h	Peptides	0.5h	8h	Peptides
NUCLEAR	0.44	0.39	5	1.097	2.382	10
CHROMATIN/BENZ-SENSITIVE	1.22	0.37	3	N/A	N/A	8
CHROMATIN/BENZ-RESISTANT	1.09	0.81	14	1.48	1.67	41

Figure 34. Mass spectrometry results of p97 pulldown.

P97 EQ (catalytically inactive therefore induces substrate/interactome trapping) pulldown after ionising radiation treatment (IR) of 2 gray and recovery of either 0.5 or 8 hours, in different nuclear fractions. Results displayed as SILAC (Stable isotope labelling using amino acids in cell culture) ratios of non-IR (time point 0) vs IR and no. of peptides interacting with p97. Highlights p97 dynamically interacting with MRE11 and RAD50 in different subcellular fractions.

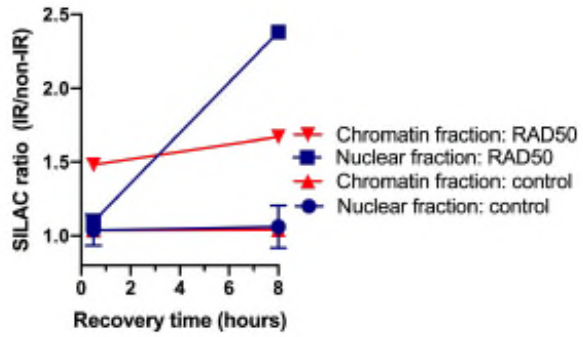


Figure 35. Graphical representation of table in Figure 17.

Showing the spatiotemporal dynamic interaction of RAD50 with p97 after ionising radiation, measured by SILAC (Stable isotope labelling using amino acids in cell culture) based mass spectrometry.

	LFQ RATIOS					
	MRE11		RAD50		NBS1	
	20m	6h	20m	6h	20m	6h
CYTOSOL	x	x	x	x	x	x
NUCLEOSOL	0.974179	-0.28349	0.138865	-0.06597	x	x
CHR-SOL	0.325067	0.607724	0.734472	0.027926	0.521749	0.478506
CHR-INS	0.069732	0.070194	-0.08982	0.127439	-1.07649	-0.23084

Figure 36. Mass spectrometry results of p97 pulldown.

P97 EQ (catalytically inactive therefore induces substrate/interactome trapping) pulldown after ionising radiation treatment (IR) of 2 gray and recovery of either 20 minutes or 6 hours, in different fractions. Results displayed as LFQ (Label free quantification) ratios of non-IR (time point 0) vs IR. Highlights p97 dynamically interacting with MRE11, RAD50 and NBS1 in different subcellular fractions

To amplify	Oligos	DNA template	Size (bp)
Mre11	322 + 323 ¦ MRE11_1_fw + MRE11_1_rv	Plasmid 507	2,145
Fragment 1	324 + 339 ¦ Mre11_2_fw + PGL35 Frag1_rev	Plasmid 317	2,584
Fragment 2	340 + 325 ¦ PGL35 Frag2_fwd + Mre11_2_rv	Plasmid 317	2,647

To amplify	Oligos	DNA template	Size (bp)
NBN	449 + 450 ¦ NBN_35_fw + NBN_35_rv	Plasmid 508	2,286
Fragment 1	436 + 448 ¦ PGL35_Frag1_fw + PGL35_Frag1_NBN_rv	Plasmid 502 (pGL35)	2,738
Fragment 2	451 + 437 ¦ PGL35_Frag2_NBN_fw + PGL35_Frag2_rv	Plasmid 502 (pGL35)	3,247

To amplify	Oligos	DNA template	Size (bp)
Rad50	330 + 331 ¦ RAD50_1_fw + RAD50_1_rv	Plasmid 505	3,960
pcDNA5	332 + 333 ¦ RAD50_2_fw + RAD50_2_rv	Plasmid 317	5,255

To amplify	Oligos	DNA template	Size (bp)
Rad50	441 + 442 ¦ RAD50_35_fw + RAD50_35_rv	Plasmid 505	3,960
Fragment 1	436 + 440 ¦ PGL35_Frag1_fw + PGL35_Frag1_RAD_rv	Plasmid 502 (pGL35)	2,738
Fragment 2	443 + 437 ¦ PGL35_Frag2_RAD_fw + PGL35_Frag2_rv	Plasmid 502 (pGL35)	3,247

To amplify	Oligos	DNA template	Size (bp)
Rad50a	441 + 435 ¦ RAD50_35_fw + Rad50_int2000_rv	Plasmid 505	1,976
Rad50b	434 + 442 ¦ Rad50_int2000_fw + RAD50_35_rv	Plasmid 505	1,984
Fragment 1	436 + 440 ¦ PGL35_Frag1_fw + PGL35_Frag1_RAD_rv	Plasmid 502 (pGL35)	2,738
Fragment 2	443 + 437 ¦ PGL35_Frag2_RAD_fw + PGL35_Frag2_rv	Plasmid 502 (pGL35)	3,247

Figure 37. Example of tables used for HiFi cloning to ensure correct PCR amplification prior to ligation.

Tables shows the oligonucleotides and DNA template used for the PCR reaction along with the expected size. This table corresponds to the agarose gels showed in Figures 6 and 7.

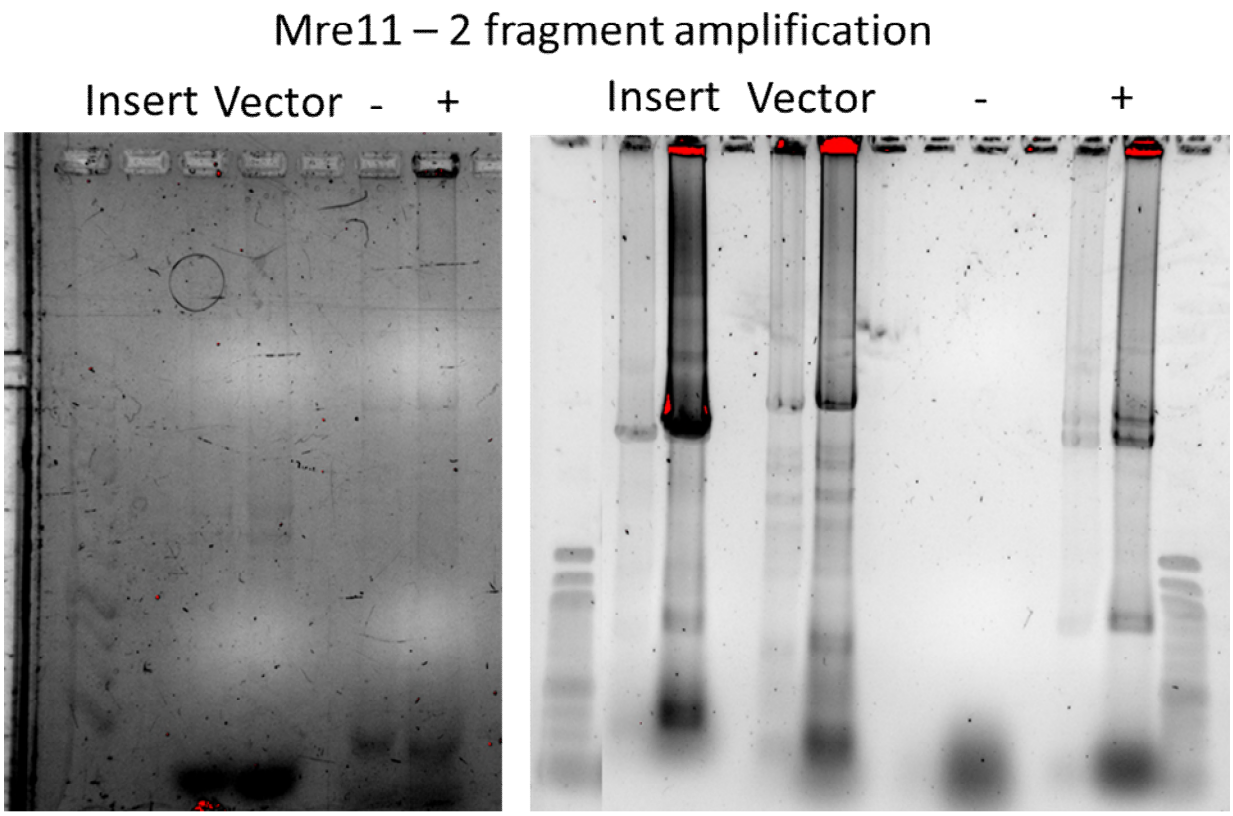


Figure 38. Candidate 1% agarose electrophoresis gel of PCR amplicons.

Highlighting the Failed amplification of MRE11 and pcDNA5. The image on the left highlights a negative result with no amplification occurring whereas the second image highlights a nonspecific amplification with multiple other bands of molecular weights more than expected. Positive control of a known MRE11 containing plasmid and negative control of no oligonucleotides in the PCR mixture are also highlighted.

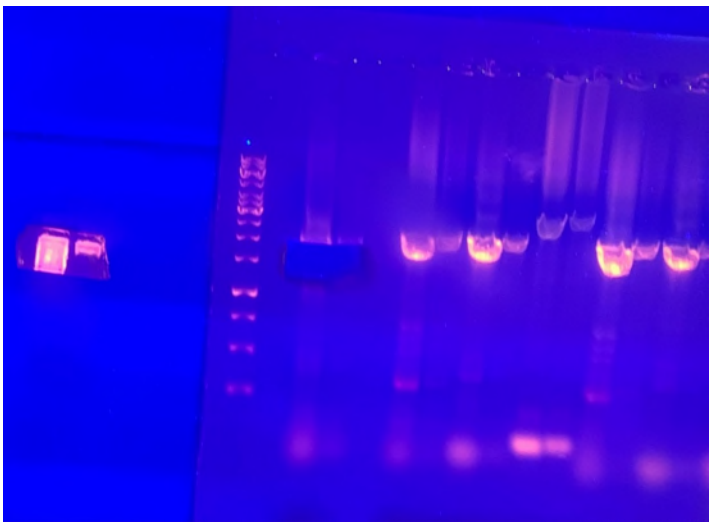


Figure 39. Band excision prior to gel extraction.

Using UV light specific bands are excised for downstream DNA purification via gel extraction allowing for the ligation to occur.

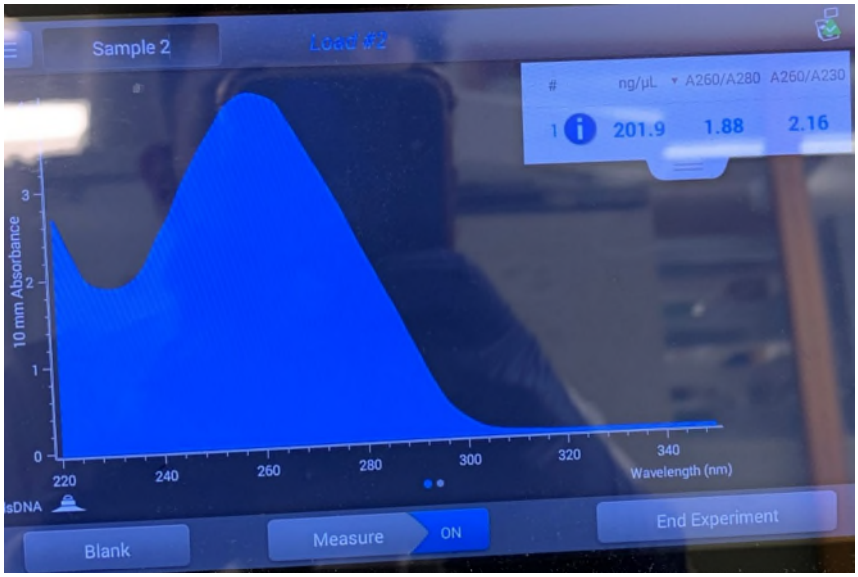


Figure 40. DNA quantification after gel extraction using nanodrop.

Showing the concentration in ng/µl as well as A260/A280 or A230 values which indicate purity. 1.8 is deemed pure for 260/280 and 2.2 for 260/230. Variations from this indicates contaminants

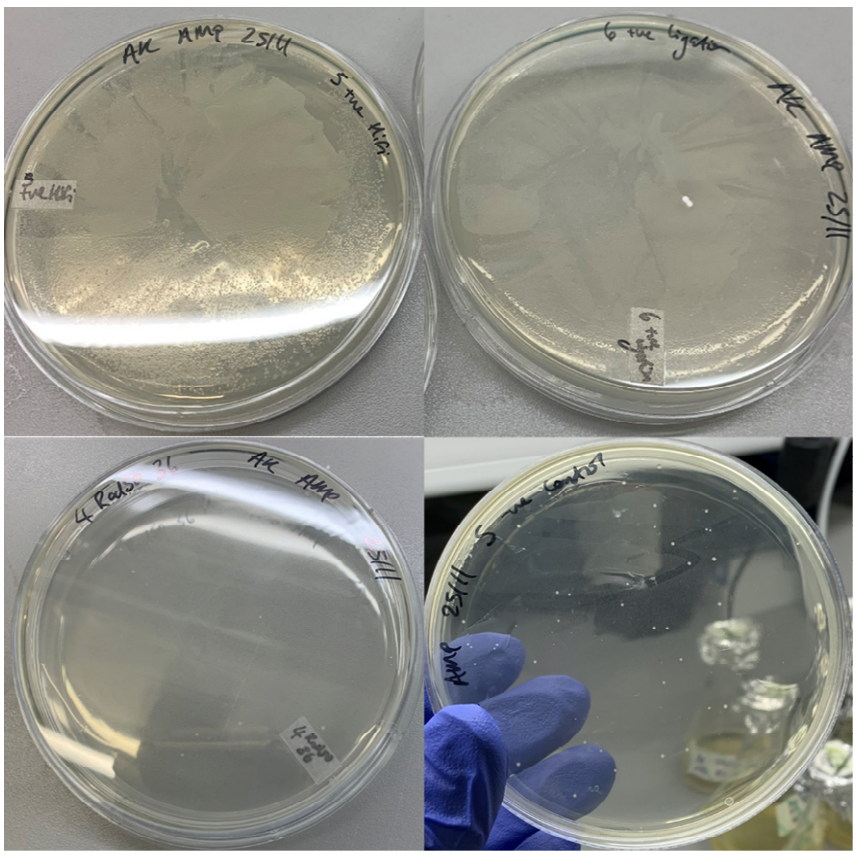


Figure 41 Agar plates containing ampicillin (50µg/ml) showing colonies transfected with synthetic DNA constructs after DNA assembly and ligation.

RAD50 in a pGL36 vector are shown along with appropriate controls, two positives, one for the ligation being a provided insert and vector from NEB and the other for the transfection where an ampicillin resistance plasmid is transfected, the

negative control is missing the insert. The number of colonies in the ligation plate does not exceed that of the negative control therefore the ligation is unlikely to have worked despite the ligation and transfection working for the positive controls.

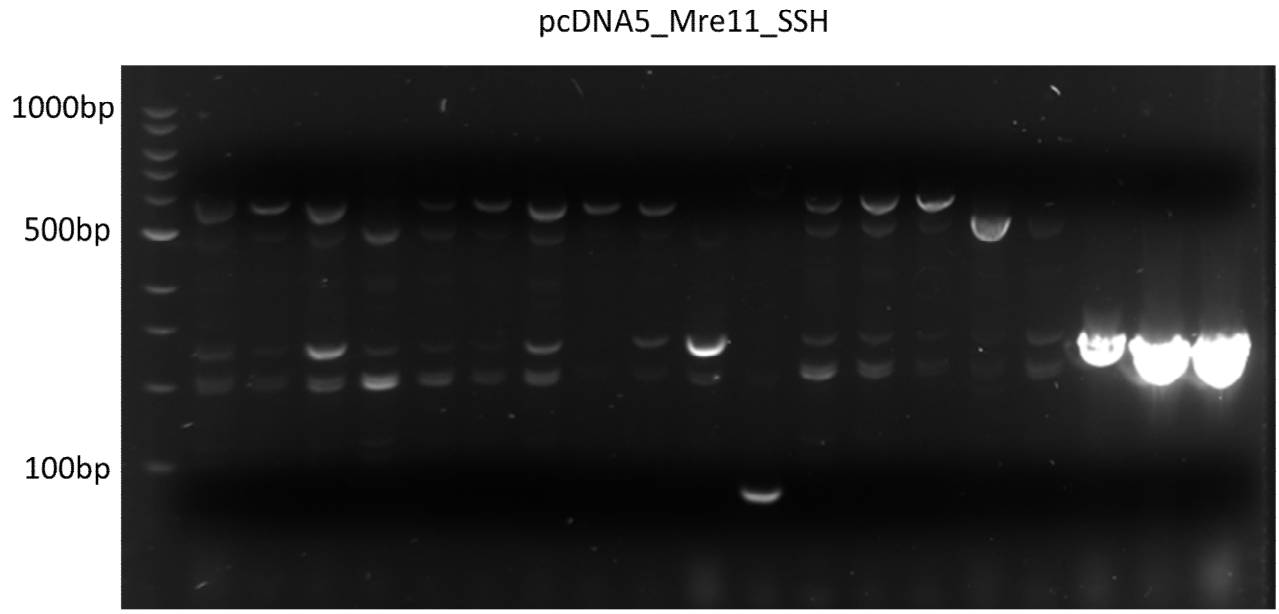


Figure 42. Candidate colony PCR result of 1% agarose electrophoresis gel from unspecific PCR amplification.

Gel showing unspecific or no PCR amplicons from N-terminally SSH tagged MRE11 pcDNA5 amplicon. Expected size of the amplicon was 546 base pairs

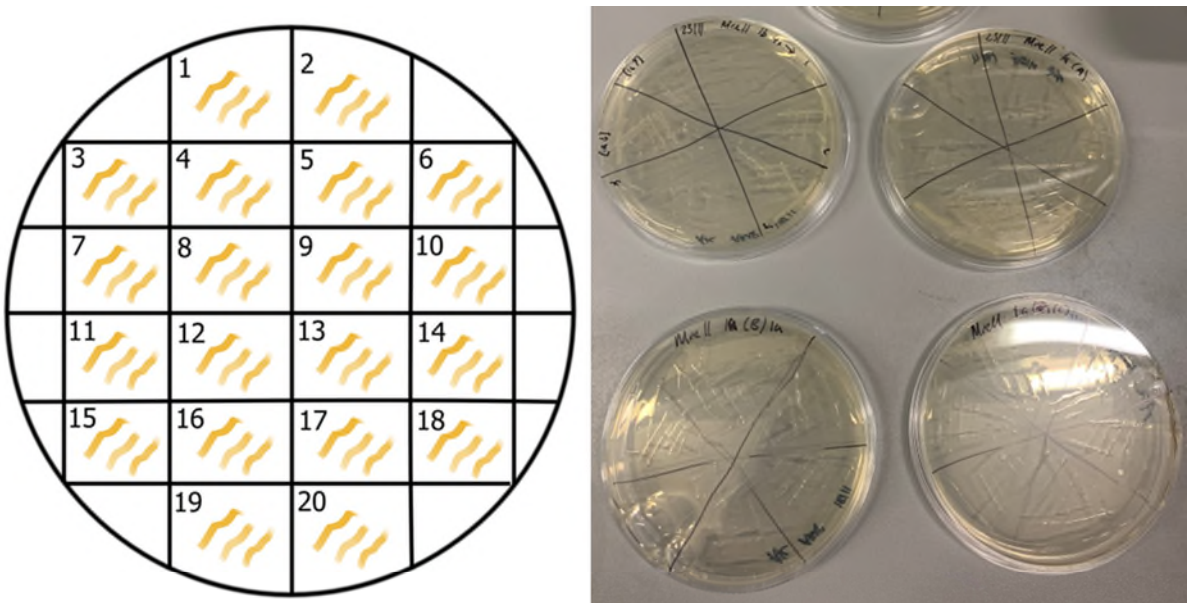


Figure 43. Patch plates of colonies screened by colony PCR.

A schematic is shown along with examples on agar plates containing ampicillin (50µg/ml).

Rad50 ligation issues pcDNA5_Rad50_SSH example

START

```
SSH             --------------------------------------------------
primer1         --------------------------------------------------
primer3         --------------------------------------------------
rad50           --------------------------------------------------
rad50pcdna5     TGATAGAGATCGTCGACGAGCTCGTTTAGTGAACCGTCAGATCGCCTGGA
seqdataend      --------------------------------------------------
seqdatast       TGATAGAGATCGTCGACGAGCTCGTTTAGTGAACCGTCAGATCGCCTGGA
tettet          TGATAGAGATCGTC----------------------------------
```

```
SSH             --------------------------------------------------
primer1         ----------------------------------------GCTCGGATC
primer3         --------------------------------------------------
rad50           --------------------------------------------------
rad50pcdna5     AGCCTCCGGACTCTAGCGTTTAAACTTAAGCTTGGTACCGAGCTCGGATC
seqdataend      --------------------------------------------------
seqdatast       AGCCTCCGGACTCTAGCGTTTAAACTTAAGCTTGGTACCGAGCTCGGATC
tettet          --------------------------------------------------
```

```
SSH             --------------------------------------------------
primer1         CATGTCCCGGATCGAAAAGATGAGC----------------------
primer3         --------------------------------------------------
rad50           -ATGTCCCGGATCGAAAAGATGAGCATTCTGGGCGTGCGGAGTTTTGGAA
rad50pcdna5     CATGTCCCGGATCGAAAAGATGAGCATTCTGGGCGTGCGGAGTTTTGGAA
seqdataend      --------------------------------------------------
seqdatast       CATGTCCCGGATCGAAAAGATAAAT----------------------
tettet          --------------------------------------------------
```

MIDDLE CONFUSION

```
SSH             --------------------------------------------------
primer1         ----------------------------------AAAAGATGAGC-----
primer3         --------------------------------------------------
rad50           ATAGCTCAACTAAGTGAATGCGAGAAACACAAAGAAAAGATAAATGAAGA
rad50pcdna5     ATAGCTCAACTAAGTGAATGCGAGAAACACAAAGAAAAGATAAATGAAGA
seqdataend      ---------------------------------AAAAGATAAATGAAGA
seqdatast       --------------------------------------------------
tettet          --------------------------------------------------
```

```
SSH             --------------------------------------------------
primer1         --------------------------------------------------
primer3         --------------------------------------------------
rad50           TATGAGACTCATGAGACAAGATATTGATACACAGAAGATACAAGAAAGGT
rad50pcdna5     TATGAGACTCATGAGACAAGATATTGATACACAGAAGATACAAGAAAGGT
seqdataend      TATGAGACTCATGAGACAAGATATTGATACACAGAAGATACAAGAAAGGT
seqdatast       --------------------------------------------------
tettet          --------------------------------------------------
```

END

```
SSH             --------------------------------------------------
primer1         --------------------------------------------------
primer3         ---------------------GGATTCAATGTTCATG---CGGCCGCTC
rad50           GAAATGCAGTGTTAGCTCCCTGGGATTCAATGTTCATTAA----------
rad50pcdna5     GAAATGCAGTGTTAGCTCCCTGGGATTCAATGTTCATTAAGCGGCCGCTC
seqdataend      GAAATGCAGTGTTAGCTCCCTGGGATTCAATGTTCATG---CGGCCGCTC
seqdatast       --------------------------------------------------
tettet          --------------------------------------------------
```

```
SSH             --------------------TGGAGCCACCCGCAGTTCGAGAAAGGTGGA
primer1         --------------------------------------------------
primer3         GAGGGAACC-------------------------------------------
rad50           --------------------------------------------------
rad50pcdna5     GAGGGAACCTTTTAGCAGAGTGGAGCCACCCGCAGTTCGAGAAAGGTGGA
seqdataend      GAGGGAACCTTTTAGCAGANNGGAGCCNCCNGCAGTTCNNNAAAGGNGGA
seqdatast       --------------------------------------------------
tettet          --------------------------------------------------
```

Figure 44. Failed DNA alignment result showing the beginning and end regions of the RAD50 insert into the pCDNA5 vector backbone as well as a region of interest where the alignment resumed.

The beginning and end of the insert is shown although the alignment stops at the beginning of the RAD50 sequence and seems to start again 1000s of base pairs downstream. The orange highlighted sequence is where I suggest the end of the primer annealed to and the red portion where the sequencing reaction continued unspecific to the primer used. The name of the sequence is labelled on the left, with those labelled without 'seq' prefix being reference sequences that the Sanger sequencing result is aligned to. The primers used to anneal the insert to the backbone are also highlighted. The sequencing results are labelled as 'seqdataend' and 'seqdatast' where the Sanger sequence result has been split into two for better visualisation and alignment.

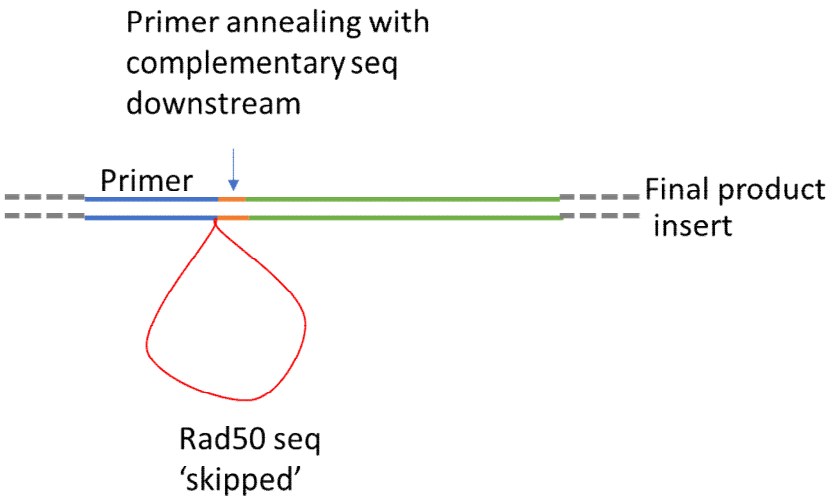


Figure 45. Schematic of the proposed ligation reaction causing the failed alignment.

Showing the primer annealing to the start of RAD50 as well as the downstream portion resulting in a large portion of the sequence 'skipped'.

NBN variant	
NP_002476.2/180-189 nibrin isoform 1 [Homo sapiens]	FLKAV**E**SKKQP
AAC39752.1/180-189 p95 [Homo sapiens]	FLKAV**Q**SKKQP
AAY15242.1/178-187 NBS1 [Xenopus laevis]	LLHAI**Q**EKRPL
NP_001191291.1/180-189 nibrin isoform 1 [Pongo abelii]	FLKAV**Q**SKKQL
NP_620228.1/180-189 nibrin [Rattus norvegicus]	FLKAV**E**SKTQP
NP_989668.2/177-186 nibrin [Gallus gallus]	LMKAV**Q**SRQQL

Figure 46. Protein alignment result of the variant found in the NBN gene (ACC39752.1) aligned to multiple different species.

Highlighted in bold is the variant.

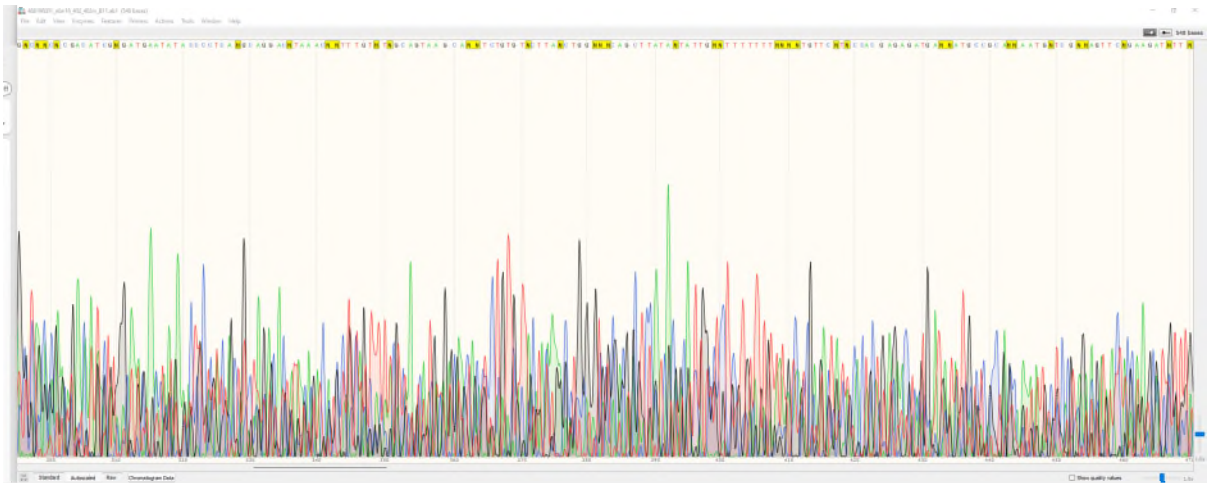


Figure 47. An example of a failed Sanger sequencing result.

The quality of the read failed assumed due to the inability of the primer to anneal. Therefore, the ligation was likely unsuccessful.

SAMPLE NAME	NUCLEIC ACID CONC (ng/µl)	A260/A280	A260/A230
MRE11-SSH	588.335	1.903	2.297
RAD50-SSH	749.109	1.889	2.372
NBS1-SSH	1196.086	1.894	2.337
APEX-MRE11	1274.79	1.863	2.293
APEX-RAD50	562.018	1.896	2.296
APEX-NBS1	665.259	1.859	2.323
MRE11-APEX	598.673	1.896	2.289
RAD50-APEX	637.616	1.901	2.29
NBS1-APEX	1213.661	1.838	2.204
EV-SSH	1116.223	1.893	2.326
APEX-EV	618.808	1.915	2.255
EV-APEX	1193.507	1.831	2.219

Figure 48. DNA concentrations in ng/µl of plasmids after maxiprep DNA purification once colony PCR and sequencing reactions.

A260/A280 or A230 values which indicate purity are shown, 1.8 is deemed pure for 260/280 and 2.2 for 260/230. Variations from this indicates contaminants.

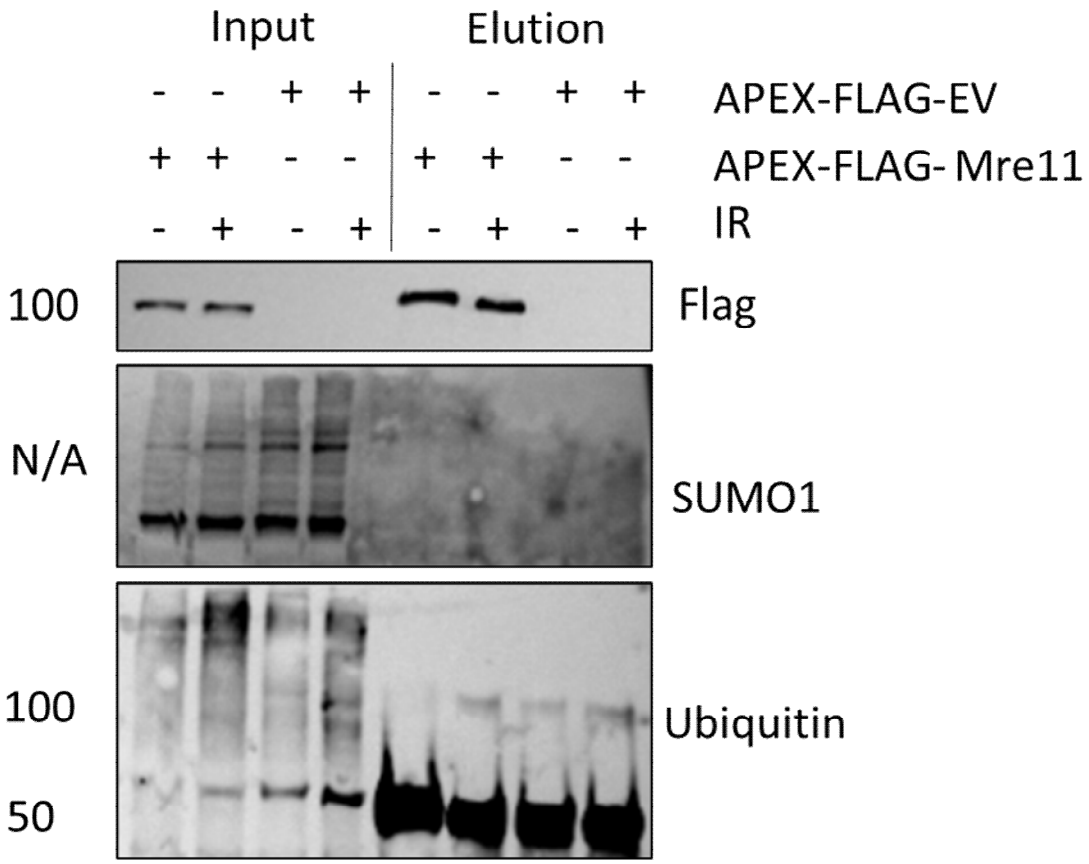


Figure 49. Candidate 'failed' denaturing IP results where MRE11 is not observed as SUMOylated or Ubiquitinated despite evidence from the literature.

The POI was expressed for 2 days where subsequent treatment with ionising radiation occurred. Recovery for 8 hours followed by lysis and chromatin digestion via benzonase was completed to study the whole cell fraction. Flagged-tagged MRE11 is pulldown using magnetic flag beads and the elution is blotted along with the input (prior to bead capture) on 9% acrylamide gels. Blotting for anti-Flag (MRE11), SUMO1, and ubiquitin. It shows MRE11 being over expressed and specifically pulled down in the elution although SUMO1 and ubiquitin cannot be observed indicating MRE11 is not modified by these residues. Strong bands in the elution for ubiquitin are the beads as the antibody on the beads is raised in mouse as well as the ubiquitin antibody. Molecular weight markers are highlighted on the left in kilodaltons.

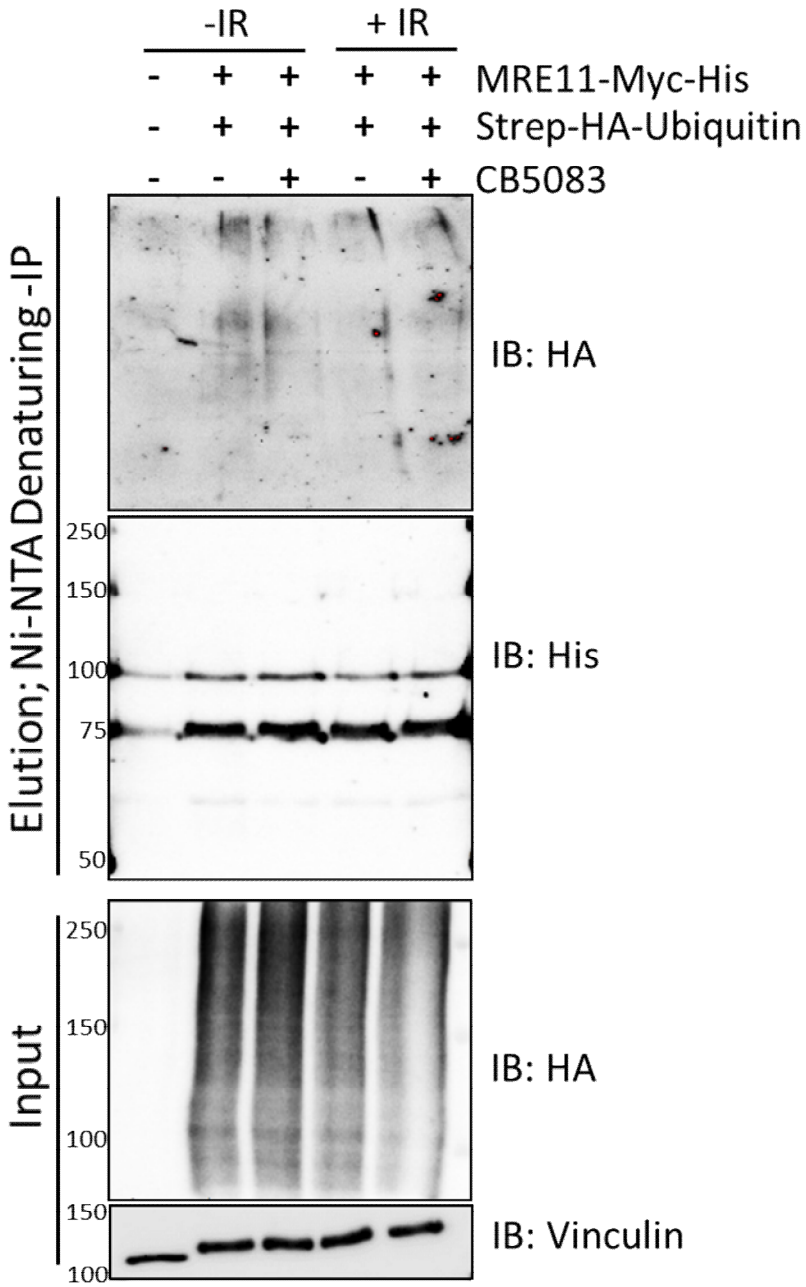


Figure 50. Candidate 'failed' denaturing IP results where MRE11 is not observed as Ubiquitinated despite evidence from the literature.

The POI was expressed for 2 days where subsequent treatment with ionising radiation and a p97 inhibitor occurred. Recovery for 8 hours followed by lysis and chromatin digestion via benzonase was completed to study the whole cell fraction. His-tagged MRE11 is pulldown using agarose His beads and the elution is blotted along with the input (prior to bead capture) on 9% acrylamide gels. Blotting for anti-HA (ubiquitin), His (MRE11), and vinculin. It shows MRE11 being over expressed and specifically pulled down in the elution although ubiquitin cannot be observed indicating MRE11 is not modified by these residues. Vinculin is used as a loading control in the input. Molecular weight markers are highlighted on the left in kilodaltons. ***This work was completed by another lab member.***

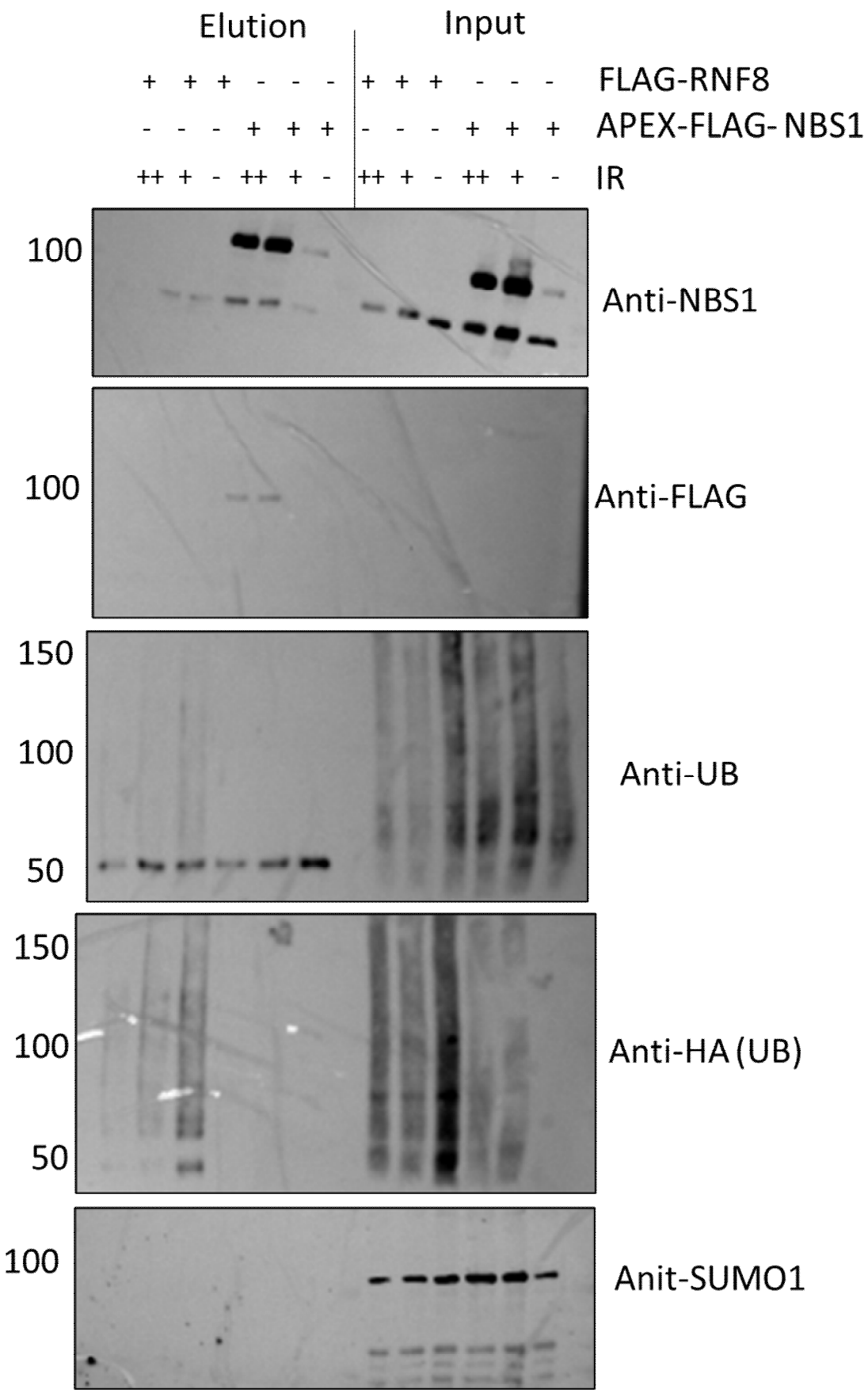

Elution
Input
+ + + - - - + + + - - - FLAG-RNF8
- - - + + + - - - + + + APEX-FLAG- NBS1
++ + - ++ + - ++ + - ++ + - IR
100
Anti-NBS1
100
Anti-FLAG
150
100
50
Anti-UB
150
100
50
Anti-HA (UB)
100
Anit-SUMO1

Figure 51. Positive control denaturing IP results where RNF8 is potentially observed as ubiquitinated although NBS1 is not.

The POI was expressed for 2 days where subsequent treatment with ionising radiation at 10 grays. Recovery after IR was 15 minutes (single +) or 8 hours (double ++). Subsequent lysis and chromatin digestion via benzonase was completed to study the whole cell fraction. FLAG-tagged NBS1 and RNF8 are pulldown using magnetic FLAG beads and the elution is blotted along with the input (prior to bead capture) on 9% acrylamide gels. Blotting for anti-HA (ubiquitin), NBS1, flag and SUMO1. It shows NBS1 being over expressed and specifically pulled down in the elution although ubiquitin cannot be observed indicating NBS1 is not modified by these residues. RNF8 cannot be observed being pulldown in the anti-FLAG blot which is thought to be a reblotting or human error issue. A species at the expected molecular weight of RNF8 (55) is seen to be ubiquitinated in the anti-HA blot due to the precise of a band around that molecular weight and a smear above that species. Neither NBS1 nor RNF8 seems to be SUMOylated by SUMO1. Anti-ubiquitin was not sensitive enough to observe ubiquitin chains. Molecular weight markers are highlighted on the left in kilodaltons

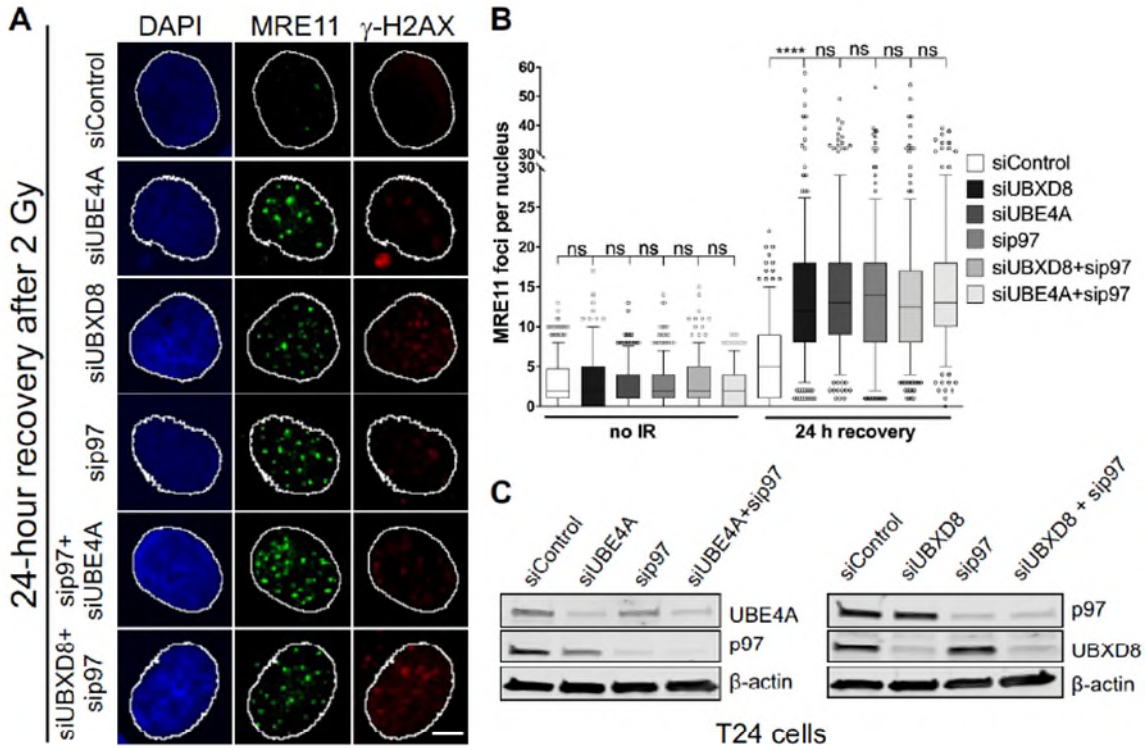


Figure 52. UBE4A and UBXD8 regulate accumulation of MRE11 on DNA damage similarly to p97.

*Representative images (A) and quantification (B) of the number of MRE11 foci over 24 hours after recovery from 2 Gy IR in UBE4A- and UBXD8- depleted T24 cells. C. Western Blot showing knockdowns of UBE4A, UBXD8 and p97. Data in (B) is presented as box plot with interquartile ranges shown and values beyond the 5th and 95th percentiles are shown as individual points and analysed by Kruskal-Wallis's test with Dunn's multiple comparisons. NS – not significant, **** p<0.0001. Scale bar: 5µm; n = 3 independent experiments.*

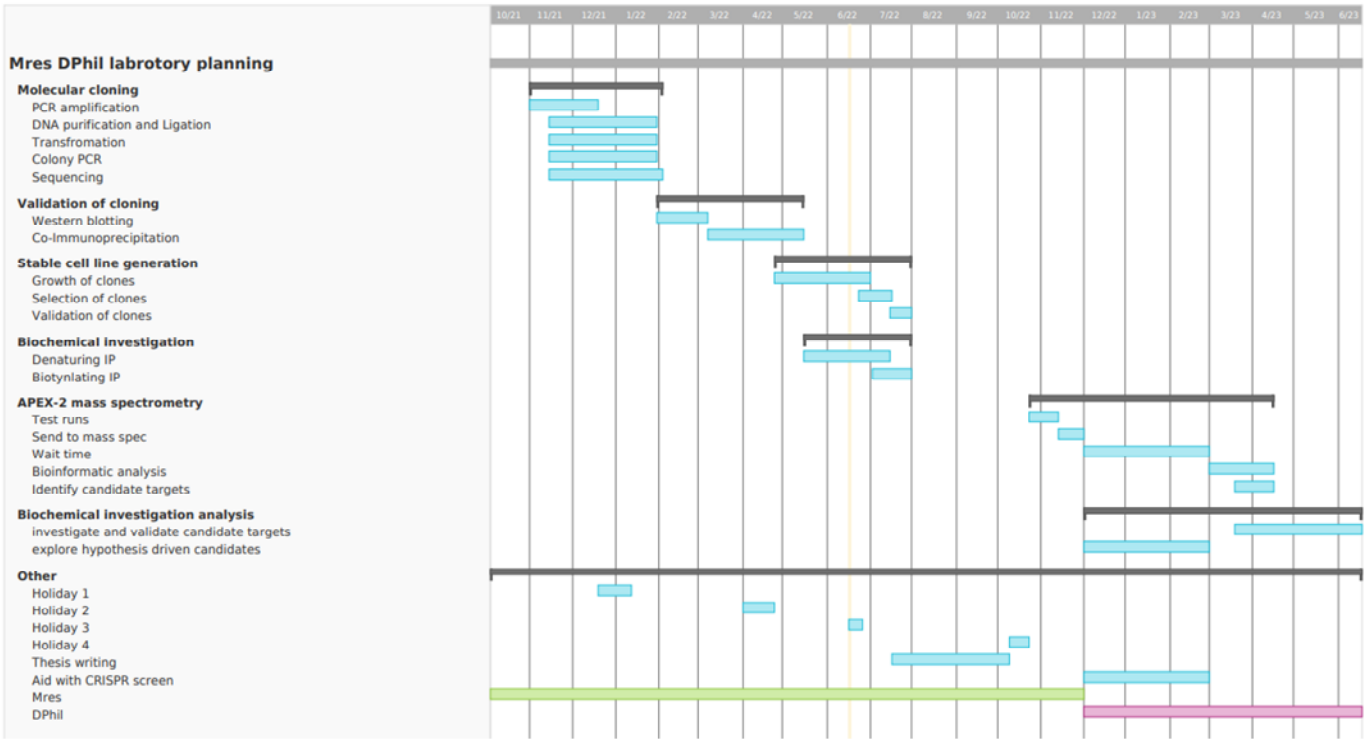


Figure 53. Gantt chart displaying masters work completed along with planned work for first couple months of DPhil.

Tasks completed and planned with an estimated time schedule.